ESI-MS AND EPR SPIN TRAPPING STUDY OF XANTHOPHYLLS:

STRUCTURAL AND ENVIRONMENTAL IMPACTS ON REACTIVITY

by

ADAM MAGYAR

LOWELL D. KISPERT, COMMITTEE CHAIR
MICHAEL K. BOWMAN, CO-CHAIR
CAROLYN J. CASSADY
KATRINA RAMONELL
DANIEL J. GOEBBERT
SHANLIN PAN

A DISSERTATION

Submitted in partial fulfillment of the requirements
for the degree of Doctor of Philosophy
in the Department of Chemistry
in the Graduate School of
The University of Alabama

TUSCALOOSA, ALABAMA

2015

ABSTRACT

Carotenoids are lipophilic pigments that provide many of the colors found in nature, including the colors found in plants, flowers, and animals. The main interest in carotenoids concerns their participation in light harvesting in biological systems and prevention of light-induced oxidative damage. Another reason for the interest in the redox properties of carotenoids is related to their use as antioxidants in medicinal formulations as a result of radical-mediated processes that occur frequently in living systems. A specific group of carotenoids, known as xanthophylls, are active in photoprotection and radical scavenging. What makes xanthophylls differ from other carotenoids is that they contain oxygen. This dissertation focuses on the interaction of three xanthophylls, Zeaxanthin, Lutein, and Astaxanthin, with damaging energetic species. Chapter 3 is focused on the deprotonation of naturally-occurring zeaxanthin (Zea) radical cations ($Zea^{\bullet+}$) to form neutral radicals ($\#Zea^{\bullet}$) and their involvement in the qE portion of non-photochemical quenching (NPQ) in the model organism *Arabidopsis thaliana*. An H/D exchange method was developed to test for the presence of $\#Zea^{\bullet}$ and was detected via liquid chromatography/mass spectrometry (LC/MS) methods and analyzed using analysis of variance (ANOVA) techniques. Chapter 4 examined the characteristics of xanthophyll carotenoids which self-assemble in aqueous solution to form J- and H-type aggregates. This aggregation significantly changes the photo-physical and optical properties of these xanthophylls, and has an impact on solar energy conversion and light induced oxidative damage. This study applied electron paramagnetic resonance (EPR) and optical absorption spectroscopy to investigate how complexation can affect the aggregation ability of the three xanthophylls mentioned above, their

photostability, and antioxidant activity. Chapter 5 demonstrates the different chemistries of geometrical isomers of zeaxanthin isolated from various sources in mass spectrometry using electrospray ionization sources. Zeaxanthin exhibits antioxidant activity and also plays a role in photo-protection in the retina. These properties have led to it being marketed as a dietary supplement as it is not formed by the body and must be consumed as part of the diet. Understanding the different chemical properties of zeaxanthin isomers is important with regards to the nutraceutical and pharmaceutical industries.

DEDICATION

This dissertation is dedicated to all those who helped make it possible. I especially would like to thank my family and close friends as well as all of my academic colleagues for helping me grow during my time as a graduate student.

LIST OF ABBREVIATIONS AND SYMBOLS

#	Proton loss
µ	micro
•	Radical
a	Hyperfine splitting
Å	Angstrom
AG	Arabinogalactan
ANOVA	Analysis of Variance
Asta	Astaxanthin
ATD	Above qE threshold, D_2O infiltrated
ATD-C	Above qE threshold, D_2O infiltrated control
ATW	Above qE threshold, water infiltrated
ATW-C	Above qE threshold, water infiltrated control
BTD	Below qE threshold, D_2O infiltrated
BTD-C	Below qE threshold, D_2O infiltrated control
BTW	Below qE threshold, water infiltrated
BTW-C	Below qE threshold, water infiltrated control
Chl	Chlorophyll
CLC	Column liquid chromatography
Col-0	Columbia wild-type seeds of Arabidopsis thaliana

CV	Cyclic Voltammetry
d_1	Deuterated
d_2	Doubly deuterated
DAD	Diode array detector
DMSO	Dimethyl sulfoxide
E	Einsteins
EIC	Extracted ion chromatogram
EPR	Electron paramagnetic resonance
ESI	Electrospray ionization
FDA	Food and Drug Administration
fs	Femtoseconds
GA	Glycyrrhizic acid
HPLC	High Pressure Liquid Chromatography
Hz	Hertz
LC/MS	Liquid Chromatography/Mass Spectrometry
Lut	Lutein
m	Meters
m/z	Mass to charge ratio
MS	Mass Spectrometry
NMR	Nuclear Magnetic Resonance
NPQ	Non-photochemical quenching
PBN	N-tert-Butyl-α-phenylnitrone
ps	picoseconds

s	Seconds
SA	Spin adduct
TIC	Total ion chromatogram
UV	Ultraviolet
V/Z	Violaxanthin/zeaxanthin
VDE	Violaxanthin deepoxidase
Viol	Violaxanthin
ZE	Zeaxanthin deepoxidase
Zea	Zeaxanthin
β	Beta
Δ	Delta
λ	Lamda

ACKNOWLEDGMENTS

This graduate research was carried out with financial support from The Chemical Sciences, Geoscience and Biosciences Division, Office of Basic Sciences, U. S. Department of Energy, grant DE-FG02-86ER-13465 (LDK). I would like to extend my thanks to the Graduate School and Department of Chemistry for giving me the opportunity to do my graduate work and pursue my Ph D at the University of Alabama in Tuscaloosa, AL.

I am most indebted to Professor Lowell D. Kispert for his advice, support, and guidance throughout my time at the University of Alabama. He was an extremely effective mentor and I would not have been able to write my dissertation without his influence.

I would also like to extend a special thank you to Professor Michael K. Bowman, co-chair of my dissertation committee, for guiding my research and undoubtedly playing a major role in my development as a scientific writer.

I would also like to thank all of my committee members, Daniel J. Goebbert, Carolyn J. Cassady, Shanlin Pan, and Katrina Ramonell for their invaluable support in both my research projects as well as during my progress through the academic requirements of the graduate program here at the University of Alabama.

I would like to express my gratitude for my current and former group members Dr. A. Ligia Focsan, Dr. Matthew Krzyaniak, Dr. Preethi Vennam, Alex Cruce, Sefadzi Tay-Agbozo, and Hanjiao Chen. I was very fortunate to have the opportunity to grow as a scientist with the support of such a great group. I would also like to thank our international collaborators Dr. Nikolay Polyakov and Dr. Péter Molnár, both of which have helped me publish work.

I would like to thank my fellow graduate students, too many to name, for helping me feel like I was home when I was so far away from where I grew up. I would like to express my appreciation for the Department of Chemistry, the faculty, the incredible support staff, and the College of Arts and Sciences for giving me the opportunity to pursue my doctoral degree at the University of Alabama.

Finally, I thank my family and friends for their support and help for getting me to where I am today.

CONTENTS

LIST OF TABLES

LIST OF FIGURES

CHAPTER 1

INTRODUCTION

1.1 Background

Carotenoids are lipophilic pigments that provide many of the colors found in nature, including the colors found in plants, flowers, and animals.[1] Examples of this coloration include the orange in carrots, the yellow in marigold, and pink in salmon. In plants these molecules also participate in light harvesting in biological systems and prevention of light-induced oxidative damage. They act as antioxidants in animals. This dissertation will examine some of the interactions a specific group of carotenoids which contain oxygen, known as xanthophylls, undergo with destructive energetic species. The main focus will be on zeaxanthin (Zea), lutein (Lut), and astaxanthin (Asta) (**Figure 1.1**) and how structure and their environment impacts their reactivity.

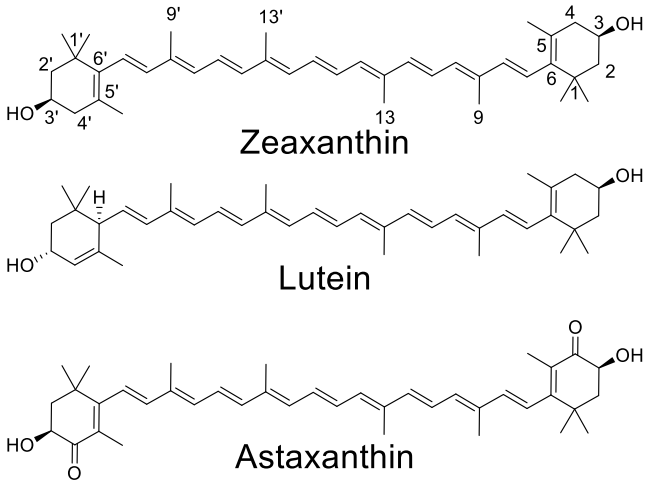

Figure 1.1: Structures of zeaxanthin, lutein, and astaxanthin. Carotenoids which contain oxygen are known as xanthophylls. The numbering system commonly used with carotenoids is shown on zeaxanthin and is based on the reference carotenoid lycopene.

The structure of carotenoids consists of a long conjugated chain and various terminal groups. The overall structure of the molecules has a direct influence on their properties, such as their color. A specific example of how the structure can affect the properties of the molecules is shown in **Figure 1.2**. The carotenoids A – E are listed in increasing order of oxidation potential, the potential at which the loss of an electron occurs at an anode in an electrochemical cell. The differences in these molecules are changes at the terminal ends.

	Name	E_1
A	β-carotene	0.634 V
B	Canthaxanthin	0.775 V
C	8’-apo-β-caroten-8’-al	0.795 V
D	Ethyl 8’-apo-β-caroten-8’-oate	0.797 V
E	7’-apo-7’,7’-dicyano-β-carotene	0.825 V

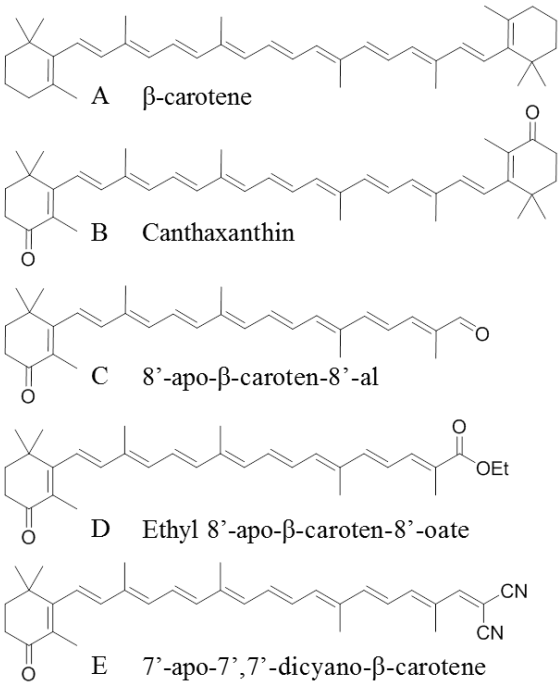

Figure 1.2: Structures and oxidation potentials of carotenoids with various terminal groups. The end groups influence the properties of the molecules, in particular the oxidation potentials.[2]

Another factor that has a major influence on the oxidation potential is the conjugation length of the molecule, the number of consecutive alternating double bonds. **Figure 1.3** gives an example on how the oxidation potentials of carotenoids change with conjugation length.

Carotenoids with the same terminal group but varying conjugation length exhibit significant differences in their oxidation potentials.[3] Longer conjugation leads to lower oxidation potentials.

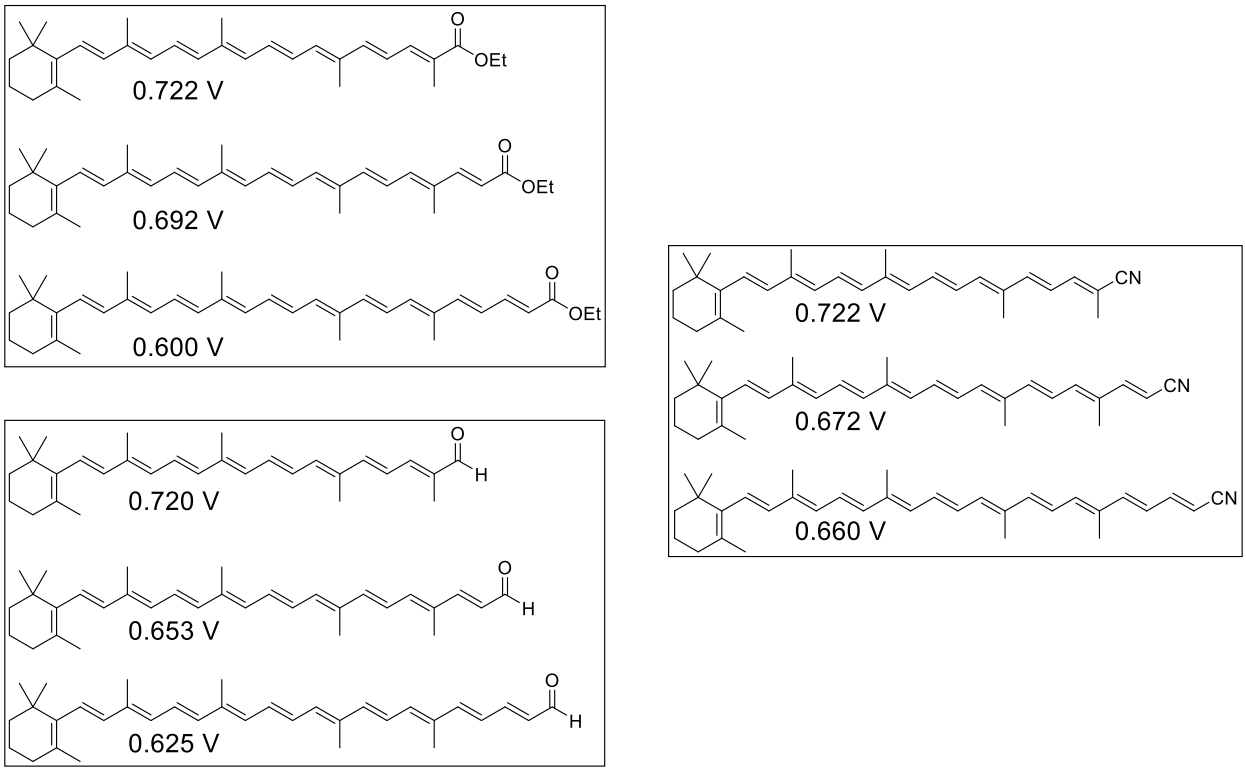

Figure 1.3: Oxidation potentials[3] of carotenoids with the same terminal groups yet varied conjugated polyene chain length. As the chain length increases, the oxidation potentials of the molecules decrease.

The oxidation potential of these molecules is of particular interest as it has been demonstrated to impact the scavenging ability of carotenoids towards the hydroperoxy radical, $^{\bullet}$OOH.[4,5] Published literature examining carotenoids **A – E** from **Figure1.2** found that a non-linear increase in reactivity with $^{\bullet}$OOH correlated with an increase in their oxidation potentials: carotenoids with higher oxidation potentials serve as better anti-oxidants.[4,5]

The values for the oxidation potentials of these carotenoids were established utilizing cyclic voltammetry electrochemical techniques. During these measurements, it was observed that

the carotenoids could undergo a variety of electrochemical and acid/base reactions. Reactions that are of particular interest are the formation of radical cations and neutral radicals. Previous work[3,6-8] has examined the reactions carotenoids undergo during CV measurements, shown in **Scheme 1.1**.

1: $Car \overset{E_1^0}{\rightleftharpoons} Car^{\bullet+} + e^-$	4: $Car^{++} + Car \overset{K_{com}}{\rightleftharpoons} 2\ Car^{\bullet+}$	7: $Car^{\bullet+} \longrightarrow$ Products
2: $Car^{\bullet+} \overset{E_2^0}{\rightleftharpoons} Car^{++} + e^-$	5: $Car^{++} \overset{K_{dp}}{\rightleftharpoons} \#Car^{+} + H^+$	8: $Car^{++} \longrightarrow$ Products
3: $\#Car^{+} + e^- \overset{E_3^0}{\rightleftharpoons} {}^{\#}Car^{\bullet}$	6: $Car^{\bullet+} \overset{K'_{dp}}{\rightleftharpoons} \#Car^{\bullet} + H^+$	9: $\#Car \longrightarrow$ Products
		10: $\#Car^{\bullet} \longrightarrow$ Products

Scheme 1.1: Reactions of carotenoids (Car) during CV measurements. The first oxidation (E_1^0) forms a radical cation ($Car^{\bullet+}$) which can undergo a second oxidation (E_2^0) to form a dication (Car^{++}). These molecules can then undergo additional reactions, including deprotonation to form neutral radicals ($\#Car^{\bullet}$).[7,8]

An equilibrium exists among the dications, the remaining carotenoid molecules, and radical cations. The equilibrium constant K_{com} is near 1 for **A** from **Figure 1.1** and approximately 1000 for **E** from **Figure 1.1**. The radical cations are weak acids (pK_{dp} = 4 for A and 7 for E).[7,8] Thus in proton accepting media, neutral radicals form from radical cations. The dications are very strong acids (pK_{dp} = −2) and easily deprotonate to form cations which upon reduction during the CV cycle, generates additional neutral radicals.

Research has been conducted to determine the most likely site for deprotonation on a variety of molecules, including Zea,[9] Lut,[10] and Asta.[11] Stable carotenoid radicals were formed on solid supports and studied via electron paramagnetic resonance (EPR).[9-14] The radical cations, and to a lesser extent neutral radicals, are readily formed on these supports. The

formation of neutral radicals increases in some cases when the samples are irradiated.[7] The formation of these neutral radicals was confirmed on solid supports via pulsed EPR techniques,[9-11] while density function theory (DFT) calculations were utilized to determine the most energetically favorable configurations.[9-11,15] The most likely site for deprotonation predicted by DFT calculations is dependent on the structure of the molecule. In the case of Zea this site is located at the 4(4') carbon on the terminal rings.[9] Zea is a symmetrical molecule and the two carbon are identical making the deprotonation equally likely at either end. Lut, an isomer of Zea, is not a symmetrical molecule and therefore does not have equivalent terminal rings. It was shown that the most likely site for deprotonation on Lut is at the 6' carbon, followed by the 4 carbon on the opposite terminal ring.[10] In the case of symmetrical Asta, the most likely site for deprotonation is at the 3(3') position of the terminal rings.[11]

1.2 Neutral Carotenoid Radicals in Photoprotection of Wild-Type *Arabidopsis thaliana*

Plants use photosynthesis to generate carbohydrates and oxygen from CO_2 and water. Light energy is necessary for this process, but excessive light is harmful to the plant. Chlorophyll (Chl) absorbs light and is transformed into its excited state. When light is absorbed at a higher rate than the photosynthetic enzymes can process, that energy must be dissipated in the form of heat or fluorescence in order to prevent unwanted reactions of the excited state Chl (Chl^*). Chl^* can generate singlet oxygen, damage proteins, and bleach Chl in a variety of photochemical reactions detrimental to the plant.[16-18] Controlled dissipation of the excess energy as heat is very important for the plant.[19,20]

Plants have several redundant mechanisms for protection from excess light, collectively known as non-photochemical quenching (NPQ).[21-24] One important form of NPQ is qE which is characterized by a decrease in Chl fluorescence. *Arabidopsis thaliana* mutants show a strong

connection between Zea[25] and the qE component of NPQ. Femtosecond transient absorption spectroscopy detects a charge transfer complex between Zea and Chl^* in some light-harvesting complexes of proteins in qE proficient plants.[26,27] Chl^* generated in these proteins is quenched by formation of the charge transfer complex with Zea, producing[26,27] a radical cation of Zea and a Chl radical anion: Zea + $Chl^* \rightarrow Zea^{\bullet+}\bullet\bullet\bullet\bullet Chl^{\bullet-}$ which has a lifetime of roughly 200 ps.[13,14] Free radicals and other paramagnetic species such as molecular oxygen are generally potent quenchers of excited states by electron exchange-induced-quenching. Quenching by free radicals is important in liquids and solids and forms the basis for fluorescence detection of reactive oxygen species.[28,29] The deprotonation of the $Zea^{\bullet+}$ in this charge transfer complex would form $\#Zea^{\bullet}$, which would become a potent free radical trap for large numbers of Chl^*. $\#Zea^{\bullet}$ would have a relatively long lifetime because Chl^{*-} and $\#Zea^{\bullet}$ can't recombine as the original charge transfer complex can. The formation of $\#Zea^{\bullet}$, even in a small quantum yield, would potentially make a major contribution to qE. Chapter 3 investigates the formation of Zea neutral radicals during the qE portion of NPQ in *A. thaliana* utilizing isotopic labeling and mass spectrometry techniques.

1.3 Chemistry of Geometrical Isomers of Zeaxanthin During Mass Spectrometry with Electrospray Ionization Source

As stated before, the structure of the carotenoids has an impact on their chemical properties. Due to the long polyene chains of these molecules, they can naturally exist in either *cis* or *trans* forms. The *cis* isomers can form from *trans* when the radical cations or dications are formed.[30] Specific isomers of Zea are regionally dominant in primate eyes.[31] An example of *cis*/*trans* isomers of carotenoids is shown in **Figure 1.4** with various geometric isomers of lycopene. Lycopene and its *cis* isomers are naturally found in ketchup.[32] These isomers are distinguishable via their optical absorption spectra.

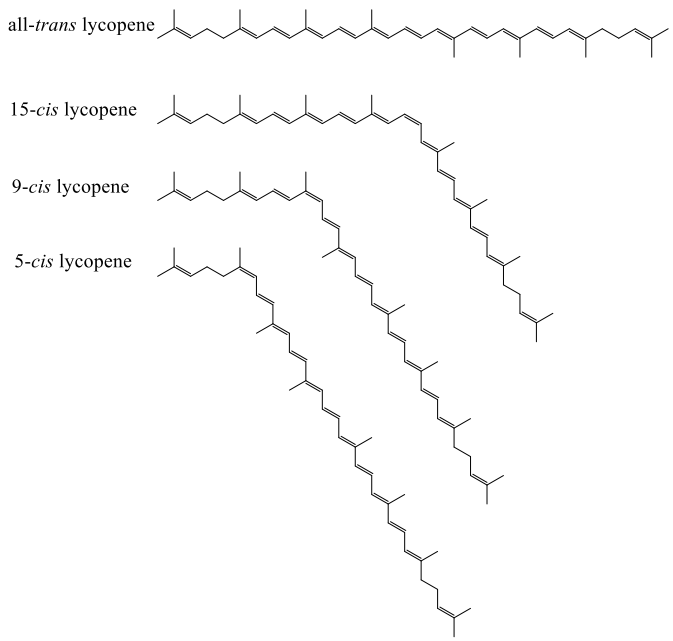

Figure 1.4: Various *cis/trans* isomers of lycopene.

In the case of β-carotene, the (all-*trans*) isomer has three absorption bands in the 400 – 500 nm range, while the various *cis* isomers have slight blue shifts in these absorption bands. Additionally an absorption band in the 300 – 400 nm range appears whose intensity relative to the absorption bands in the 400 – 500 nm range again depends on the isomer.[33] Other carotenoids have similar trends.

Since carotenoids are not manufactured by the body and must be consumed as part of the diet, they have been marketed and sold as dietary supplements. However, some supplements do not isolate specific carotenoid isomers. This is an important detail to consider because of the regional dominance of Zea isomers in the eye.[31] Much work has demonstrated that subtle changes in the structure of the carotenoids lead to changes in their chemical properties as discussed earlier in this chapter. Geometric isomers of the same carotenoid may exhibit different chemistry and therefore have different roles in cells. Chapter 4 compares the chemistry of (all-*trans*)-Zea and (13-*cis*)-Zea during electrospray ionization mass (ESI) spectrometry as previous

work has demonstrated carotenoids undergo multiple chemical and electrochemical reactions during ESI.[34]

1.4 Photochemical and Optical Properties of Water-Soluble Xanthophyll Antioxidants: Aggregation vs. Complexation

Practical application of carotenoids as nutritional antioxidants or components of medicinal preparations has been limited since carotenoids are highly hydrophobic, air- and light-sensitive compounds. The majority of carotenoids are lipophilic molecules with poor aqueous solubility. Moving carotenoids into a pharmaceutical application requires a chemical delivery system that overcomes the problems with parenteral administration of a highly lipophilic, low molecular weight compound. Many different methods have been developed to make the carotenoids "water dispersible", as true water solubility has not been found. Most of the attempts to increase the solubility of carotenoids depended on the preparation of cyclodextrin inclusion complexes.[35-41] However, cyclodextrin complexes demonstrate low solubility and fast aggregation in aqueous solution. Moreover, using cyclodextrin complexes does not allow control of the antioxidant activity of the carotenoids due to the fast dissociation of these complexes in biological media. Thus, identifying complexing agents without these drawbacks continues to be of considerable interest.

The unique properties of these complexes were demonstrated for two natural carotenoids: β-carotene and canthaxanthin.[1,42-45] An interesting property of xanthophylls which contain hydroxyl groups at each end of the molecules is that they form aggregates in aqueous media.[46-53] Two types of carotenoid aggregates can be distinguished according to their absorption spectra. The first type, associated with a large blue shift of the absorption spectrum and loss of

vibrational structure of the S_2 excited state, is suggested to take the form of H-aggregates, in which the molecules are stacked with the conjugated chains oriented more or less parallel to each other and closely packed. The blue shift of the absorption spectrum is explained in terms of excitonic interaction between the closely packed carotenoid chromophores.[47-49] The second aggregation type, characterized by a red shift of the absorption spectrum also caused by excitonic interactions where the resolution of vibrational bands is preserved, is attributed to J-type aggregation, in which there is a more head-to-tail organization of the conjugated chains. Examples of the aggregates are shown in **Figure 1.5.** The self-assembly of xanthophyll carotenoids leads to new photophysical properties which are not available to the monomer.

However no data has been reported in the literature on the chemical properties of carotenoid aggregates. This section studies the reactivity of the xanthophylls Zea, Lut, and Asta H-aggregates in some practically important processes, namely photodegradation and antioxidant activity and to compare these properties to the monomer.

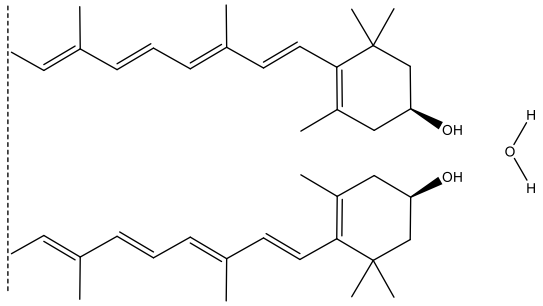

H-type Aggregate

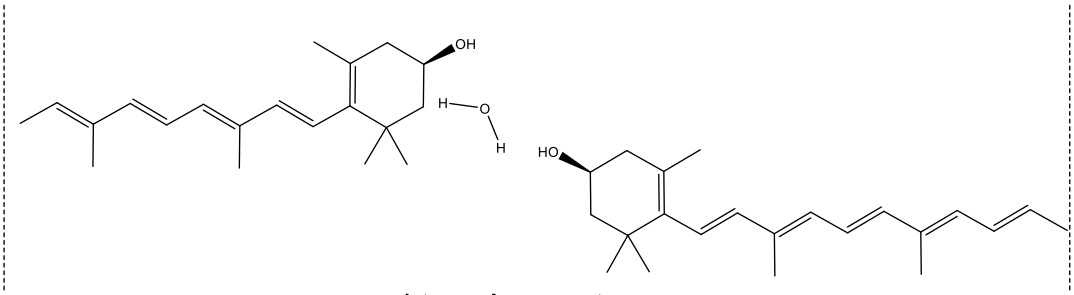

J-type Aggregate

Figure 1.5: H- and J-type aggregates of Zea. The H-aggregates are closely packed with the polyene chains aligned with each other, while the J-type has a head to tail orientation. The aggregates are held in place by hydrogen bonding around the terminal hydroxyl groups from the addition of water. H-aggregates can be identified optically by a large blue shift in the absorption spectrum, while J-aggregates exhibit a large red shift.

1.5 References

(1) Haugen, L.; Bjornson, T. *Beta Carotene: Dietary Sources, Cancer and Cognition*; Nova Biomedical Books, 2009.

(2) Focsan, A. L.; Pan, S.; Kispert, L. D. Electrochemical Study of Astaxanthin and Astaxanthin n-Octanoic Monoester and Diester: Tendency to Form Radicals, *J Phys Chem B* **2014**, *118*, 2331-2339.

(3) Deng, Y.; Gao, G. Q.; He, Z. F.; Kispert, L. D. Effects of Polyene Chain Length and Acceptor Substituents on the Stability of Carotenoid Radical Cations, *J Phys Chem B* **2000**, *104*, 5651-5656.

(4) Polyakov, N. E.; Kruppa, A. I.; Leshina, T. V.; Konovalova, T. A.; Kispert, L. D. Carotenoids as Antioxidants: Spin Trapping EPR and Optical Study, *Free Radical Bio Med* **2001**, *31*, 43-52.

(5) Polyakov, N. E.; Leshina, T. V.; Konovalova, T. A.; Kispert, L. D. Carotenoids as Scavengers of Free Radicals in a Fenton Reaction: Antioxidants or Pro-Oxidants?, *Free Radical Bio Med* **2001**, *31*, 398-404.

(6) He, Z. F.; Gosztola, D.; Deng, Y.; Gao, G. Q.; Wasielewski, M. R.; Kispert, L. D. Effect of Terminal Groups, Polyene Chain Length, and Solvent on the First Excited Singlet States of Carotenoids, *J Phys Chem B* **2000**, *104*, 6668-6673.

(7) Liu, D. Z.; Gao, Y. L.; Kispert, L. D. Electrochemical Properties of Natural Carotenoids, *J Electroanal Chem* **2000**, *488*, 140-150.

(8) Liu, D.; Kispert, L. Electrochemical Aspects of Carotenoids, *Recent Res Dev Electrochem* **1999**, *2*, 139-157.

(9) Focsan, A. L.; Bowman, M. K.; Konovalova, T. A.; Molnar, P.; Deli, J.; Dixon, D. A.; Kispert, L. D. Pulsed EPR and DFT Characterization of Radicals Produced by Photo-Oxidation of Zeaxanthin and Violaxanthin on Silica-Alumina, *J Phys Chem B* **2008**, *112*, 1806-1819.

(10) Lawrence, J.; Focsan, A. L.; Konovalova, T. A.; Molnar, P.; Deli, J.; Bowman, M. K.; Kispert, L. D. Pulsed Electron Nuclear Double Resonance Studies of Carotenoid Oxidation in Cu(Il)-Substituted MCM-41 Molecular Sieves, *J Phys Chem B* **2008**, *112*, 5449-5457.

(11) Polyakov, N. E.; Focsan, A. L.; Bowman, M. K.; Kispert, L. D. Free Radical Formation in Novel Carotenoid Metal Ion Complexes of Astaxanthin, *J Phys Chem B* **2010**, *114*, 16968-16977.

(12) Focsan, A. L.; Molnar, P.; Deli, J.; Kispert, L. Structure and Properties of 9'-Cis Neoxanthin Carotenoid Radicals by Electron Paramagnetic Resonance Measurements and Density Functional Theory Calculations: Present in LHC II?, *J Phys Chem B* **2009**, *113*, 6087-6096.

(13) Focsan, A. L.; Bowman, M. K.; Molnar, P.; Deli, J.; Kispert, L. D. Carotenoid Radical Formation: Dependence on Conjugation Length, *J Phys Chem B* **2011**, *115*, 9495-9506.

(14) Focsan, A. L.; Bowman, M. K.; Shamshina, J.; Krzyaniak, M. D.; Magyar, A.; Polyakov, N. E.; Kispert, L. D. Epr Study of the Astaxanthin N-Octanoic Acid Monoester and Diester Radicals on Silica-Alumina, *J Phys Chem B* **2012**, *116*, 13200-13210.

(15) Gao, Y. L.; Focsan, A. L.; Kispert, L. D.; Dixon, D. A. Density Functional Theory Study of the Beta-Carotene Radical Cation and Deprotonated Radicals, *J Phys Chem B* **2006**, *110*, 24750-24756.

(16) Koyama, Y. Structures and Functions of Carotenoids in Photosynthetic Systems, *J Photoch Photobio B* **1991**, *9*, 265-280.

(17) Renger, G.; Wolff, C. Further Evidence for Dissipative Energy Migration Via Triplet-States in Photosynthesis - Protective Mechanism of Carotenoids in Rhodopseudomonas-Spheroides Chromatophores, *Biochim Biophys Acta* **1977**, *460*, 47-57.
(18) Boucher, F.; Vanderrest, M.; Gingras, G. Structure and Function of Carotenoids in Photoreaction Center from Rhodospirillum-Rubrum, *Biochim Biophys Acta* **1977**, *461*, 339-357.
(19) Holt, N. E.; Fleming, G. R.; Niyogi, K. K. Toward an Understanding of the Mechanism of Nonphotochemical Quenching in Green Plants, *Biochemistry-Us* **2004**, *43*, 8281-8289.
(20) Pascal, A. A.; Liu, Z. F.; Broess, K.; van Oort, B.; van Amerongen, H.; Wang, C.; Horton, P.; Robert, B.; Chang, W. R.; Ruban, A. Molecular Basis of Photoprotection and Control of Photosynthetic Light-Harvesting, *Nature* **2005**, *436*, 134-137.
(21) Mozzo, M.; Dall'Osto, L.; Hienerwadel, R.; Bassi, R.; Croce, R. Photoprotection in the Antenna Complexes of Photosystem II - Role of Individual Xanthophylls in Chlorophyll Triplet Quenching, *J Biol Chem* **2008**, *283*, 6184-6192.
(22) Bautista, J. A.; Tracewell, C. A.; Schlodder, E.; Cunningham, F. X.; Brudvig, G. W.; Diner, B. A. Construction and Characterization of Genetically Modified Synechocystis Sp. Pcc 6803 Photosystem II Core Complexes Containing Carotenoids with Shorter pi-Conjugation Than Beta-Carotene, *J Biol Chem* **2005**, *280*, 38839-38850.
(23) Lakshmi, K. V.; Poluektov, O. G.; Reifler, M. J.; Wagner, A. M.; Thurnauer, M. C.; Brudvig, G. W. Pulsed High-Frequency EPR Study on the Location of Carotenoid and Chlorophyll Cation Radicals in Photosystem II, *J Am Chem Soc* **2003**, *125*, 5005-5014.
(24) Vasil'ev, S.; Brudvig, G. W.; Bruce, D. The X-Ray Structure of Photosystem II Reveals a Novel Electron Transport Pathway between P680, Cytochrome b(559) and the Energy-Quenching Cation, Chl(Z)(+), *Febs Lett* **2003**, *543*, 159-163.
(25) Niyogi, K. K.; Grossman, A. R.; Bjorkman, O. Arabidopsis Mutants Define a Central Role for the Xanthophyll Cycle in the Regulation of Photosynthetic Energy Conversion, *Plant Cell* **1998**, *10*, 1121-1134.
(26) Ahn, T. K.; Avenson, T. J.; Ballottari, M.; Cheng, Y. C.; Niyogi, K. K.; Bassi, R.; Fleming, G. R. Architecture of a Charge-Transfer State Regulating Light Harvesting in a Plant Antenna Protein, *Science* **2008**, *320*, 794-797.
(27) Avenson, T. J.; Ahn, T. K.; Zigmantas, D.; Niyogi, K. K.; Li, Z.; Ballottari, M.; Bassi, R.; Fleming, G. R. Zeaxanthin Radical Cation Formation in Minor Light-Harvesting Complexes of Higher Plant Antenna, *J Biol Chem* **2008**, *283*, 3550-3558.
(28) Green, J. A.; Singer, L. A.; Parks, J. H. Fluorescence Quenching by Stable Free-Radical Di-tert-Butylnitroxide, *J Chem Phys* **1973**, *58*, 2690-2695.
(29) Hideg, E.; Barta, C.; Kalai, T.; Vass, I.; Hideg, K.; Asada, K. Detection of Singlet Oxygen and Superoxide with Fluorescent Sensors in Leaves under Stress by Photoinhibition or UV Radiation, *Plant Cell Physiol* **2002**, *43*, 1154-1164.
(30) Gao, G.; Wei, C. C.; Jeevarajan, A. S.; Kispert, L. D. Geometrical Isomerization of Carotenoids Mediated by Cation Radical Dication Formation, *J Phys Chem-Us* **1996**, *100*, 5362-5366.
(31) Nolan, J. M.; Meagher, K.; Kashani, S.; Beatty, S. What Is Meso-Zeaxanthin, and Where Does It Come From?, *Eye* **2013**, *27*, 899-905.
(32) Vallverdú-Queralt, A.; Martínez-Huélamo, M.; Arranz-Martinez, S.; Miralles, E.; Lamuela-Raventós, R. M. Differences in the Carotenoid Content of Ketchups and Gazpachos through HPLC/ESI(Li+)-MS/MS Correlated with Their Antioxidant Capacity, *J Sci Food Agr* **2012**, *92*, 2043-2049.

(33) Stahl, W.; Sundquist, A. R.; Hanusch, M.; Schwarz, W.; Sies, H. Separation of Beta-Carotene and Lycopene Geometrical-Isomers in Biological Samples, *Clin Chem* **1993**, *39*, 810-814.
(34) Guaratini, T.; Vessecchi, R.; Pinto, E.; Colepicolo, P.; Lopes, N. P. Balance of Xanthophylls Molecular and Protonated Molecular Ions in Electrospray Ionization, *J Mass Spectrom* **2005**, *40*, 963-968.
(35) Loftsson, T.; Brewster, M. E. Pharmaceutical Applications of Cyclodextrins. 1. Drug Solubilization and Stabilization, *J Pharm Sci* **1996**, *85*, 1017-1025.
(36) Szejtli, J. *Cyclodextrin Technology*; Springer, 1988; Vol. 1.
(37) Mele, A.; Mendichi, R.; Selva, A. Non-Covalent Associations of Cyclomaltooligosaccharides (Cyclodextrins) with Trans-Beta-Carotene in Water: Evidence for the Formation of Large Aggregates by Light Scattering and NMR Spectroscopy, *Carbohyd Res* **1998**, *310*, 261-267.
(38) Mele, A.; Mendichi, R.; Selva, A.; Molnar, P.; Toth, G. Non-Covalent Associations of Cyclomaltooligosaccharides (Cyclodextrins) with Carotenoids in Water. A Study on the Alpha- and Beta-Cyclodextrin/Psi,Psi-Carotene (Lycopene) Systems by Light Scattering, Ionspray Ionization and Tandem Mass Spectrometry, *Carbohyd Res* **2002**, *337*, 1129-1136.
(39) Szente, L.; Mikuni, K.; Hashimoto, H.; Szejtli, J. Stabilization and Solubilization of Lipophilic Natural Colorants with Cyclodextrins, *J Inclus Phenom Mol* **1998**, *32*, 81-89.
(40) Lancrajan, I.; Diehl, H. A.; Socaciu, C.; Engelke, M.; Zorn-Kruppa, M. Carotenoid Incorporation into Natural Membranes from Artificial Carriers: Liposomes and Beta-Cyclodextrins, *Chem Phys Lipids* **2001**, *112*, 1-10.
(41) Polyakov, N. E.; Leshina, T. V.; Konovalova, T. A.; Hand, E. O.; Kispert, L. D. Inclusion Complexes of Carotenoids with Cyclodextrins: H-1 NMR, EPR, and Optical Studies, *Free Radical Bio Med* **2004**, *36*, 872-880.
(42) Polyakov, N. E.; Leshina, T. V.; Salakhutdinov, N. F.; Kispert, L. D. Host-Guest Complexes of Carotenoids with Beta-Glycyrrhizic Acid, *J Phys Chem B* **2006**, *110*, 6991-6998.
(43) Polyakov, N. E.; Leshina, T. V.; Salakhutdinov, N. F.; Konovalova, T. A.; Kispert, L. D. Antioxidant and Redox Properties of Supramolecular Complexes of Carotenoids with Beta-Glycyrrhizic Acid, *Free Radical Bio Med* **2006**, *40*, 1804-1809.
(44) Polyakov, N. E.; Leshina, T. V.; Meteleva, E. S.; Dushkin, A. V.; Konovalova, T. A.; Kispert, L. D. Water Soluble Complexes of Carotenoids with Arabinogalactan, *J Phys Chem B* **2009**, *113*, 275-282.
(45) Polyakov, N. E.; Leshina, I. V.; Meteleva, E. S.; Dushkin, A. V.; Konovalova, T. A.; Kispert, L. D. Enhancement of the Photocatalytic Activity of TiO_2 Nanoparticles by Water-Soluble Complexes of Carotenoids, *J Phys Chem B* **2010**, *114*, 14200-14204.
(46) Mosquera, M. I. M.; Galán, M. J.; Méndez, D. H. *Pigments in Food Technology: Proceedings of 1st International Congress Pft*, 1999.
(47) Ruban, A. V.; Horton, P.; Young, A. J. Aggregation of Higher-Plant Xanthophylls - Differences in Absorption-Spectra and in the Dependency on Solvent Polarity, *J Photoch Photobio B* **1993**, *21*, 229-234.
(48) Billsten, H. H.; Sundstrom, V.; Polivka, T. Self-Assembled Aggregates of the Carotenoid Zeaxanthin: Time-Resolved Study of Excited States, *J Phys Chem A* **2005**, *109*, 1521-1529.
(49) Wang, C.; Berg, C. J.; Hsu, C. C.; Merrill, B. A.; Tauber, M. J. Characterization of Carotenoid Aggregates by Steady-State Optical Spectroscopy, *J Phys Chem B* **2012**, *116*, 10617-10630.

(50) Krinsky, N. I.; Mathews-Roth, M. M.; Taylor, R. F. *Carotenoids: Chemistry and Biology*; Plenum Press, 1989.
(51) Goulinet, S.; Chapman, M. J. Plasma LDL and HDL Subspecies Are Heterogenous in Particle Content of Tocopherols Oxygenated and Hydrocarbon Carotenoids - Relevance to Oxidative Resistance and Atherogenesis, *Arterioscl Throm Vas* **1997**, *17*, 786-796.
(52) Sujak, A.; Gabrielska, J.; Grudzinski, W.; Borc, R.; Mazurek, P.; Gruszecki, W. I. Lutein and Zeaxanthin as Protectors of Lipid Membranes against Oxidative Damage: The Structural Aspects, *Arch Biochem Biophys* **1999**, *371*, 301-307.
(53) Sujak, A.; Okulski, W.; Gruszecki, W. I. Organisation of Xanthophyll Pigments Lutein and Zeaxanthin in Lipid Membranes Formed with Dipalmitoylphosphatidylcholine, *Bba-Biomembranes* **2000**, *1509*, 255-263.

CHAPTER 2

EXPERIMENTAL

2.1 Role of Zeaxanthin Neutral Radicals in NPQ

2.1.1 Plant Material

Columbia wild-type (Col-0) seeds of *A. thaliana* were planted in 4" x 4" x 3.75" pots (Hummert International) in Pro-Mix HP soil (Premier). Plants were grown under 16/8 hour day/night cycles at approximately 23˚C/21˚C respectively. The average light intensity at the top of the pots was approximately 100 µE $m^{-2}s^{-1}$. Plants were watered with fertilizer (Petersen's 20-20-20) twice a week or as needed. Leaves were collected from 4-5 week old *A. thaliana* plants.

2.1.2 H_2O and D_2O Infiltration of Leaves

A. thaliana leaves were placed into a syringe. Distilled water or D_2O was added until the leaves were completely submerged. The syringe needles were plugged into a cork and the plunger was drawn to create a vacuum which was held for two minutes and then released. This process infiltrated the leaves with either H_2O or D_2O.

2.1.3 Light Exposure

Infiltrated leaves were exposed to light intensity less than needed to induce qE by placing half of the leaves from each syringe outside on a cloudy day for 30 minutes at approximately 150 µE $m^{-2}s^{-1}$ light intensity. This intensity is sufficient to initiate the xanthophyll cycle, but not qE. These will be referred to as the **below qE threshold** samples and denoted "**BTW**" for the **water** infiltrated and "**BTD**" for the **D_2O** infiltrated. The other half of the leaves from each syringe was used as **controls** (**C**) and received a sham exposure in a closed styrofoam shipping box. These

will be referred to as the **below qE threshold controls** or "**BTW-C**" for the **water** infiltrated control and "**BTD-C**" for the **D_2O** infiltrated control.

Infiltrated leaves were exposed to light intensity greater than needed to induce qE by placing half of the leaves from each syringe outside on a sunny day for 30 minutes at approximately 370 µE $m^{-2}s^{-1}$ light intensity. This intensity is sufficient to initiate both the xanthophyll cycle and qE. These will be referred to as the **above qE threshold** samples and denoted "**ATW**" for the **water** infiltrated and "**ATD**" for the **D_2O** infiltrated. The other half of the leaves from each syringe was used as **controls** (**C**) and received a sham exposure in a closed styrofoam shipping box. These will be referred to as the **above qE threshold controls** or "**ATW-C**" for the **water** infiltrated control and "**ATD-C**" for the **D_2O** infiltrated control.

2.1.4 Carotenoid Extraction

The exposed leaves from the *A. thaliana* plant were placed into eppendorf tubes and crushed with a tissue homogenizer. A small amount of anhydrous sodium sulfate was added and crushed with the homogenizer again. Then, 0.5 mL of HPLC-grade acetone was added and vigorously shaken for 30 seconds. Another 0.5 mL of HPLC-grade acetone was added and shaken again for 30 seconds. 0.5 mL of this acetone solution was transferred to a new eppendorf tube while the rest was discarded. 0.8 mL of HPLC-grade hexane was then added to the extracted acetone solution.[1] The tubes were centrifuged until two visible layers formed. The upper green layer was placed into a glass storage vial while the rest was discarded. The extract was then dried under a stream of N_2 gas and capped. The dried extract was dissolved in 2.5 mL of dichloromethane for LC/MS analysis.

2.1.5 Liquid Chromatography/Mass Spectrometry Analysis

Samples were analyzed using liquid chromatography/mass spectrometry with an Agilent Technologies 1200 series, with an Agilent Technologies Zorbax SB-C18 5 µm 150x0.5 mm column. The mass spectrometer was a Bruker HCTultra PTM Discovery system. The flow rate of the chromatography was 18 µL/second. The solvent system was an isocratic mixture of 92% methanol diluted with high-purity water (95) and LC/MS grade acetonitrile (5). Both solutions contained 0.1% formic acid by volume. The mass spectrum was generated by using electrospray ionization (ESI) technique in positive ion mode.[2] The chromatograms were analyzed using DataAnalysis version 4.0 (Build 234) from Bruker Daltonic. The unprocessed chromatograms can be found in Appendix A in Figures A1 – A38.

2.1.6 Statistical Evaluation

The data was subject to statistical analysis by one way analysis of variance (ANOVA) using Microsoft Excel 2010 Analysis Toolpak with α set to 0.05. This corresponds to a confidence level of 95%. A p value, the probability that differences between samples are due entirely to random processes, of less than 0.05 was considered statistically significant. The full data sets can be found in Appendix A in Tables A1-A13.

2.1.7 Chemical Formation of Zea Radicals

The radicals were generated via addition of Fe(III)[3] (from $FeCl_3$) dissolved in either water or D_2O equal to 10% molar concentration of the carotenoid solution. Five separate samples were prepared. One sample was left untouched, two samples had Fe(III) added as well as 1% by volume of D_2O (one a few hours prior to LC/MS injection and one 10 minutes prior), and the other two had Fe(III) added as well as 1% by volume H_2O (one a few hours prior to LC/MS injection and one 10 minutes prior). These five samples will be referred to as: Normal, Short

Term H_2O, Long Term H_2O, Short Term D_2O, and Long Term D_2O. The formation of the radicals was confirmed via optical spectroscopy by the appearance of a peak in the 800 – 900 nm range.[3]

2.2 Chemistry of geometrical isomers of zeaxanthin during ESI-MS analysis

2.2.1 Crude zeaxanthin extract

This process was undergone as described in section **2.1.4**

2.2.2 Isolation of purified zeaxanthin isomers

The Zeaxanthin standard used as a reference in our ESI/MS system was isolated from berries of *Lycium halimifolium* L. or *Lycium barbarum* L. The berries of *L. halimifolium* or *L. barbarum* were extracted three times with MeOH and once with Et_2O. The ethereal solution was evaporated, dried by anhydrous Na_2SO_4 and the residue was crystallized from toluene:MeOH mixture (ca. 1:5 mixture). This process resulted in "rough" physaliene (zeaxanthin-dipalmitate). Physaliene was saponified in Et_2O with 30% KOH-MeOH in heterogenous phase (overnight). After washing alkali-free, the solution was evaporated, dried by anhydrous Na_2SO_4 and crystallized from toluene:hexane (ca. 1:5 mixture). This process resulted in crystalline zeaxanthin with the purity of 92-93% (HPLC). This sample contained ca. 3% β-cryptoxanthin and other impurities; (*Z*)-isomers of zeaxanthin and β-cryptoxanthin, furanoids e.g. mutatoxanthin- and auroxanthin-epimers and β-citraurin) in traces (3-4%). The final purification was carried out by column liquid chromatography (CLC) using $CaCO_3$ (Ph. Hg. VI.; Biogal, Hungary; precipitated pharmaceutical) as adsorbent and toluene:hexane (ca. 1:1 mixture) as eluent. After removing of the zone of β-cryptoxanthin and of the zones of other impurities, the main zone (zone of zeaxanthin) was eluted and after the usual work-up it was crystallized from toluene:hexane (ca. 1:5 mixture) resulting in pure (<95%; HPLC) Zeaxanthin.

2.2.3 Liquid chromatography/mass spectrometry analysis

This process was undergone as described in section **2.1.5.**

2.3 Photochemical and Optical Properties of Water Soluble Xanthophyll Antioxidants: Aggregation vs. Complexation

2.3.1 Complexation Methods

Astaxanthin was purchased from Sigma (97%), lutein (90%) from Kemin and zeaxanthin (90%) is from Kalsec. All carotenoids were stored at -14°C in a desiccator. Synthesis and properties of n-octanoic acid diester of astaxanthin is described in.[4] The purity was checked by ^{1}H NMR spectroscopy (360 MHz, $CDCl_3$) and TLC. Glycyrrhizic acid is extracted from the Ural licorice root. For the methods of GA purification see.[5] AG is extracted from *Larix sibirica*.[6-8] All complexes were prepared by standard liquid phase method, although a mechanico-chemical method[9] has been used when high (~5 mM) concentrations of carotenoids are required in AG. Complexes with GA were prepared by dissolving carotenoids and GA in ethanol or DMSO, and then water was added in required proportion. Complexes with AG were prepared by mixing ethanol solution of carotenoid with water solution of polysaccharide in the required proportion resulting in the xanthophyll being located in the polymer matrix as part of a supramolecule.

The stoichiometry and stability of complexes were measured by conventional methods[10,11] and were detected by changes in the absorption spectra of carotenoids as a function of GA concentration. Absorption spectra were recorded using a Shimadzu UV-visible 1601 spectrophotometer. All measurements were performed in a 10 mm path length quartz cuvette at 293 K.

2.3.2 Radical scavenging in organic solution

The competitive spin trapping reaction was carried out in DMSO solution. The solution contained 500 mM H_2O_2, 5 mM PBN spin trap, varying concentrations of xanthophylls, and the radical generation via Fenton chemistry was triggered via addition of 1 mM $FeCl_2$. The spectra were recorded using a Bruker ELEXYS E540 CW X-band (9.7 GHz) EPR spectrometer at room temperature. The signal intensity was determined using Bruker's X-EPR spinfit software. Spin adducts with hyperfine splittings (A) of A_N = 13.96 G and A_H = 2.33 G were observed in the spin trapping system.

2.3.3 Radical scavenging in aqueous solution

The competitive spin trapping mechanism was carried out in 80% DMSO/water solution. The solution contained 500 mM H_2O_2, 5 mM PBN spin trap, varying concentrations of xanthophylls or dimer complexed xanthophylls, and the radical generation via Fenton chemistry was triggered by addition of 1 mM $FeCl_2$. The EPR spectra were recorded using a Bruker ELEXYS E540 CW X-band (9.7 GHz) EPR spectrometer at room temperature. The signal intensity was fit using Bruker's X-EPR spinfit software. Spin adducts with hyperfine splittings (A) of A_N = 13.96 G and A_H = 2.33 G were observed in the spin trapping system.

2.4 References

(1) Lakshminarayana, R.; Raju, M.; Krishnakantha, T. P.; Baskaran, V. Determination of Major Carotenoids in a Few Indian Leafy Vegetables by High-Performance Liquid Chromatography, *J Agr Food Chem* **2005**, *53*, 2838-2842.

(2) Van Breemen, R. B. Liquid Chromatography/Mass Spectrometry of Carotenoids, *Pure Appl Chem* **1997**, *69*, 2061-2066.

(3) Gao, Y. L.; Kispert, L. D. Reaction of Carotenoids and Ferric Chloride: Equilibria, Isomerization, and Products, *J Phys Chem B* **2003**, *107*, 5333-5338.

(4) Focsan, A. L.; Bowman, M. K.; Shamshina, J.; Krzyaniak, M. D.; Magyar, A.; Polyakov, N. E.; Kispert, L. D. Epr Study of the Astaxanthin n-Octanoic Acid Monoester and Diester Radicals on Silica-Alumina, *J Phys Chem B* **2012**, *116*, 13200-13210.

(5) Kondratenko, R.; Baltina, L.; Mustafina, S.; Makarova, N.; Nasyrov, K. M.; Tolstikov, G. Crystalline Glycyrrhizic Acid Synthesized from Commercial Glycyrram. Immunomodulant Properties of High-Purity Glycyrrhizic Acid, *Pharmaceutical Chemistry Journal* **2001**, *35*, 101-104.

(6) Odonmazig, P.; Ebringerova, A.; Machova, E.; Alfoldi, J. Structural and Molecular-Properties of the Arabinogalactan Isolated from Mongolian Larchwood (Larix-dahurica L), *Carbohyd Res* **1994**, *252*, 317-324.

(7) Medvedev, E. N.; Vavkin, V. A.; Ostroukhova, L. A. Larch Arabinogalactan - Properties and Prospects (Review) (Russian), *Chem. Nat. Comp.* **2003**, *1*, 27-37.

(8) D'Adamo, P. Larch Arabinogalactan, *J. Naturopath. Med.* **1996**, *6*, 1997.

(9) Polyakov, N. E.; Leshina, T. V.; Meteleva, E. S.; Dushkin, A. V.; Konovalova, T. A.; Kispert, L. D. Water Soluble Complexes of Carotenoids with Arabinogalactan, *J Phys Chem B* **2009**, *113*, 275-282.

(10) Polyakov, N. E.; Leshina, T. V.; Salakhutdinov, N. F.; Kispert, L. D. Host-Guest Complexes of Carotenoids with Beta-Glycyrrhizic Acid, *J Phys Chem B* **2006**, *110*, 6991-6998.

(11) Martin, L.; Leon, A.; Olives, A. I.; del Castillo, B.; Martin, M. A. Spectrofluorimetric Determination of Stoichiometry and Association Constants of the Complexes of Harmane and Harmine with Beta-Cyclodextrin and Chemically Modified Beta-Cyclodextrins, *Talanta* **2003**, *60*, 493-503.

CHAPTER 3

NEUTRAL CAROTENOID RADICALS IN PHOTOPROTECTION OF WILD-TYPE *Arabidopsis thaliana*

Adapted with permission from: [1]Magyar, A.; Bowman, M. K.; Molnár, P.; Kispert, L. Neutral Carotenoid Radicals in Photoprotection of Wild-Type Arabidopsis thaliana, *The Journal of Physical Chemistry B* **2013**, *117*, 2239-2246

3.1 Introduction

Plants use photosynthesis to generate carbohydrates and oxygen from CO_2 and water. Light energy is necessary for this process, but excessive light is harmful to the plant. Chlorophyll (Chl) absorbs light and is transformed into its excited state. When light is absorbed at a higher rate than the photosynthetic enzymes can process, that energy must be dissipated in the form of heat or fluorescence in order to prevent unwanted reactions of the excited state Chl which can generate singlet oxygen, damage proteins, and bleach Chl in a variety of photochemical reactions detrimental to the plant.[2-4] Controlled dissipation of the excess energy as heat is very important for the plant.[5,6] Previous studies[7] have pointed out that the favorable formation of carotenoid neutral radicals at the terminal end groups for zeaxanthin (Zea) and lutein (Lut) radical cations correlates with their ability to quench excess energy in addition to their role as antennae. However, neutral radicals do not form at the terminal end groups of carotenoid radical cations that are not involved in quenching, such as violaxanthin (Viol) and 9-cis-neoxanthin.[7]

Plants have several redundant mechanisms for protection from excess light, collectively known as non-photochemical quenching (NPQ).[8-11] One important form of NPQ is qE which is characterized by a decrease in fluorescence. *Arabidopsis thaliana* mutants show a strong

connection between Zea[12] and the qE component of NPQ. Femtosecond transient absorption spectroscopy detects a charge transfer complex between Zea and Chl in light-harvesting complex proteins CP24, CP26, and CP29 in qE proficient plants.[13,14] Excited Chl generated in these proteins are quenched by formation of a charge transfer complex with Zea producing[13,14] a radical cation of Zea and a Chl radical anion: Zea + Chl + hv $\rightarrow$ $Zea^{\bullet+}$••••$Chl^{\bullet-}$.

At low light levels, the photosynthetic apparatus needs every light photon available and qE becomes detrimental to the plant. So at low light, Zea is converted into Viol which does not support qE. The light-intensity-dependent interconversion of Zea and Viol is known as the xanthophyll cycle (**Scheme 3.1**). Zea is formed from Viol by violaxanthin deepoxidase (VDE) which is triggered by excess protons and low pH.[15] The epoxide groups of Viol are removed by VDE to form Zea. At low light VDE is no longer activated and Zea is epoxidized by zeaxanthin epoxidase (ZE) to reform Viol. The Zea made by the xanthophyll cycle replaces Viol. The *A. thaliana* npq1 mutant which is inhibited in its ability to convert Viol to Zea shows very little qE,[16] while the mutant npq2 which accumulates Zea yet lacks Viol showed unimpaired qE.[12] It was also found that the nearly maximal level (80%) of qE and maximum concentration of Zea was already observed after preillumination at 300 µE $m^{-2}s^{-1}$ of *A. thaliana*.[17]

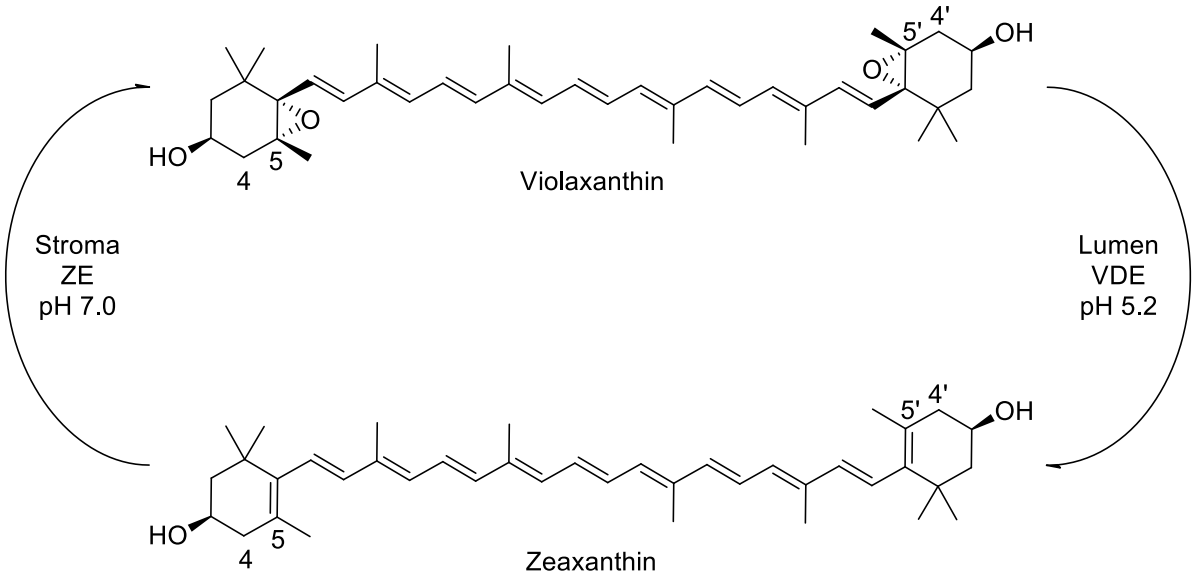

Scheme 3.1: Illustration of the xanthophyll cycle. In the presence of as little as room light (4 μE $m^{-2}s^{-1}$), violaxanthin deepoxidase (VDE) is triggered by excess protons in the lumen lowering the pH. VDE deepoxidizes Viol to form Zea. In the absence of light zeaxanthin epoxidase (ZE) is generated which epoxidizes Zea to form Viol.

These results indicate a vital role for Zea in qE and the femtosecond absorption spectroscopy was interpreted as showing formation of a charge transfer complex from excited Chl and ground state Zea to form $Chl^{\bullet-}$ and $Zea^{\bullet+}$, which then recombined to the ground state in 200 ps.[13] Although this recombination is fast, other chemical reactions can compete with it, notably deprotonation of $Zea^{\bullet+}$. The timescale for proton transfer is measured in femtoseconds[18-20] when proton donors and acceptors are pre-assembled. For instance, proton transfer from an amine to an oxygen takes place with a time constant[21] of 35 fs in photo-excited 2-(2'-hydroxyphenyl)benzothiazole with the donor/acceptor groups separated by a distance of 2.8 Å.[22] Similarly, proton-coupled electron transfer reactions can be quite fast.[23-25] It is not possible to dismiss the possibility of deprotonation competing with collapse of the charge transfer state.

Electrochemistry studies[26-28] show that carotenoid radical cations are weak acids (pK_a 4-7). The most acidic protons are at carbon atoms where their loss results in the largest conjugation length and depends on the donor/acceptor substituents of a carotenoid.[26-28] In the case of $Zea^{\bullet+}$, proton loss occurs from the terminal rings at the C4(4') methylene or from the methyl groups at the C5(5') carbon with the C4(4') being the most favorable.[7] On the other hand, the epoxide groups on the terminal rings of Viol prevent proton loss from the rings and proton loss occurs only from the methyl protons located in the center of the polyene chain. Proton loss to form neutral radicals occurs in the electrochemical solutions for both Viol and Zea.[7] In the solid state, #$Zea^{\bullet}$ forms from $Zea^{\bullet+}$ very efficiently even at 77 K after photo-oxidation[29] of Zea on silica alumina solid supports at λ ~350 nm. In electrochemical solutions and in the solid supports, all protons on the carotenoid radical cations have similar access to proton acceptors so that deprotonation is determined mainly by the acidity of the radical cation. However in proteins, this is not the case because the carotenoids are typically in a highly-ordered environment and the long chain typically is embedded in a very non-polar region, lacking proton acceptors, while the rings are in more polar environments.

The crystal structure of the CP29 minor antenna component (Protein Data Bank 3PL9) where qE was found shows that in one terminal ring the C4(4') of Viol XAT662, is in close proximity (< 4 Å) to an axial water ligand HOH307 on Chl CLA604 and another water HOH244 which could act as proton acceptors. A network of water molecules lies within hydrogen bonding distance of each other, as well as the hydroxyl at C3(3') and another oxygen on Chl CLA604. This network suggests that the water plays a functional or structural role in the protein and would remain in place after the Viol XAT662 is replaced by Zea during light stress. Any $Zea^{\bullet+}$ that is formed has proton-accepting groups nearby the acidic C4(4') positions so that deprotonation is

possible. These conditions could allow formation of #Zea$^{\bullet}$. On the other hand, any Viol$^{\bullet+}$ would be unable to lose protons from the ring and proton loss from the chain is prevented because no proton acceptors are available in the non-polar protein region holding the chain.[7,29]

If #Zea$^{\bullet}$ is formed, what is its relevance to qE? Deprotonation would leave Chl$^{\bullet-}$ and #Zea$^{\bullet}$ in the protein. Recombination is prevented because deprotonation drastically shifts the redox potential of Zea.[26] The radical ions of Chl undergo facile electron transfer with Chl in photosystem I and II as well as in light harvesting complexes.[30-37] The Chl radical is likely to jump to other Chls in the protein complex to separate the #Zea$^{\bullet}$ and Chl$^{\bullet-}$. This extends their lifetimes because they would need to come together again, transfer a proton back to Zea to form the charge transfer complex, before they could recombine. However, in the time before they recombine, both radicals can encounter many Chl excited states.

Free radicals and other paramagnetic species such as molecular oxygen are generally potent quenchers of excited states by electron exchange-induced-quenching. Quenching by free radicals[38,39] is important in liquids and solids and forms the basis for fluorescence detection of reactive oxygen species. Quenching of fluorescence by J exchange for either an excited single or triplet state has been accomplished by attaching a stable nitroxide neutral radical as far away as 9 Å from a fluorescing molecule. This is demonstrated by Hideg[39] via fluorescence quenching in two reactive oxygen species sensors; singlet oxygen specific DanePy and OH-1889NH which reacts with both singlet oxygen and superoxide radicals. A similar situation would occur if #Zea$^{\bullet}$ is near an excited Chl in CP29 or similar proteins. Each #Zea$^{\bullet}$ would become a potent free radical trap for large numbers of excited Chl, potentially making a major contribution to qE even if its quantum yield is small. Yet, possible impact of #Zea$^{\bullet}$ in qE seems to have been overlooked.

Evidence is sought for #Zea$^{\bullet}$ formation during qE in the form of H/D exchange in Zea. To accomplish this, wild-type *A. thaliana* leaves were infiltrated with D_2O and examined the relative isotopic distribution of Zea via liquid chromatography/mass spectrometry (LC/MS). If deprotonation of Zea$^{\bullet+}$ occurs, the #Zea$^{\bullet}$ could re-protonate with a deuterium to d_1Zea$^{\bullet+}$ and subsequently could be reduced to d_1Zea. This would shift the relative distribution of the different isotopic species: Zea, d_1Zea, and d_2Zea. Zea has a molecular mass of 568.9 g/mol, denoted as "M" while d_1Zea and d_2Zea have masses of M+1 and M+2 respectively. Zea has an OH group on each terminal ring which readily exchange with H or D in the solvent. To prevent exchange of OH groups from affecting the mass distributions, all extracted carotenoid samples were equilibrated with protonated solvents before and during LC/MS. This ensured that all OH groups had the natural isotopic abundance and that the mass distribution reflected primarily the H/D distribution of the C-H groups. The theoretical distribution of the M, M+1, and M+2 mass peaks should be approximately 100, 44, and 10 due to the natural abundance of ^{13}C. Zea is readily protonated during electrospray ionization[40] forming a mixture of $[Zea+H]^+$ and $[Zea^{\bullet}]^+$ ions which skews our isotopic distribution from the theoretical distribution. To compensate for this, it was important to compare consecutive sets of experiments measured under identical conditions using single factor analysis of variance (ANOVA). This analysis determines if any there are statistically significant differences in the amount of d_1Zea and d_2Zea between the various samples.

H/D exchange can be caused by processes other than qE and it is necessary to determine whether non-qE processes are involved. One approach is to use mutants deficient in qE as in the femtosecond absorption measurements. This approach has the major drawback that exposing the

mutants to high light levels will cause photochemical damage that is not present in leaves protected by qE, making it problematic to attribute results to qE or photodamage. We therefore used the light level in wild-type *A. thaliana* to modulate qE and other physiological processes that might lead to H/D exchange.

Leaves were infiltrated with either D_2O or H_2O and exposed to varying levels of light intensity; both above and below that needed to induce NPQ in *A. thaliana* (300 μE $m^{-2}s^{-1}$).[41] Leaves exposed to light intensity less than needed to induce NPQ but high enough to trigger the xanthophyll cycle were measured to determine if any H/D exchange occurred during interconversion of Zea and Viol in the xanthophyll cycle. Control samples were kept in the dark to check if other physiological processes or Zea isolation caused H/D exchange. We expected that only a fraction of Zea would undergo H/D exchange since only a fraction of the Zea participates in qE. Avenson et al[14] demonstrated that a majority of Zea binding proteins do not undergo charge transfer quenching and thus could not undergo H/D exchange. The amount of H/D exchange is also limited because not all water molecules can be replaced by D_2O. Following infiltration of wild type *A. thaliana* leaves with D_2O or H_2O and exposure to light intensity less than or greater than that needed to induce NPQ, the carotenoids were extracted and analyzed via LC/MS. The relative mass distribution of Zea was measured to check for formation of #$Zea^{\bullet}$ during qE.

The ability to form neutral radicals depends on the local environment of the carotenoid in its complex with the protein, the terminal groups, and the presence of nearby proton acceptors. All of these conditions are satisfied by Zea in the CP29 minor antennae component where qE seems to occur. It is not known if they do in the other antenna proteins, CP24 and CP26, that also support $Zea^{\bullet+}$ formation during qE because there is no structure of those complexes in the

structural databases. Although we suggested that #Zea$^{\bullet}$ may be present during qE, based on the known chemistry of Zea$^{\bullet+}$, there has been no experimental evidence of its presence during qE until the H/D exchange measurements reported by our group.[1]

3.2 Results and Discussion

3.2.1 Confirmation of Zea/Viol Extraction

Confirmation of the extraction of Zea and Viol was done by comparing the LC/MS peaks with purified samples[42,43] used as standards. The extracted ion chromatograms (EIC) at *m/z* 568.9 of both the Zea standard (**Figure 3.1a**) and ATW-C extract (**Figure 3.1b**) showed similar retention times. The same technique was used to identify Viol peaks in the EICs at *m/z* 601.9 (**Figure 3.1c,d**). Viol has a molecular weight of 600.9 g/mol, but is readily protonated during the ESI process[40] leading to the analysis of the Viol EIC at *m/z* 601.9.

The chromatograms showed different patterns of multiple peaks for both Zea and Viol due to the *cis/trans* isomers of the carotenoids in the extract[44]. The standards were originally produced from the all-*trans* isomer, but it converts into a mixture over time. Also, previous work has demonstrated that radical cations readily form *cis* isomers from the all *trans* isomer as illustrated in **Scheme 3.2**.[45] Due to this chemistry, the H/D exchange should be most noticeable in the *cis* isomers. In the Zea samples, the earliest peak is the *trans* isomer and the later are various *cis* isomers.

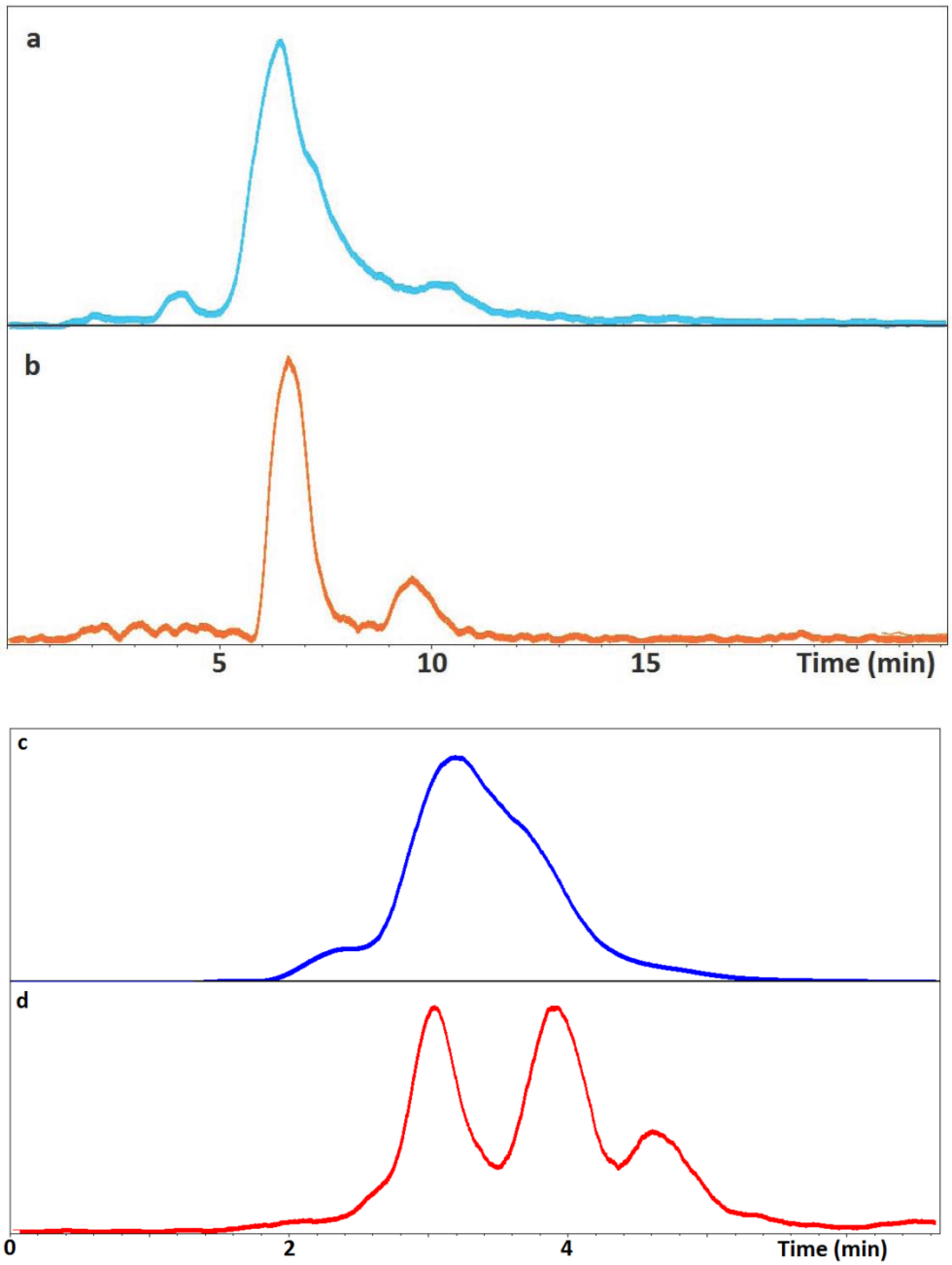

Figure 3.1a,b,c,d: EIC at *m/z* 568.9 of extract from the Zea standard (a) and ATD-C (b). EIC at *m/z* 601.9 of Viol standard (c) and ATD-C (d). The differences in peak shapes result from the distribution of the cis/trans isomers.

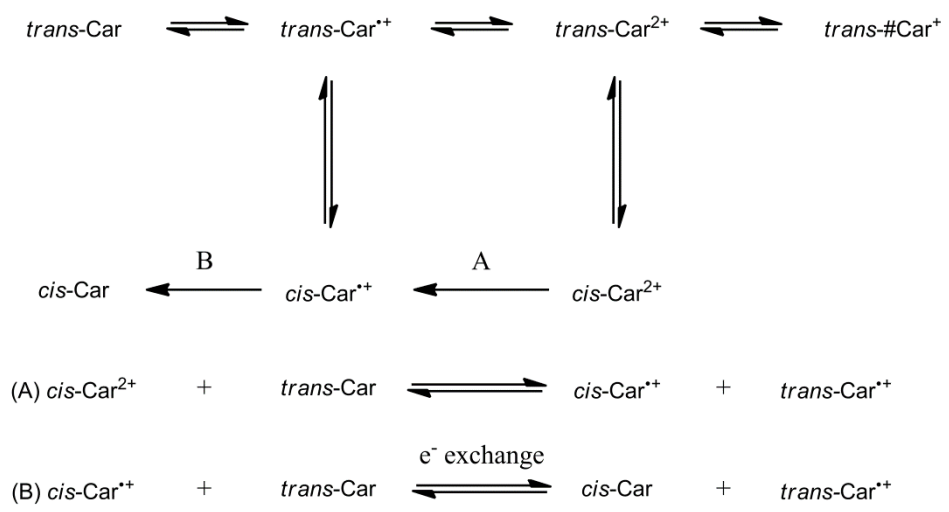

Scheme 3.2: Possible routes the carotenoids undergo by electron transfer to form various isomers.

3.2.2 Xanthophyll Cycle Activity

Demonstrating that the xanthophyll cycle is active in the leaves after they have been harvested is essential to the current study. This was shown by comparing the relative mass peak areas of Viol and Zea (V/Z) in the different samples (**Figure 3.2**). The V/Z ratio of the BTW sample was 0.51 while the V/Z ratio from the BTW-C was 0.78 (figure not shown). The V/Z ratio of the ATW sample was 0.54 while the V/Z ratio from the ATW-C was 1.27 (figure not shown). The decrease in the amount of Viol relative to Zea in the samples exposed to light demonstrates the xanthophyll cycle is active under the experimental conditions.

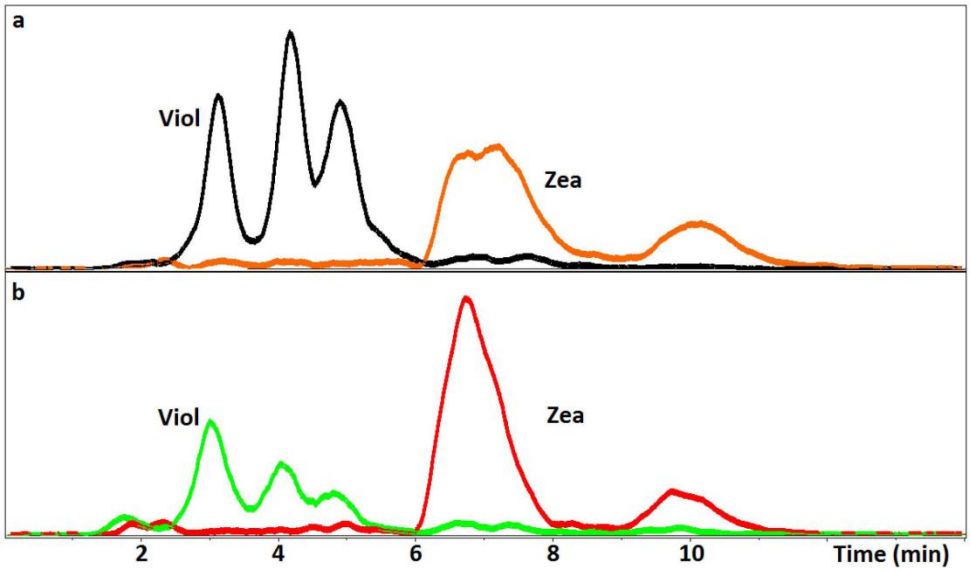

Figure 3.2a,b: Extracted ion chromatograms (EIC) from ATW-C (a) and ATW (b). The shifts in the relative intensities from the control samples placed in the box (a) and the samples exposed to light (b) demonstrate xanthophyll cycle activity.

3.2.3 H/D Exchange in Chemically-Generated Zea Radicals

The EIC at *m/z* 568.9 has two distinct peaks (**Figure 3.3**) due to *cis/trans* isomers as discussed above. The first peak is identified as the all *trans* isomer and shows no significant H/D exchange in the chemically generated radical samples.

The second EIC peak was identified as the *cis* isomers. Mass peak M was normalized to 100, and the relative intensity of the M+1 peak compared to Normal and Short Term D_2O increased from 55 to 65 with $p < 10^{-5}$ reported from ANOVA. This translates to a < 0.01% chance the difference is due to random errors in the measurement process. The M+2 mass peak increased from 14 to 22 ($p < 10^{-6}$) relative to M as seen in **Figure 3.4**. A statistically significant increase of both the M+1 and M+2 peaks from Long Term D_2O compared to Normal (both p = .004) is also observed.

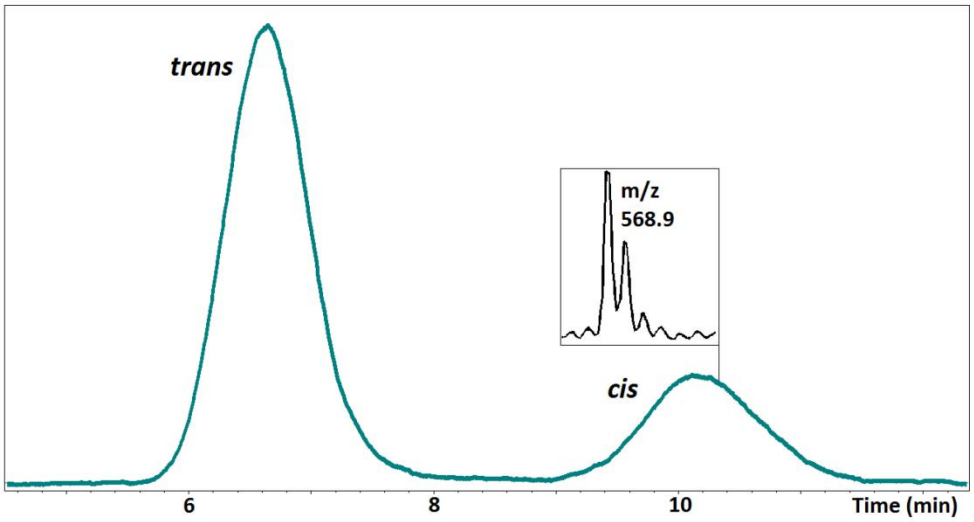

Figure 3.3: EIC at 568.9 *m/z* of short term D_2O Fe(III) added sample with mass spectrum inlay. Two distinct peaks can be seen. The first is from the all trans configuration of Zea. The second is from the *cis* configurations caused by naturally occurring isomers and from the isomerization of Zea during the chemical formation of the radical cations.

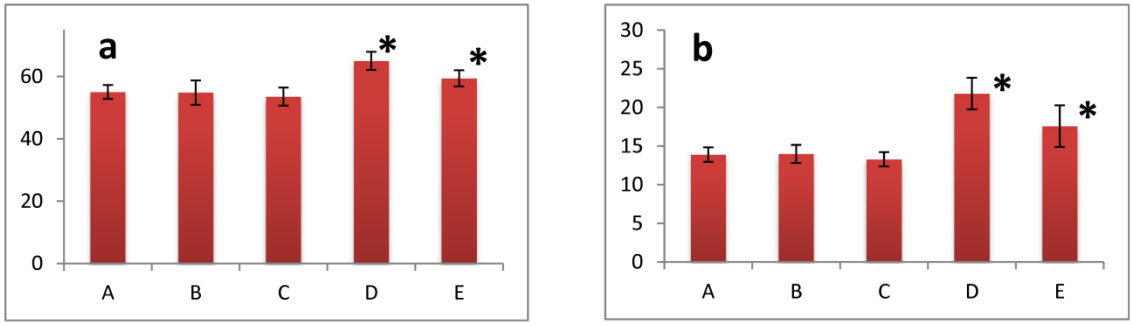

Figure 3.4: Relative intensities of the M+1 mass peak (a) and M+2 mass peak (b) of the chemically formed *cis* isomer where; A = Normal, B = Short H_2O, C = Long H_2O, D = Short D_2O, and E = Long D_2O. The D_2O samples showed an increase in relative intensity compared to the normal and H_2O treated samples. This indicates that H/D exchange is occurring and is detectable via LC/MS. *Denotes statistically significant differences from all other samples. ($p < 0.05$)

This isotopic shift is also be seen in comparisons of the M+1 and M+2 peak intensities of long term D_2O samples and long term H_2O samples (both $p = .001$). No statistically significant differences were found in comparisons of the Normal and Short Term H_2O samples. These

results indicated H/D exchange readily occurs when chemically formed Zea radical cations are in the presence of D_2O and is detectable via LC/MS.

3.2.4 Zea H/D Exchange in Leaves

It was demonstrated that H/D exchange is detectable via LC/MS in the case of chemically formed radicals, the deprotonation of $Zea^{\bullet+}$ during qE is now examined. The xanthophyll cycle was shown to be active in the below qE-inducing light intensity samples shown in **Figure 3.2**. **Figure 3.5** shows the relative mass peak intensities of these samples.

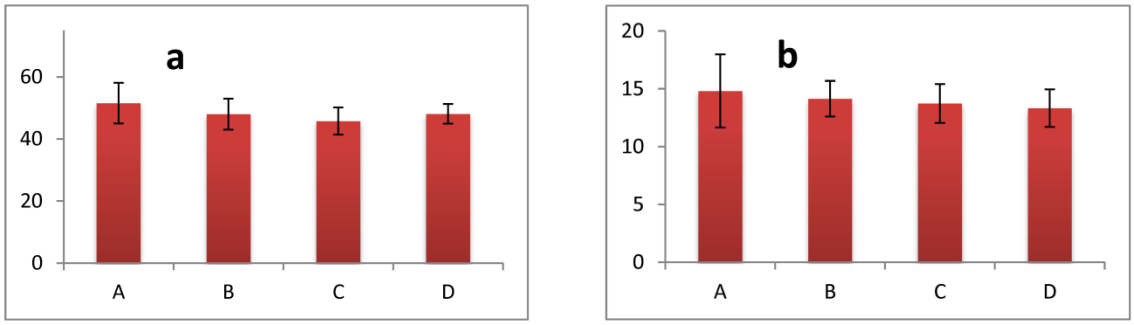

Figure 3.5: Relative intensities of the M+1 mass peak (a) and M+2 mass peak (b) of the *cis* isomer with; A = BTD, B = BTW, C = BTW-C, and D = BTD-C. No statistically significant differences were found when comparing all of the samples.

No statistically significant difference in mass distribution for both the M+1 and M+2 data sets ($p = 0.20$ and 0.60, respectively) between leaves infiltrated with H_2O vs. D_2O was found using ANOVA. Although the xanthophyll cycle is active in these leaves, no statistically significant differences in the mass distribution between any of the sample sets were observed. This demonstrates neither the presence of H_2O or D_2O during the xanthophyll cycle nor does the extraction/measurement cause a detectable difference in isotopic composition of the Zea. This indicates that there is no H/D exchange from the xanthophyll cycle or the analysis.

Above qE-inducing light samples

Comparing the M+1 data sets of the above qE inducing light samples demonstrated a statistically significant difference ($p < 10^{-3}$) among all the groups (**Figure 3.6**). More comparisons were done to determine what was causing the variation.

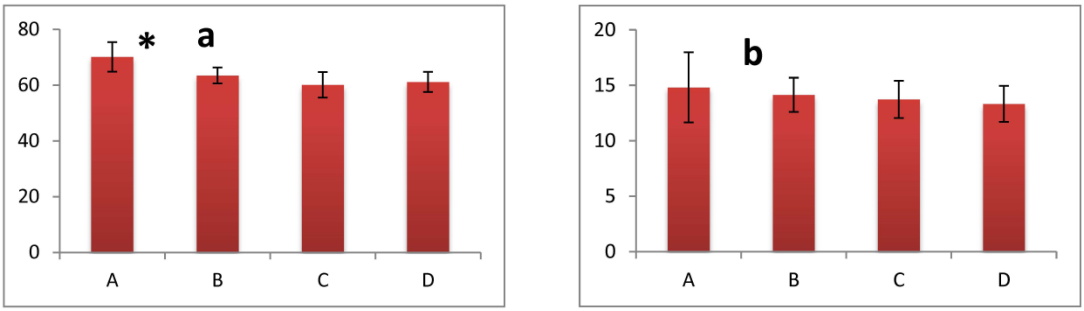

Figure 3.6: Relative intensities of the M+1 mass peak (a) and M+2 mass peak (b) of the *cis* isomer with; A = ATD, B = ATW, C = ATW-C, and D = ATD-C. There is an increase in the size of A in the M+1 mass peak compared to the other samples though not M+2. This is an indication that #Zea• underwent H/D exchange according to the proposed mechanism. *Denotes statistically significant differences from all other samples. ($p < 0.05$)

No statistically significant differences were found in comparisons of the ATW, ATW-C, and ATD-C samples ($p = 0.12 – 0.63$). Therefore neither the light exposure by itself nor D_2O infiltration by itself affected the relative M+1 peak intensity. This is consistent with the BTW and BTD results. Intense light exposure coupled with D_2O infiltration in the ATD samples demonstrates a statistically significant increase in the M+1 relative peak intensity vs ATW ($p = .011$), ATD-C ($p = .002$), and ATW-C ($p = .002$). The ANOVA of the mass profile indicates H/D exchange did occur only when there is D_2O infiltration coupled with light intensity that induces qE.

No statistically significant differences were observed in the M+2 mass peaks. This can be explained due to the orientation of Viol/Zea in the crystal structure of CP29. Only one terminal ring of Viol (and presumably Zea) within close range to potential proton acceptors. The two CH_2 protons of the terminal rings at C4(4') are "inequivelant" as they exist in different protein environments. This may cause each end to have substantial differences in their ability to undergo proton transfer in the protein complex. Charge transfer quenching in CP29 most likely involves two Chl (CLA 602 and CLA609) as suggested by Ahn et al.[13] These two Chl are located on the opposite terminal ring from the potential proton acceptors. This configuration suggests that the initial charge transfer complex between Zea and Chl occurs via electron transfer at one end while #Zea$^{\bullet}$ is formed by proton loss at the other. Zea's extensive delocalization of electrons allows the protein to carry out electron and proton transfer at different ends of Zea, making it feasible to repeatedly optimize and control these reactions.

3.2.5 Possible Mechanisms for H/D Exchange

The statistically significant difference in the relative M+1 mass peak was shown only in our results when D_2O is present during qE. The origin of this H/D exchange can now be answered by process of elimination. The exchange did not occur during the conversion of Viol to Zea during the xanthophyll cycle in presence of D_2O in light conditions less than needed to trigger qE. These results show that the xanthophyll cycle by itself cannot be the source of the detected H/D exchange. They also indicate that the de novo synthesis of Viol and Zea, and similar metabolic processes, is too slow to have an impact on the isotopic composition of the bulk Zea in the leaves under our experimental conditions.

The only statistically significant difference in the relative M+1 mass peaks was in the leaves with D_2O infiltration and exposed to qE-inducing light intensity. These results are consistent with the predicted formation of #Zea$^{\bullet}$ via deprotonation of Zea$^{\bullet+}$ during qE. We are unaware of other routes to produce isotopically-altered Zea that operates only at light intensity above the threshold for qE. This work was the first to explore the role of #Zea$^{\bullet}$ in qE.[1]

3.3 Conclusion

The formation of energy quenching #Zea$^{\bullet}$ from the charge-transfer complex Zea$^{\bullet+}$••••Chl^{-} during qE was examined. The acidic Zea$^{\bullet+}$ may form #Zea$^{\bullet}$ via deprotonation which would act as a long-lived and efficient quencher of excited state Chl. For the #Zea$^{\bullet}$ to form, several conditions must be met. It is imperative that the charge transfer complex has a long enough lifetime for the deprotonation to occur. Examples in the literature show proton transfer can occur in the ~30 femtosecond time range, while Fleming's group found the charge transfer complex to last ~200 picoseconds. The Zea$^{\bullet+}$ must be able to undergo deprotonation, which is evident from previous electrochemical, EPR, and DFT studies. These experiments demonstrate that the Zea$^{\bullet+}$ are weak acids and form neutral radicals on solid supports with the most likely site for deprotonation being the C4(4') position of the terminal rings. Finally the protein environment must be favorable for this deprotonation to occur. The crystal structure of the qE active protein CP29 (Protein Data Bank 3PL9) shows the C4(4') of Zea is within 4 Å of potential proton acceptors.

H/D exchange is detectable via LC/MS and ANOVA when #Zea$^{\bullet}$ is formed in the presence of D_2O in solution. H/D exchange was observed in leaves from wild-type *A. thaliana* which were infiltrated with D_2O and exposed to light intensity above the threshold needed to induce qE (> 300 µE $m^{-2}s^{-1}$). These results are consistent with the deprotonation of Zea$^{\bullet+}$ to form

#Zea$^{\bullet}$ during qE. #Zea$^{\bullet}$ is more difficult to reduce than the Zea$^{\bullet+}$ and should have a much longer lifetime in the leaf and act as a potent quencher of excited state Chl.

3.4 References

(1) Magyar, A.; Bowman, M. K.; Molnár, P.; Kispert, L. Neutral Carotenoid Radicals in Photoprotection of Wild-Type Arabidopsis thaliana, *J Phys Chem B* **2013**, *117*, 2239-2246.

(2) Koyama, Y. Structures and Functions of Carotenoids in Photosynthetic Systems, *J Photoch Photobio B* **1991**, *9*, 265-280.

(3) Renger, G.; Wolff, C. Further Evidence for Dissipative Energy Migration Via Triplet-States in Photosynthesis - Protective Mechanism of Carotenoids in Rhodopseudomonas-spheroides Chromatophores, *Biochim Biophys Acta* **1977**, *460*, 47-57.

(4) Boucher, F.; Vanderrest, M.; Gingras, G. Structure and Function of Carotenoids in Photoreaction Center from Rhodospirillum-rubrum, *Biochim Biophys Acta* **1977**, *461*, 339-357.

(5) Holt, N. E.; Fleming, G. R.; Niyogi, K. K. Toward an Understanding of the Mechanism of Nonphotochemical Quenching in Green Plants, *Biochemistry-Us* **2004**, *43*, 8281-8289.

(6) Pascal, A. A.; Liu, Z. F.; Broess, K.; van Oort, B.; van Amerongen, H.; Wang, C.; Horton, P.; Robert, B.; Chang, W. R.; Ruban, A. Molecular Basis of Photoprotection and Control of Photosynthetic Light-Harvesting, *Nature* **2005**, *436*, 134-137.

(7) Focsan, A. L.; Molnar, P.; Deli, J.; Kispert, L. Structure and Properties of 9 '-Cis Neoxanthin Carotenoid Radicals by Electron Paramagnetic Resonance Measurements and Density Functional Theory Calculations: Present in LHC II?, *J Phys Chem B* **2009**, *113*, 6087-6096.

(8) Mozzo, M.; Dall'Osto, L.; Hienerwadel, R.; Bassi, R.; Croce, R. Photoprotection in the Antenna Complexes of Photosystem Ii - Role of Individual Xanthophylls in Chlorophyll Triplet Quenching, *J Biol Chem* **2008**, *283*, 6184-6192.

(9) Bautista, J. A.; Tracewell, C. A.; Schlodder, E.; Cunningham, F. X.; Brudvig, G. W.; Diner, B. A. Construction and Characterization of Genetically Modified Synechocystis Sp. Pcc 6803 Photosystem II Core Complexes Containing Carotenoids with Shorter pi-Conjugation Than Beta-Carotene, *J Biol Chem* **2005**, *280*, 38839-38850.

(10) Lakshmi, K. V.; Poluektov, O. G.; Reifler, M. J.; Wagner, A. M.; Thurnauer, M. C.; Brudvig, G. W. Pulsed High-Frequency EPR Study on the Location of Carotenoid and Chlorophyll Cation Radicals in Photosystem II, *J Am Chem Soc* **2003**, *125*, 5005-5014.

(11) Vasil'ev, S.; Brudvig, G. W.; Bruce, D. The X-Ray Structure of Photosystem II Reveals a Novel Electron Transport Pathway between P680, Cytochrome b(559) and the Energy-Quenching Cation, Chl(Z)(+), *Febs Lett* **2003**, *543*, 159-163.

(12) Niyogi, K. K.; Grossman, A. R.; Bjorkman, O. Arabidopsis Mutants Define a Central Role for the Xanthophyll Cycle in the Regulation of Photosynthetic Energy Conversion, *Plant Cell* **1998**, *10*, 1121-1134.

(13) Ahn, T. K.; Avenson, T. J.; Ballottari, M.; Cheng, Y. C.; Niyogi, K. K.; Bassi, R.; Fleming, G. R. Architecture of a Charge-Transfer State Regulating Light Harvesting in a Plant Antenna Protein, *Science* **2008**, *320*, 794-797.

(14) Avenson, T. J.; Ahn, T. K.; Zigmantas, D.; Niyogi, K. K.; Li, Z.; Ballottari, M.; Bassi, R.; Fleming, G. R. Zeaxanthin Radical Cation Formation in Minor Light-Harvesting Complexes of Higher Plant Antenna, *J Biol Chem* **2008**, *283*, 3550-3558.

(15) Muller-Moule, P.; Conklin, P. L.; Niyogi, K. K. Ascorbate Deficiency Can Limit Violaxanthin De-Epoxidase Activity in vivo, *Plant Physiol* **2002**, *128*, 970-977.

(16) Havaux, M.; Niyogi, K. K. The Violaxanthin Cycle Protects Plants from Photooxidative Damage by More Than One Mechanism, *P Natl Acad Sci USA* **1999**, *96*, 8762-8767.

(17) Kalituho, L.; Beran, K. C.; Jahns, P. The Transiently Generated Nonphotochemical Quenching of Excitation Energy in Arabidopsis Leaves Is Modulated by Zeaxanthin, *Plant Physiol* **2007**, *143*, 1861-1870.
(18) Formosinho, S. J.; Arnaut, L. G. Excited-State Proton-Transfer Reactions. 2. Intramolecular Reactions, *J Photoch Photobio A* **1993**, *75*, 21-48.
(19) Kim, C. H.; Park, J.; Seo, J.; Park, S. Y.; Joo, T. Excited State Intramolecular Proton Transfer and Charge Transfer Dynamics of a 2-(2 '-Hydroxyphenyl)Benzoxazole Derivative in Solution, *J Phys Chem A* **2010**, *114*, 5618-5629.
(20) Kim, C. H.; Joo, T. Coherent Excited State Intramolecular Proton Transfer Probed by Time-Resolved Fluorescence, *Phys Chem Chem Phys* **2009**, *11*, 10266-10269.
(21) Barbatti, M.; Aquino, A. J. A.; Lischka, H.; Schriever, C.; Lochbrunner, S.; Riedle, E. Ultrafast Internal Conversion Pathway and Mechanism in 2-(2 '-Hydroxyphenyl) Benzothiazole: A Case Study for Excited-State Intramolecular Proton Transfer Systems, *Phys Chem Chem Phys* **2009**, *11*, 1406-1415.
(22) Aquino, A. J. A.; Lischka, H.; Hattig, C. Excited-State Intramolecular Proton Transfer: A Survey of TDDFT and RI-CC2 Excited-State Potential Energy Surfaces, *J Phys Chem A* **2005**, *109*, 3201-3208.
(23) Hazra, A.; Soudackov, A. V.; Hammes-Schiffer, S. Role of Solvent Dynamics in Ultrafast Photoinduced Proton-Coupled Electron Transfer Reactions in Solution, *J Phys Chem B* **2010**, *114*, 12319-12332.
(24) Saveant, J. M. Electrochemical Approach to Proton-Coupled Electron Transfers: Recent Advances, *Energ Environ Sci* **2012**, *5*, 7718-7731.
(25) Weinberg, D. R.; Gagliardi, C. J.; Hull, J. F.; Murphy, C. F.; Kent, C. A.; Westlake, B. C.; Paul, A.; Ess, D. H.; McCafferty, D. G.; Meyer, T. J. Proton-Coupled Electron Transfer, *Chem Rev* **2012**, *112*, 4016-4093.
(26) Liu, D. Z.; Gao, Y. L.; Kispert, L. D. Electrochemical Properties of Natural Carotenoids, *J Electroanal Chem* **2000**, *488*, 140-150.
(27) Liu, D.; Kispert, L. Electrochemical Aspects of Carotenoids, *Recent Res Dev Electrochem* **1999**, *2*, 139-157.
(28) Khaled, M.; Hadjipetrou, A.; Kispert, L. D. Simultaneous Electrochemical and Electron-Paramagnetic Resonance Studies of Carotenoid Cation Radicals and Dications, *J Phys Chem-Us* **1991**, *95*, 2438-2442.
(29) Focsan, A. L.; Bowman, M. K.; Konovalova, T. A.; Molnar, P.; Deli, J.; Dixon, D. A.; Kispert, L. D. Pulsed EPR and DFT Characterization of Radicals Produced by Photo-Oxidation of Zeaxanthin and Violaxanthin on Silica-Alumina, *J Phys Chem B* **2008**, *112*, 1806-1819.
(30) Hasjim, P. L.; Lendzian, F.; Ponomarenko, N.; Norris, J. R. Basic Molecular Unit Involved in Charge Migration in Oxidized Light-Harvesting Complex 1 of Rhodobacter sphaeroides, *J Phys Chem Lett* **2010**, *1*, 1687-1689.
(31) Hasjim, P. L.; Lendzian, F.; Ponomarenko, N.; Weber, S.; Norris, J. R. ENDOR Study of Charge Migration in Photosynthetic Arrays of Rhodobacter sphaeroides, *Chemphyschem* **2010**, *11*, 1258-1264.
(32) Srivatsan, N.; Kolbasov, D.; Ponomarenko, N.; Weber, S.; Ostafin, A. E.; Norris, J. R. Cryogenic Charge Transport in Oxidized Purple Bacterial Light-Harvesting 1 Complexes, *J Phys Chem B* **2003**, *107*, 7867-7876.

(33) Srivatsan, N.; Weber, S.; Kolbasov, D.; Norris, J. R. Exploring Charge Migration in Light-Harvesting Complexes Using Electron Paramagnetic Resonance Line Narrowing, *J Phys Chem B* **2003**, *107*, 2127-2138.
(34) Kolbasoy, D.; Srivatsan, N.; Ponomarenko, N.; Jager, M.; Norris, J. R. Modeling Charge Transfer in Oxidized Bacterial Antenna Complexes, *J Phys Chem B* **2003**, *107*, 2386-2393.
(35) Ostafin, A. E.; Ponomarenko, N. S.; Popova, J. A.; Jager, M.; Bylina, E. J.; Norris, J. R. Characterization of Expressed Pigmented Core Light Harvesting Complex (LH 1) in a Reaction Center Deficient Mutant of Blastochloris viridis, *Photosynth Res* **2003**, *77*, 53-68.
(36) Srivatsan, N.; Norris, J. R. Electron Paramagnetic Resonance Study of Oxidized B820 Complexes, *J Phys Chem B* **2001**, *105*, 12391-12398.
(37) Norris, J. R.; Scheer, H.; Katz, J. J. Models for Antenna and Reaction Center Chlorophylls, *Ann Ny Acad Sci* **1975**, *244*, 260-280.
(38) Green, J. A.; Singer, L. A.; Parks, J. H. Fluorescence Quenching by Stable Free-Radical Di-tert-Butylnitroxide, *J Chem Phys* **1973**, *58*, 2690-2695.
(39) Hideg, E.; Barta, C.; Kalai, T.; Vass, I.; Hideg, K.; Asada, K. Detection of Singlet Oxygen and Superoxide with Fluorescent Sensors in Leaves under Stress by Photoinhibition or UV Radiation, *Plant Cell Physiol* **2002**, *43*, 1154-1164.
(40) Guaratini, T.; Vessecchi, R.; Pinto, E.; Colepicolo, P.; Lopes, N. P. Balance of Xanthophylls Molecular and Protonated Molecular Ions in Electrospray Ionization, *J Mass Spectrom* **2005**, *40*, 963-968.
(41) Shikanai, T.; Munekage, Y.; Shimizu, K.; Endo, T.; Hashimoto, T. Identification and Characterization of Arabidopsis Mutants with Reduced Quenching of Chlorophyll Fluorescence, *Plant Cell Physiol* **1999**, *40*, 1134-1142.
(42) Molnar, P.; Szabolcs, J.; Radics, L. Naturally-Occurring Di-cis-Violaxanthins from Viola-Tricolor - Isolation and Identification by H-1-Nmr Spectroscopy of 4 Di-Cis-Isomers, *Phytochemistry* **1986**, *25*, 195-199.
(43) Molnar, P.; Szabolcs, J. Occurrence of 15-cis-Violaxanthin in Viola-tricolor, *Phytochemistry* **1980**, *19*, 623-627.
(44) Jeevarajan, A. S.; Wei, C. C.; Kispert, L. D. Geometrical Isomerization of Carotenoids in Dichloromethane, *J Chem Soc Perk T 2* **1994**, *4*, 861-869.
(45) Gao, G.; Wei, C. C.; Jeevarajan, A. S.; Kispert, L. D. Geometrical Isomerization of Carotenoids Mediated by Cation Radical Dication Formation, *J Phys Chem-Us* **1996**, *100*, 5362-5366.

CHAPTER 4

CHEMISTRY OF GEOMETRICAL ISOMERS OF ZEAXANTHIN DURING MASS SPECTROMETRY WITH ELECTROSPRAY IONIZATION SOURCE

Adapted with permission from: Magyar, A.; Focsan, A. L.; Molnar, P.; Kispert, L. D.; Bowman, M. K. Chemistry of Geometrical Isomers of Zeaxanthin During Mass Spectrometry with Electrospray Ionization Source, *Carotenoid Science.* (In Press)

4.1 Introduction

Due to their polyene structure, carotenoids exist in both *cis* (*Z*)- and *trans* (*E*)-isomers and are naturally occurring. An example of geometrical isomers of Zea is shown in **Figure 4.1**. A review of the (*E/Z*)-isomerization has been published by Péter Molnár[1] as well as other work on isolating geometrical isomers of carotenoids.[2,3] Several other examples of naturally occurring carotenoid (*Z*)-isomers include (5*Z*)-, (9*Z*)-, (13*Z*)-isomers of lycopene in ketchup,[4] (9'*Z*)-, (13*Z*)-, (13'*Z*)-isomers of fucoxanthin in *Isochrysis* sp.,[5] and (9*Z*)-, (13*Z*)-, (15*Z*)-isomers of violaxanthin in orange juice.[6]

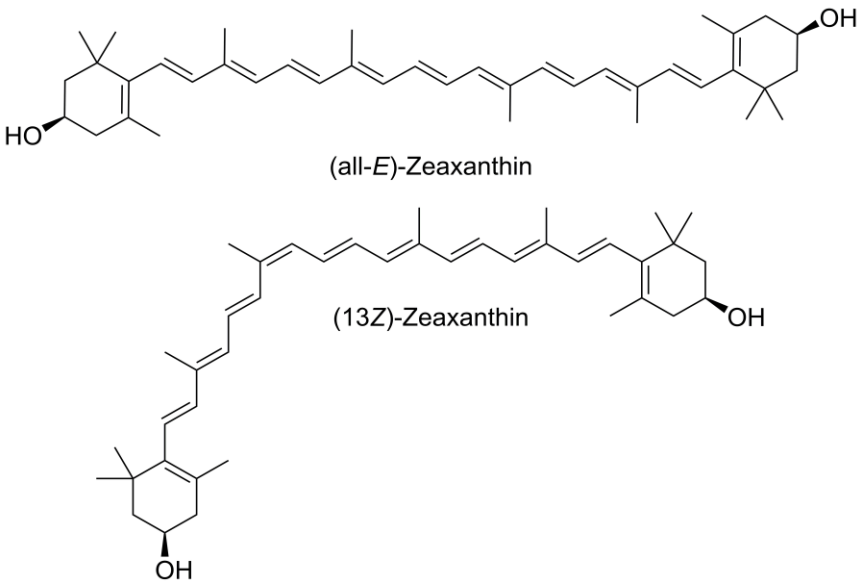

Figure 4.1: Structures of (all-*E*)-zeaxanthin and of (13*Z*)-zeaxanthin.

Despite their natural occurrence, the reasons for utilizing these different isomers are not well understood. (All-*E*)-zeaxanthin has been shown to participate in non-photochemical quenching in plants, specifically qE, by forming a charge transfer complex with Chl to help quench excess energy from light.[7-9] The crystal structure of the minor antenna component CP29 (Protein Data Bank 3PL9), where the Zea – Chl charge transfer complex was observed during qE, shows (all-*E*)-violaxanthin XAT622 (which is converted to Zea by the xanthophyll cycle[10]) in the protein in close proximity to Chl CLA602 which is suggested to be the site of the formation of the charge transfer complex.[8] The other end of the (all-*E*)-violaxanthin lies in very close proximity to an axial water ligand HOH307 on Chl CLA604, where recent work has suggested deprotonation occurs to form a carotenoid neutral radical which would aid in the energy quenching mechanism.[11] The orientation of the xanthophyll with regards to Chls in CP29 is illustrated in **Figure 4.2**. If various (*Z*)-isomers were in this position instead of the (all-*E*)-isomer, the energy quenching mechanism would not be able to proceed as previously described.

The orientation of the (all-*E*)-violaxanthin/(all-*E*)-zeaxanthin suggests the geometrical isomers may have different biological roles.

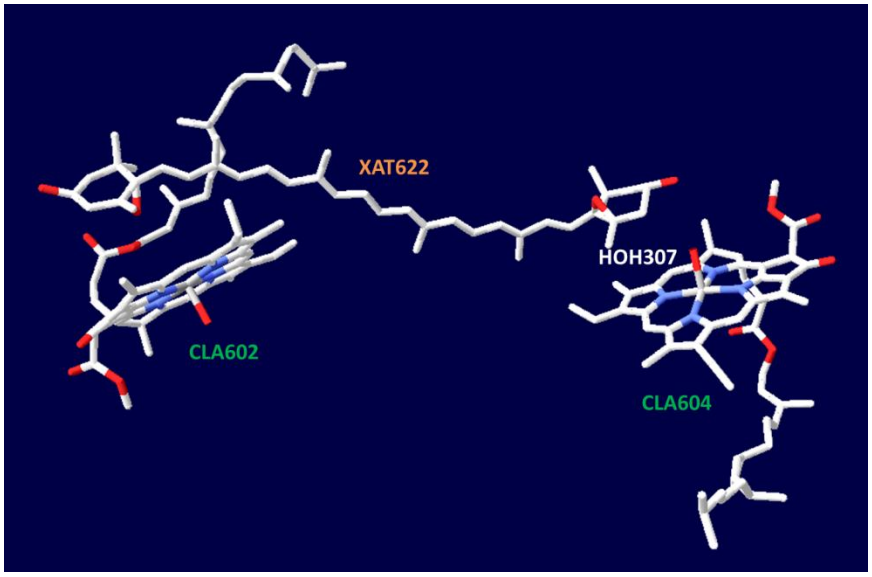

Figure 4.2: Orientation of (all-*E*)-violaxanthin/(all-*E*)-zeaxanthin XAT622 in qE active protein CP29 (Protein Data Bank 3PL9). A charge transfer complex is formed with Zea XAT622 and Chl CLA602 at one end, while proton transfer from Zea XAT622 to Chl CLA604 occurs on the other. The structure inside the protein is crucial for this energy quenching mechanism to occur, and is not likely to happen with a (*Z*)-isomer of Zea present instead of the (all-*E*)-zeaxanthin.

The formation of the *cis* (*Z*)-isomers from the all-*trans* [(all-*E*)]-isomers can be triggered by a variety of external factors, such as light exposure or thermal processing. The study of these various isomers has attracted great interest since their properties have been observed to differ from that of the (all-*E*)-isomers.[12,13] The various isomers are identifiable via changes in their optical absorption spectra.[14] Electrochemistry work[15-17] has demonstrated that carotenoids undergo a variety of chemical and electrochemical reactions, which can be seen in **Figure 4.3** This behavior has also been demonstrated to occur during electrospray ionization.[18]

Upon oxidation (**Equation 1**), the carotenoid radical cation is formed. This species is further oxidized to form a dication (**Equation 2**) that is a strong acid ($pK_a \sim 1$) and rapidly loses

a proton to form a cation (**Equation 5**). This cation can be reduced to form a carotenoid neutral radical (**Equation 3**) that is missing a proton. The carotenoid radical cations being weak acids ($pK_a \sim 4 - 7$) can deprotonate to form a neutral radical: (**Equation 6**). These various ions react chemically to form unknown products shown in **Equations 7-10**. The formation of carotenoid radical cations also facilitates the formation of (*Z*)-isomers from the (all-*E*)-isomers.[11,19] Electrochemistry work has also demonstrated carotenoid (*Z*)-isomers possess different redox potentials than their (all-*E*) counterparts. Cyclic voltammetry (CV) measurements at low temperatures (-25°C) where the (*Z*)-isomers are more stable show a drastic change in the CV compared to electrochemistry measurements undertaken at room temperature where the (*Z*)-isomers are less stable and therefore less abundant.[20]

Heterogenous Electrode Reactions	Homogeneous Chemical Reactions	Chemical Decay Reactions
1: $Car \underset{}{\overset{E_1^0}{\rightleftharpoons}} Car^{\bullet+} + e^-$	4: $Car^{++} + Car \overset{K_{com}}{\rightleftharpoons} 2\ Car^{\bullet+}$	7: $Car^{\bullet+} \longrightarrow$ Products
2: $Car^{\bullet+} \overset{E_2^0}{\rightleftharpoons} Car^{++} + e^-$	5: $Car^{++} \overset{K_{dp}}{\rightleftharpoons} \#Car^{+} + H^+$	8: $Car^{++} \longrightarrow$ Products
3: $\#Car^{+} + e^- \overset{E_3^0}{\rightleftharpoons} {}^{\#}Car^{\bullet}$	6: $Car^{\bullet+} \overset{K'_{dp}}{\rightleftharpoons} \#Car^{\bullet} + H^+$	9: $\#Car \longrightarrow$ Products
		10: $\#Car^{\bullet} \longrightarrow$ Products

Symbol	Description
CAR	neutral species of the carotenoid
$CAR^{\bullet+}$	radical cation of the carotenoid
CAR^{2+}	dication of the carotenoid
${}^{\#}CAR^{+}$	deprotonated carotenoid cation
${}^{\#}CAR^{\bullet}$	deprotonated carotenoid radical

Equation	Symbol	Description
1	E_1^0	First oxidation potential of the carotenoid for electrode reaction
2	E_2^0	Second oxidation potential of the carotenoid for electrode reaction
3	E_3^0	Reduction potential of the deprotonated carotenoid cation for electrode reaction
4	K_{com}	Comproportionation equilibrium constant of reaction
5	K_{dp}	Deprotonation equilibrium constant for the dication in reaction
6	K'_{dp}	Deprotonation equilibrium constant for the radical cation in reaction

Figure 4.3: Chemical reactions carotenoids can undergo.

Zea is found in high concentrations in the macula of human eyes.[21] It has been suggested that the role of Zea in the eye is to filter out high energy blue light from reaching the underlying structures of the human retina.[22] It can also act as an antioxidant with free radicals and reactive oxygen species to prevent peroxidation and photodamage to the retina.[23-27] The biological chemistry of Zea has led to it being marketed as a health food supplement as it is not produced naturally by the body and must be consumed as part of the diet. Therefore, it is crucial to examine the different chemical properties the geometrical isomers of Zea.

The aim of this work was to examine the chemistry of geometrical isomers of Zea during analysis utilizing mass spectrometry with electrospray ionization techniques. Mass spectrometry is a powerful tool for both quantitative and qualitative analysis of the xanthophyll carotenoids.[28] Zea was crudely extracted from wild-type *A. thaliana* leaves, and more carefully extracted from berries of *Lycium halimifolium* L. or *L. barbarum* L. The purified extracts were separated into (all-*E*)-zeaxanthin and (13*Z*)-zeaxanthin. Differences in the mass spectra from the Zea samples are highlighted and discussed. This work is important to consider when utilizing Zea as a health food supplement in the nutraceutical industry.

4.2 Results and Discussion

4.2.1 Identification of Isomers via HPLC and Optical Absorption Methods

Due to the long polyene chain of carotenoids, many different geometrical isomers are possible. The majority of these isomers are not observed in practice though, due to steric hindrance that some conformations would cause. This study utilized various isolated geometrical isomers of Zea. The identification of the isomers was carried out based on their spectroscopic features measured by an inline DAD on the LC/MS system. The chromatograms produced from the various Zea samples can be seen in **Figure 4.4**. The (13*Z*)-zeaxanthin extract produced a broad peak, beginning at a similar retention time to the (all-*E*)-zeaxanthin and ending much later.

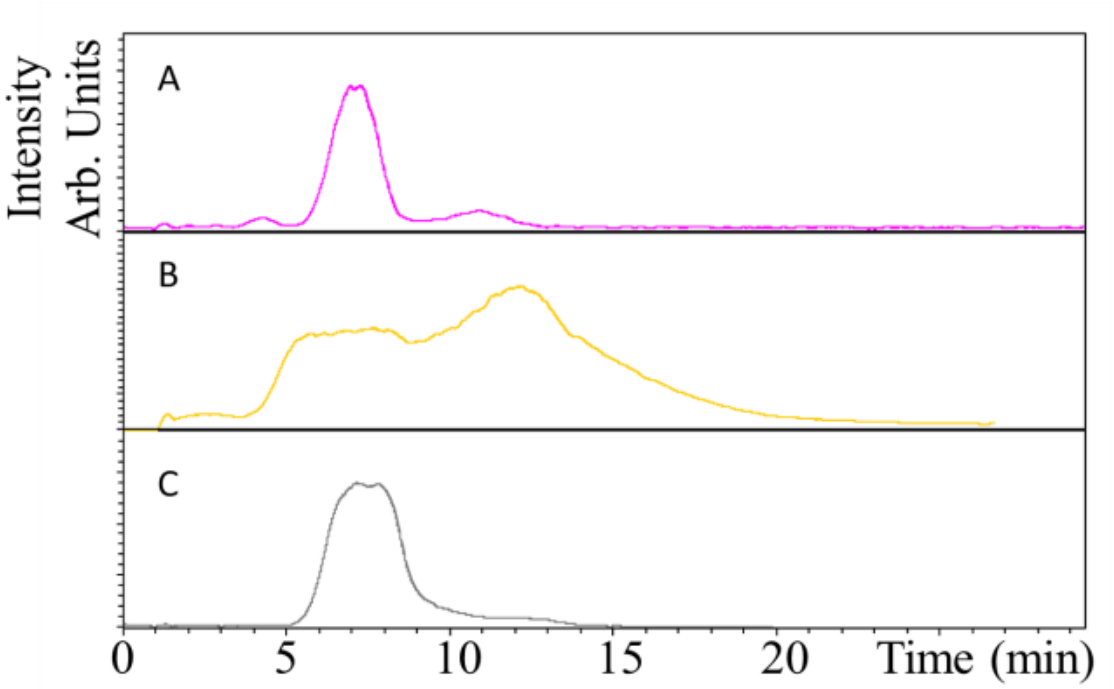

Figure 4.4: Extracted Ion Chromatograms (EIC) at *m/z* 568.5, which is the Zea radical cation. (A) Crude Zea extract; (B) (13*Z*)-zeaxanthin; (C) (all-*E*)-zeaxanthin.

The optical absorption spectra of (13*Z*)-zeaxanthin from 6.1 - 6.9 mins (**Figure 4.5A**) showed a small absorption band in near 325 nm, suggesting the presence of some (*Z*)-isomers.[14] The optical absorption spectra of (all-*E*)-zeaxanthin from 6.1 - 6.9 mins (**Figure 4.5B**) did not show the band at 325 nm, suggesting only the (all-*E*)-zeaxanthin was present. The optical absorption spectra of (13*Z*)-zeaxanthin from 8.8 - 9.4 mins (**Figure 4.5C**) has a strong band at 325 nm, and also a slight blue shift of the absorption bands in the 400 - 500 nm bands to show the presence of (13*Z*)-zeaxanthin. The optical absorption spectra for the crude Zea extract were not strong enough to identify the peaks, though comparing retention times to the (13*Z*)- and (all-*E*)-extracts can be used in identifying them.

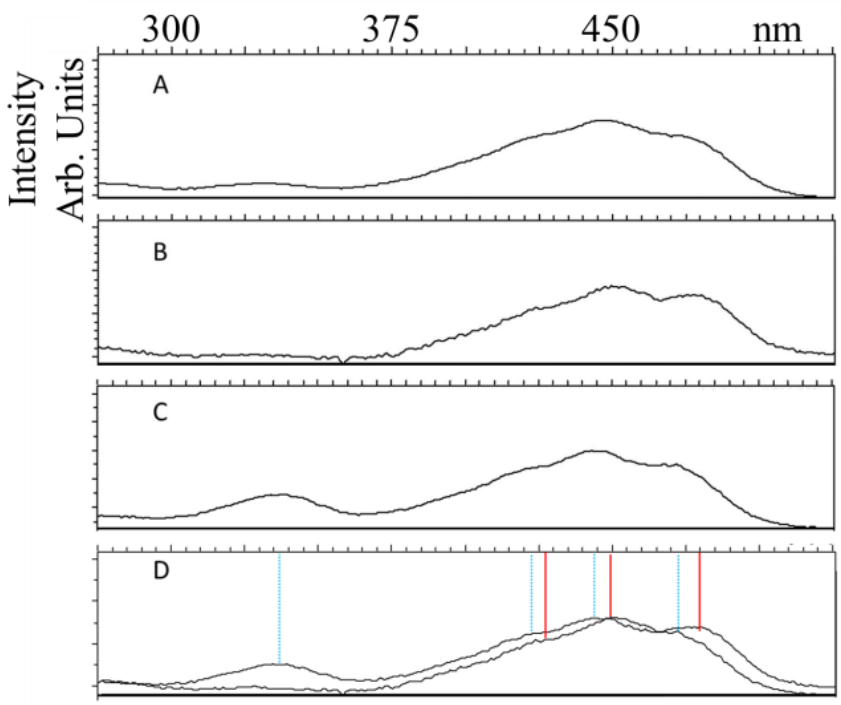

Figure 4.5: Optical absorption spectra of zeaxanthin (13*Z*)-isomer (A) and (all-*E*)-isomer (B) from 6.1 - 6.9 mins and (C) (13*Z*)-zeaxanthin from 8.8 - 9.4 mins. The small absorption band around 325 nm in A demonstrates the presence of (*Z*)-isomers although the main bands in the 400 - 500 nm range are consistent with the (all-*E*)-zeaxanthin. This suggests that a mixure of the (*E*)- and (*Z*)-isomers are present. The absence of the 325 nm band in B demonstrates that only the (all-*E*)-isomer is present. The larger absorption band in C around 325 nm as well as the slight blue shift from the bands in the 400-500 nm range shows the presence of only (13*Z*)-zeaxanthin. (D) Difference of Zea isomers optical absorption bands. The (all-*E*)-zeaxanthin absorption maxima are marked with solid red lines and the (13*Z*)-zeaxanthin is marked with dotted blue lines. The appearance of an absorption band at ~325 nm is characteristic of the (*Z*)-isomer.

4.2.2 Analyses of Mass Spectra

With the peaks identified, the mass spectra of the isomers can be examined. The mass spectrometry raw data is found in **Table B1** and **Table B2** in Appendix B. The discrepancy between the times the mass spectra are examined with the times the optical absorption spectra are examined is due to compensation for the travel time from the optical detector to the MS inlet. Signals were ignored if less than 2% of main ion peak intensity. Zea has a molecular formula of $C_{40}H_{56}O_2$ and a molar mass of 568.88 g/mol. The theoretical peak distribution due to naturally

occurring C^{13} isotopes is approximately 100/44/10 for *m/z* 568/569/570. Variation of this peak distribution will be examined to determine if the molecules have undergone any protonation/deprotonation during the analysis. The first mass spectra examined will be from the crude plant extract, **Figure 4.6A**, from 6.8 - 7.7 mins.

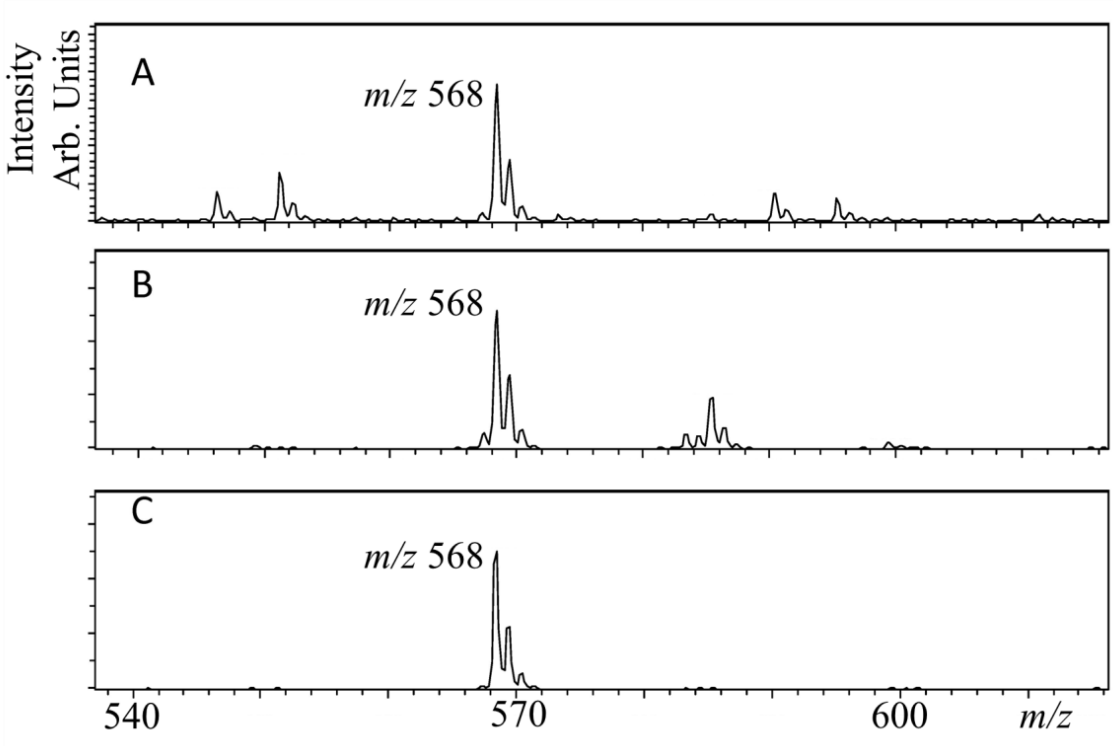

Figure 4.6: Mass spectra of (A) crude zeaxanthin, (B) (13*Z*)-zeaxanthin, and (C) (all-*E*)-zeaxanthin from 6.8-7.7 mins.

The Zea radical cation peak can be seen at *m/z* 568 with an isotopic profile of 100/45/11, closely matching the theoretical distribution expected for Zea. There is also the presence of the $[Zea – H]^+$ ion at *m/z* 567 which was approximately 7% the intensity of the main ion at *m/z* 568. This peak is consistent with **Equation 5**, where an acidic dication Zea^{++} is formed which deprotonates to give the $[Zea – H]^+$ ion. There is a strong peak at *m/z* 551 which is a commonly reported fragment for Zea $[Zea + H – H_2O]^+$ during ESI MS analysis.[18,29] There is a small set of peaks at *m/z* 585 which is approx. 5% the intensity of *m/z* 568. This is indicative of [Zea + H +

O]$^+$, the addition of an oxygen and a proton, possibly as an epoxide group forming on one terminal ring of Zea. This could be the formation of antheraxanthin which has a molar mass of 584.87 g/mol. Antheraxanthin is naturally formed from Zea as an intermediate during the inter-conversion Zea and violaxanthin during the xanthophyll cycle, a photo-protection mechanism in plants.

There are three more sets of significant peaks at *m/z* 546, 590, and 595 which appear only in the crude plant extract samples. These peaks are not consistent with reported data from ESI mass spectrometry analysis of Zea.[29] These values are similar to fragments reportedly associated with Chl, pheophytin, and pheophorbide,[30] which is reasonable considering the crude extract was green.

The extract (13*Z*)-zeaxanthin mass spectra is analyzed next from 6.8 - 7.7 mins, **Figure 4.6B.** The optical spectrum showed that there was a mixture of both the (all-*E*)-zeaxanthin and (*Z*)-isomers. The distribution of the set of peaks at *m/z* 568 is 100/54/15. This distribution differs from the theoretical value, suggesting that there is some chemistry occurring. Zea is known to protonate to form [Zea + H]$^+$ during ESI mass spectrometry[18] which is consistent with this measurement. There is also a peak at *m/z* 567, 11% relative to *m/z* 568, which again is consistent with **Equation 5**. The peak at *m/z* 585 is 38% the intensity of *m/z* 568 consistent with antheraxanthin. There is also a set of peaks at *m/z* 599 at approx. 5% the intensity of *m/z* 568. The *m/z* 599 peak is indicative of [Zea + 2O – H]$^+$ the addition of two oxygen and loss of one proton, possibly as epoxide groups forming at both ends of Zea. This could be another xanthophyll, violaxanthin, which has a molar mass of 600.85 g/mol.

Moving on to the (all-*E*)-zeaxanthin, **Figure 4.6C**, there is a different story altogether. The optical spectrum demonstrated that only the (all-*E*)-zeaxanthin was present. The mass spectrum shows only a distribution of peaks at *m/z* 568. The ratio of these peaks (starting at *m/z* 568) is 100/46/12, closely matching the theoretical distribution. The (all-*E*)-zeaxanthin isomer does not appear to undergo the same protonation/deprotonation or epoxidation demonstrated by the crude Zea extract and the (13*Z*)-zeaxanthin.

The next set of data to examine is the set of chromatographic peaks from 9.9 mins – 11.8 mins, which is most prominent in the (13*Z*)-zeaxanthin measurement. The crude plant extract will be analyzed first, **Figure 4.7A**. The same sets of peaks as the 6.8 - 7.7 mins analysis still appear, though they differ in relative intensity. In this case, the most intense peak is the $[Zea + H - H_2O]^+$ ion at *m/z* 551, approximately 200% the intensity of the *m/z* 568. The peak distribution for the *m/z* 568 (starting at *m/z* 567) is 48/100/52/21/18 signifying substantial chemical reactions occurring from proton loss consistent with **Equation 5** as well as protonation. The peak at *m/z* 585 is 63% the intensity of *m/z* 568. The other sets of peaks at *m/z* 546, 590, and 595 are again attributed to chlorophyll, pheophytin, and pheophorbide.

Figure 4.7B shows the mass spectra of the (13*Z*)-zeaxanthin from 9.9 - 11.8 mins. The most intense peak is at *m/z* 568, and the peak distribution (starting at *m/z* 567) is 14/100/73/23. In this case, the effects of **Equation 5** as well as the formation of $[Zea + H]^+$ ions is very prevalent. The peak at *m/z* 551 from the $[Zea + H - H_2O]^+$ ion is approx. 8% as intense as the *m/z* 568 peak. There is also the presence of peaks at *m/z* 585 which is 6% the intensity of *m/z* 568 and the *m/z* 599 peak is 24% as intense as *m/z* 568.

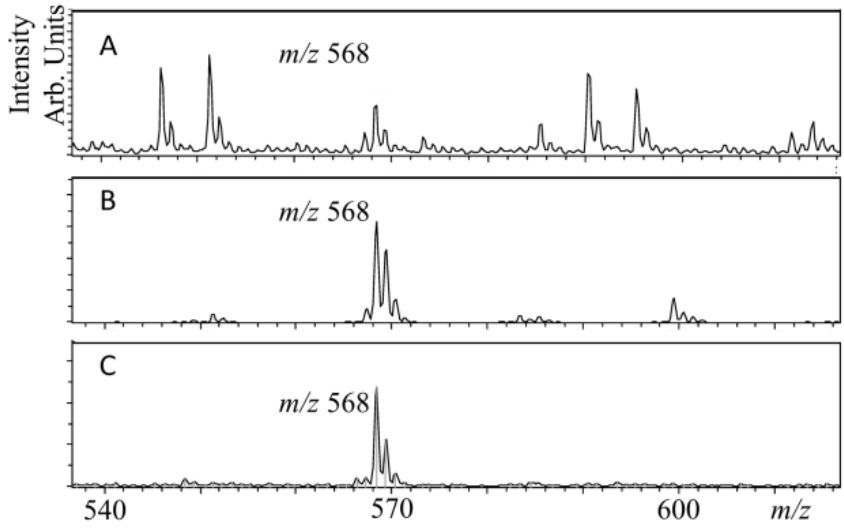

Figure 4.7: Mass spectra of (A) crude zeaxanthin, (B) (13*Z*)-zeaxanthin, and (C) (all-*E*)-zeaxanthin from 9.9 – 11.1 mins.

For the (all-*E*)-zeaxanthin from 9.9 - 11.1 mins, **Figure 4.7C**, the mass spectra shows only a set of peaks at *m/z* 568. The ratio of the peaks (starting at *m/z* 567) is 11/100/48/14. The only notable difference in this spectra compared to the (all-*E*)-zeaxanthin spectra from 6.8 - 7.7 mins is the rise in the *m/z* 567 peak relative to the *m/z* 568, indicating that proton loss is occurring via **Equation 5**. It is reasonable to assume the deprotonation is due to the presence of (*Z*)-isomers at this point in the chromatogram based on the retention time of the (13*Z*)-zeaxanthin standard.

4.3 Conclusion

Unique chemistry from geometrical isomers of Zea from different sources during mass spectrometry electrospray ionization has been shown. (All-*E*)-zeaxanthin was the most stable sample, showing little or no chemistry with the analytical environment with respect to proton loss, protonation, fragmentation, or epoxidation. (13*Z*)-zeaxanthin and crude Zea extract experience various chemistry during the analysis that was not observed in (all-*E*)-zeaxanthin.

The crude extract experience more fragmentation in the form of $[Zea + H - H_2O]^+$ than (13*Z*)-Zea, though this may be due to interference from other species that were present during the analysis. (13*Z*)-zeaxanthin samples experienced significantly more protonation/proton loss than the other Zea samples. This is consistent with previous work that demonstrated carotenoid (*Z*)-isomers have different redox properties than their (all-*E*) counterparts.[20]

To the best of our knowledge, this is the first report comparing the different behavior of geometrical isomers of Zea in mass spectrometry using electrospray ionization sources. The antioxidant properties of geometrical isomers of Zea have been shown to vary.[13] (All-*E*)-Zea has been observed in energy dissipating mechanisms in photosynthetic systems.[8] This work along with previous publications demonstrates that proper extraction and isolation techniques of the geometrical isomers of Zea are needed due to their unique chemistry. (All-*E*)- and (*Z*)-isomers do not undergo the same chemistry, suggesting certain isomers are required for a specific biological process. It behooves the processor to select the correct isomer to achieve the maximum desired result.

4.4 References

(1) Molnar, P. Research of the (E/Z)-Isomerization of Carotenoids in Pecs since the 1970s, *Arch Biochem Biophys* **2009**, *483*, 156-164.

(2) Molnar, P.; Deli, J.; Toth, G.; Haberli, A.; Pfander, H.; Bernhard, K. (9z)-Capsanthin-5,6-Epoxide, a New Carotenoid from the Fruits of Asparagus falcatus, *J Nat Prod* **2001**, *64*, 1254-1255.

(3) Molnár, P.; Ősz, E.; Tóth, G.; Zsila, F.; Deli, J. Preparation and Spectroscopic Characterization of (9z,9′Z)-Lutein (Neolutein C), *Helv Chim Acta* **2006**, *89*, 667-674.

(4) Vallverdú-Queralt, A.; Martínez-Huélamo, M.; Arranz-Martinez, S.; Miralles, E.; Lamuela-Raventós, R. M. Differences in the Carotenoid Content of Ketchups and Gazpachos through HPLC/ESi(Li+)-MS/MS Correlated with Their Antioxidant Capacity, *J Sci Food Agr* **2012**, *92*, 2043-2049.

(5) Crupi, P.; Toci, A. T.; Mangini, S.; Wrubl, F.; Rodolfi, L.; Tredici, M. R.; Coletta, A.; Antonacci, D. Determination of Fucoxanthin Isomers in Microalgae (Isochrysis sp.) by High-Performance Liquid Chromatography Coupled with Diode-Array Detector Multistage Mass Spectrometry Coupled with Positive Electrospray Ionization, *Rapid Commun Mass Sp* **2013**, *27*, 1027-1035.

(6) Melendez-Martinez, A. J.; Vicario, I. M.; Heredia, F. J. Geometrical Isomers of Violaxanthin in Orange Juice, *Food Chem* **2007**, *104*, 169-175.

(7) Niyogi, K. K.; Grossman, A. R.; Bjorkman, O. Arabidopsis Mutants Define a Central Role for the Xanthophyll Cycle in the Regulation of Photosynthetic Energy Conversion, *Plant Cell* **1998**, *10*, 1121-1134.

(8) Ahn, T. K.; Avenson, T. J.; Ballottari, M.; Cheng, Y. C.; Niyogi, K. K.; Bassi, R.; Fleming, G. R. Architecture of a Charge-Transfer State Regulating Light Harvesting in a Plant Antenna Protein, *Science* **2008**, *320*, 794-797.

(9) Avenson, T. J.; Ahn, T. K.; Zigmantas, D.; Niyogi, K. K.; Li, Z.; Ballottari, M.; Bassi, R.; Fleming, G. R. Zeaxanthin Radical Cation Formation in Minor Light-Harvesting Complexes of Higher Plant Antenna, *J Biol Chem* **2008**, *283*, 3550-3558.

(10) Muller-Moule, P.; Conklin, P. L.; Niyogi, K. K. Ascorbate Deficiency Can Limit Violaxanthin De-Epoxidase Activity in Vivo, *Plant Physiol* **2002**, *128*, 970-977.

(11) Magyar, A.; Bowman, M. K.; Molnár, P.; Kispert, L. Neutral Carotenoid Radicals in Photoprotection of Wild-Type Arabidopsis thaliana, *J Phys Chem B* **2013**, *117*, 2239-2246.

(12) Melendez-Martinez, A. J.; Britton, G.; Vicario, I. M.; Heredia, F. J. HPLC Analysis of Geometrical Isomers of Lutein Epoxide Isolated from Dandelion (Taraxacum officinale F. Weber Ex Wiggers), *Phytochemistry* **2006**, *67*, 771-777.

(13) Bohm, V.; Puspitasari-Nienaber, N. L.; Ferruzzi, M. G.; Schwartz, S. J. Trolox Equivalent Antioxidant Capacity of Different Geometrical Isomers of Alpha-Carotene, Beta-Carotene, Lycopene, and Zeaxanthin, *J Agr Food Chem* **2002**, *50*, 221-226.

(14) Grudzinski, W.; Matula, M.; Sielewiesiuk, J.; Kernen, P.; Krupa, Z.; Gruszecki, W. I. Effect of 13-cis Violaxanthin on Organization of Light Harvesting Complex II in Monomolecular Layers, *Bba-Bioenergetics* **2001**, *1503*, 291-302.

(15) Liu, D.; Kispert, L. D. Recent Research Development in Electrochemistry, *Res. Devel. Electrochem.* **1999**, *2*, 139-157 and references therein.

(16) Liu, D. Z.; Gao, Y. L.; Kispert, L. D. Electrochemical Properties of Natural Carotenoids, *J Electroanal Chem* **2000**, *488*, 140-150.

(17) Jeevarajan, A.; Khaled, M.; Forbes, M.; Kispert, L. CIDEP Studies of Carotenoid Radical Cations*, *Zeitschrift für Physikalische Chemie* **1993**, *182*, 51-61.
(18) Guaratini, T.; Vessecchi, R.; Pinto, E.; Colepicolo, P.; Lopes, N. P. Balance of Xanthophylls Molecular and Protonated Molecular Ions in Electrospray Ionization, *J Mass Spectrom* **2005**, *40*, 963-968.
(19) Gao, G.; Wei, C. C.; Jeevarajan, A. S.; Kispert, L. D. Geometrical Isomerization of Carotenoids Mediated by Cation Radical Dication Formation, *J Phys Chem-Us* **1996**, *100*, 5362-5366.
(20) He, Z. F.; Kispert, L. D. Effect of Electrolytes and Temperature on Dications and Radical Cations of Carotenoids: Electrochemical, Optical Absorption, and High-Performance Liquid Chromatography Studies, *J Phys Chem B* **1999**, *103*, 10524-10531.
(21) Li, B. X.; Vachali, P.; Bernstein, P. S. Human Ocular Carotenoid-Binding Proteins, *Photoch Photobio Sci* **2010**, *9*, 1418-1425.
(22) Kirschfeld, K. Carotenoid-Pigments - Their Possible Role in Protecting against Photo-Oxidation in Eyes and Photoreceptor Cells, *P Roy Soc B-Biol Sci* **1982**, *216*, 71-85.
(23) Krinsky, N. I. Antioxidant Functions of Carotenoids, *Free Radical Bio Med* **1989**, *7*, 617-635.
(24) Jorgensen, K.; Skibsted, L. H. Carotenoid Scavenging of Radicals - Effect of Carotenoid Structure and Oxygen Partial-Pressure on Antioxidative Activity, *Z Lebensm Unters For* **1993**, *196*, 423-429.
(25) Edge, R.; McGarvey, D. J.; Truscott, T. G. The Carotenoids as Anti-Oxidants - a Review, *J Photoch Photobio B* **1997**, *41*, 189-200.
(26) Woodall, A. A.; Lee, S. W. M.; Weesie, R. J.; Jackson, M. J.; Britton, G. Oxidation of Carotenoids by Free Radicals: Relationship between Structure and Reactivity, *Bba-Gen Subjects* **1997**, *1336*, 33-42.
(27) El-Agamey, A.; Lowe, G. M.; McGarvey, D. J.; Mortensen, A.; Phillip, D. M.; Truscott, T. G.; Young, A. J. Carotenoid Radical Chemistry and Antioxidant/Pro-Oxidant Properties, *Arch Biochem Biophys* **2004**, *430*, 37-48.
(28) van Breemen, R. B. Electrospray Liquid Chromatography-Mass Spectrometry of Carotenoids, *Anal Chem* **1995**, *67*, 2004-2009.
(29) Rivera, S. M.; Christou, P.; Canela-Garayoa, R. Identification of Carotenoids Using Mass Spectrometry, *Mass Spectrom Rev* **2013**, 353-372.
(30) Vanbreemen, R. B.; Canjura, F. L.; Schwartz, S. J. Identification of Chlorophyll Derivatives by Mass-Spectrometry, *J Agr Food Chem* **1991**, *39*, 1452-1456.

CHAPTER 5

PHOTOCHEMICAL AND OPTICAL PROPERTIES OF WATER-SOLUBLE XANTHOPHYLL ANTIOXIDANTS: AGGREGATION VS COMPLEXATION

Adapted with permission from: [1] Polyakov, N. E.; Magyar, A.; Kispert, L. D. Photochemical and Optical Properties of Water-Soluble Xanthophyll Antioxidants: Aggregation Vs Complexation, *The Journal of Physical Chemistry B* **2013**, *117*, 10173-10182.

5.1 Introduction

Practical application of carotenoids as nutritional antioxidants or components of medicinal preparations has been limited since carotenoids are highly hydrophobic, air and light-sensitive compounds. The majority of carotenoids are lipophilic molecules with near zero inherent aqueous solubility. Moving carotenoids into a pharmaceutical application requires a chemical delivery system that overcomes the problems with parenteral administration of a highly lipophilic, low molecular weight compound. Many different methods have been developed to make the carotenoids "water dispersible", as true water solubility has not been found. Most of the attempts to increase the solubility of carotenoids depended on the preparation of cyclodextrin inclusion complexes[2-8] However, cyclodextrin complexes demonstrate low solubility and fast aggregation in aqueous solution. Moreover, using cyclodextrin complexes does not allow control of the antioxidant activity of the carotenoids due to the fast dissociation of these complexes in biological media. Thus, identifying complexing agents without these drawbacks continues to be of considerable interest. Recently the synthesis of novel carotenoid complexes with unique physicochemical properties have been described.[9-13] In these studies two natural complexants derived from the plant: the triterpene glycoside glycyrrhizic acid (GA), a natural compound extracted from the licorice root,[14,15] and arabinogalactan (AG), a natural water soluble

polysaccharide extracted from Siberian larch.[16-18] (See **Figure 5.1**) β-Glycyrrhizic acid forms a head to tail dimer containing a hydrophobic and hydrophilic component in a donut like shape.[9] The polyene chains of the xanthophylls can reside within the hydrophobic area while allowing the hydrophilic terminal rings to stick out on each end. Arabinogalactan is a highly branched polysaccharide polymer composed of galactose and arabinose molecules in a 6:1 ratio previously reported as a complexing agent to make carotenoids water dispersible resulting in increased photostability[11] and photocatalytic activity.[12] Larch arabinogalactan is approved by the U.S. Food and Drug Administration (FDA) as a source of dietary fiber, but it also has potential therapeutic benefits as an immune stimulating agent and cancer protocol adjunct.[18] The unique properties of these complexes were demonstrated for two natural carotenoids: β-carotene and canthaxanthin.[9-13]

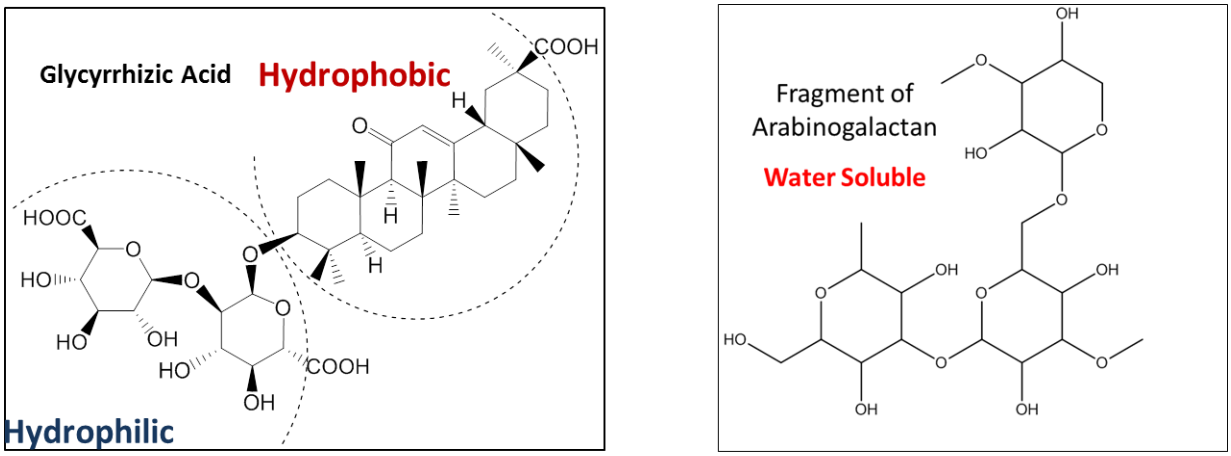

Figure 5.1: Molecular structures arabinogalactan and β-glycyrrhizic acid.

This study investigated the xanthophylls and their aggregates. Hydroxyl groups at each end of the molecules provide their unique biochemical properties. These hydroxyl groups are responsible for the xanthophylls characteristics which allow them to orient within cell

membranes in ways other carotenoids cannot.[19-22] This study is devoted to three representatives of xanthophyll carotenoids, Lut, Zea, and astaxanthin (Asta), which play a special role in the prevention and treatment of visual diseases. These carotenoids are not produced by the human body and must be consumed in the diet.

Lut and Zea – dipolar, terminally dihydroxylated carotenoids – selectively accumulate at an extremely high concentration in the macula of the primate eye retina through the action of specific high-affinity binding proteins[23] from blood plasma, where more than 20 other carotenoids are available.[24,25] These two carotenoids can impede the onset of age-related macular degeneration[26,27] and have been recently added to the list of potentially beneficial nutrients provided by leafy greens. The role of Lut and Zea is suggested to be blue light filtration and antioxidant function.[28,29] Data has shown that the high-energy, blue wavelengths of visible light are 100 times more effective at inducing free radical formation in the cells of the retina than the low-energy, red wavelengths of visible light.[30] Reacting as antioxidants with free radicals and reactive oxygen species, macular xanthophylls protect the retina against peroxidation and photo-damage.[31-35] The ability of macular xanthophylls to quench singlet oxygen and triplet states of photoactive molecules is especially significant.

Asta, a carotenoid similar to Zea with a keto group in addition to the OH on the terminal cyclohexene rings, has the highest antioxidant activity among natural carotenoids. Asta is 10 times more effective an antioxidant than β-carotene, and >100 times more effective than vitamin E.[36-38] The two adjacent oxygen atoms on the cyclohexene ring permit formation of stable complexes with metal ions such as Ca^{2+}, Fe^{2+} and Zn^{2+}.[39] The unusual metal complexing ability may be an important feature of Asta in some organisms. For example, in some unicellular green algae, Asta accumulates in huge amount (up to 30 mg/g) under high light conditions, often in the

presence of excess metal ions. This accumulation is generally thought to be a survival strategy of the algae under photooxidative and salt stress.[40] Some studies indicate also the benefit of Asta for vision. In particular, it is capable in vitro of protecting porcine lens proteins from oxidative insult and degradation by calcium-induced calpain.[41] Also, it is known that UVB exposure induces cell death and thinning of the corneal epithelium. However, the epithelium was morphologically well preserved after irradiation in Asta-treated corneas.[42] Irradiated corneal epithelium was significantly thicker in eyes treated with Asta eye drops, in a doses dependent manner. So, topical Asta administration may be a candidate treatment to limit the damages by UV irradiation with wide clinical applications.

The important feature of xanthophyll carotenoids is their ability to form self-assemblies in aqueous media and even in lipid membrane.[22,43-46] Molecular self-assembly in biological systems attracts considerable attention, since it is important for the functioning of living organisms. It is well known that carotenoids form aggregates when dissolved in hydrated polar solvents and that this aggregation is characterized by dramatic changes in their absorption spectra and photophysical properties. Two types of carotenoid aggregates can be distinguished according to their absorption spectra. The first type, associated with a large blue shift of the absorption spectrum and loss of vibrational structure of the S_2 excited state, is suggested to take the form of H-aggregates, in which the molecules are stacked with the conjugated chains oriented more or less parallel to each other and closely packed. The blue shift of the absorption spectrum is explained in terms of excitonic interaction between the closely packed carotenoid chromophores.[44-46] The second aggregation type, characterized by a red shift of the absorption spectrum where the resolution of vibrational bands is preserved, is attributed to J-type aggregation, in which there is a more head-to-tail organization of the conjugated chains.

Examples of the aggregates are shown in **Figure 5.2.** The self-assembly of xanthophyll carotenoids leads to new photo-physical properties that are not available to the monomer. The photo-physics that emerge upon coupling of carotenoid chromophores have an impact on various applications, in particular, to solar energy conversion.[47] One photo-physical mechanism that generally requires the proximity of two chromophores is singlet fission. In this mechanism, a chromophore is photoexcited to its singlet excited state and subsequently partitions its energy over two neighboring chromophores both remaining in triplet excited states. The chromophore of Zea is favorable for the production of triplet excited states via fission, and a high yield of triplet excited states via singlet fission was found for its aggregate.[48]

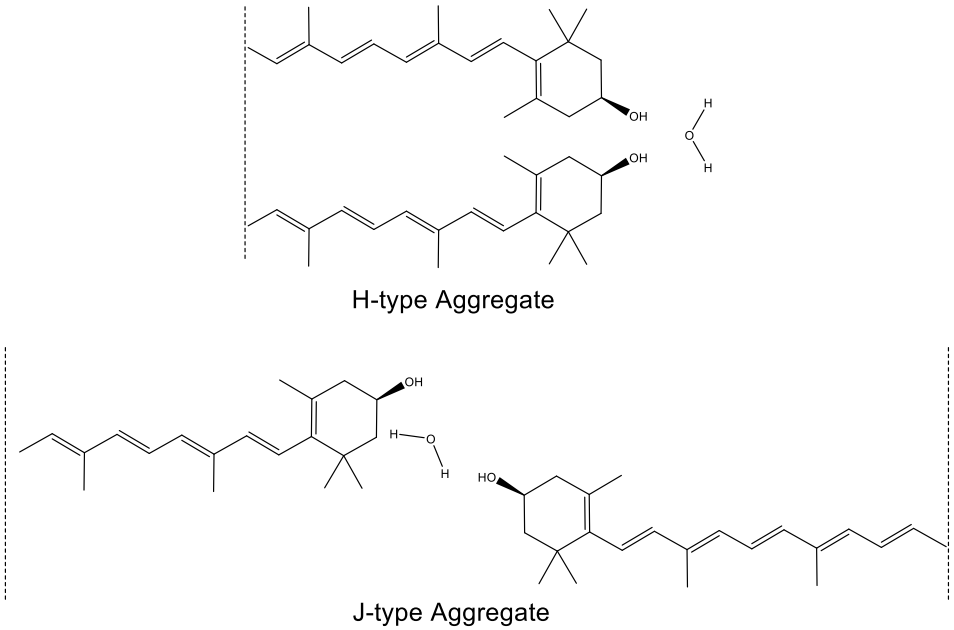

Figure 5.2: H- and J-type aggregates of Zea. The H-aggregates are closely packed with the polyene chains aligned with each other, while the J-type has a head to tail orientation. The aggregates are held in place by hydrogen bonding around the terminal hydroxyl groups from the addition of water. H-aggregates can be identified optically by a large blue shift in the absorption spectrum, while J-aggregates exhibit a large red shift.

5.2 Results and Discussion

5.2.1 Evidence of Complex Formation Of Xanthophyll Carotenoids With the Triterpene Glycoside Glycyrrhizic Acid

Earlier it was found that the inclusion complexes of lipophilic carotenoid molecules formed from water soluble oligosaccharides or polysaccharides result in significant changes in the optical (absorption wavelength and fluorescence intensity) and chemical properties of carotenoids.[8,11-13] This chapter used the sensitivity of the absorption wavelength of carotenoids to the surrounding environment to prove formation of the inclusion complex in a water-ethanol mixture and to measure its stoichiometry and stability constant. However it was found that even at micromolar (0.5-10 μM) concentrations the aggregation of Lut and Zea is very fast and occurs immediately after addition of water into ethanol solutions of the carotenoids. Note that these concentrations correspond to real Lut and Zea concentrations in serum and macular tissue (0.4-0.7 μM).[56] Only Asta supramolecular complexes were measured, as they show slow aggregation over several minutes with a gradual decrease of the monomer peak at 460 nm and growth of H-aggregate at 380 nm in the absorption spectrum. It was demonstrated also that the ability to form molecular aggregates is the specific feature of OH containing xanthophylls. The substitution of OH groups of Asta to ester groups inhibits aggregation completely **(Figure 5.3)**.

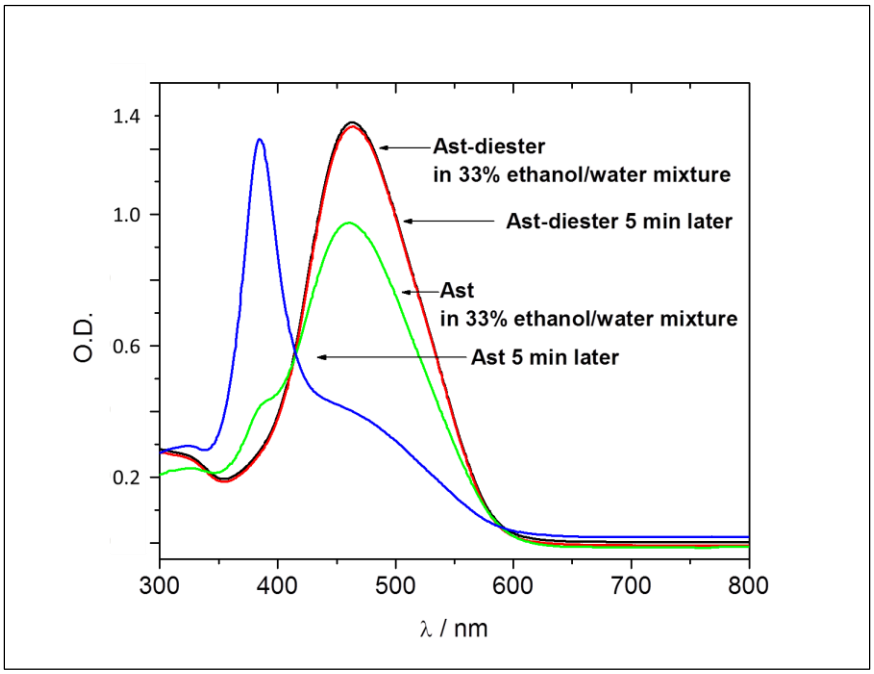

Figure 5.3: Optical absorption spectra of Asta (7.5 μM) and its n-octanoic acid ester (10 μM) in 33% ethanol/water mixture immediately after mixing and after 5 minutes delay.

An interesting feature of the water-ethanol mixture is the dependence of the aggregation rate on the water/ethanol ratio. In 25% ethanol, aggregation of Asta occurs much slower than in 33%. **Figure 5.4** shows the Benesi-Hildebrand plot of the shift of absorption maximum of Asta as a function of GA concentration in 25% ethanol where the monomer is stable for at least 10 minutes. The linear dependence of $1/\Delta\lambda$ vs. $1/[GA]^n$ was observed only for n = 2. This means that Asta forms a non-covalent supramolecular complex with the dimer of GA. It is evident also that the structure of the complex is different for low (< 1 mM) and high (> 1 mM) GA concentrations. The same result was obtained earlier for GA complexes of the carotenoid canthaxanthin and some drug molecules.[9,57,58] From the slope of the concentration dependence, the stability constant of this complex for low concentration was calculated as $k_2 = 1.7\times10^7 \pm 5\times10^5\ M^{-2}$.

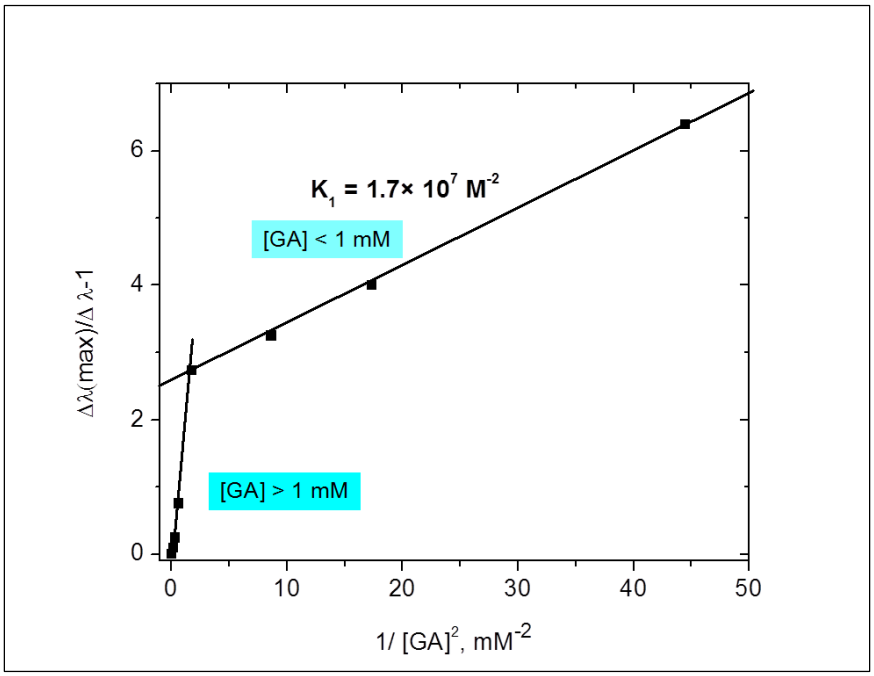

Figure 5.4: Benesi-Hildebrand diagram of the shift of absorption maximum of Asta as a function of GA concentration in 25% ethanol.

Figure 5.4 also confirms the previous conclusion that the complex stability decreases with the growth of GA concentration. It was demonstrated by various physical methods that at concentrations higher than 1 mM, GA forms micelle like aggregates.[58,59]

For Zea and Lut, the absorption spectrum also changes in the presence of GA in a concentration and time dependent manner. **Figure 5.5** shows an example of the change in the absorption spectrum of Lut in the presence of GA at 2.5 and 5 mM in a 25% ethanol solution. Increasing the GA concentration shifts the equilibrium from the H-aggregate (λ_{max}= 380 nm) to the monomer (λ_{max}= 460 nm). Note, that similar to the Asta complex, complexation of Lut with GA results in a red shift of the monomer absorption maximum relative to a pure ethanol solution (addition of water to ethanol results in small blue shift).

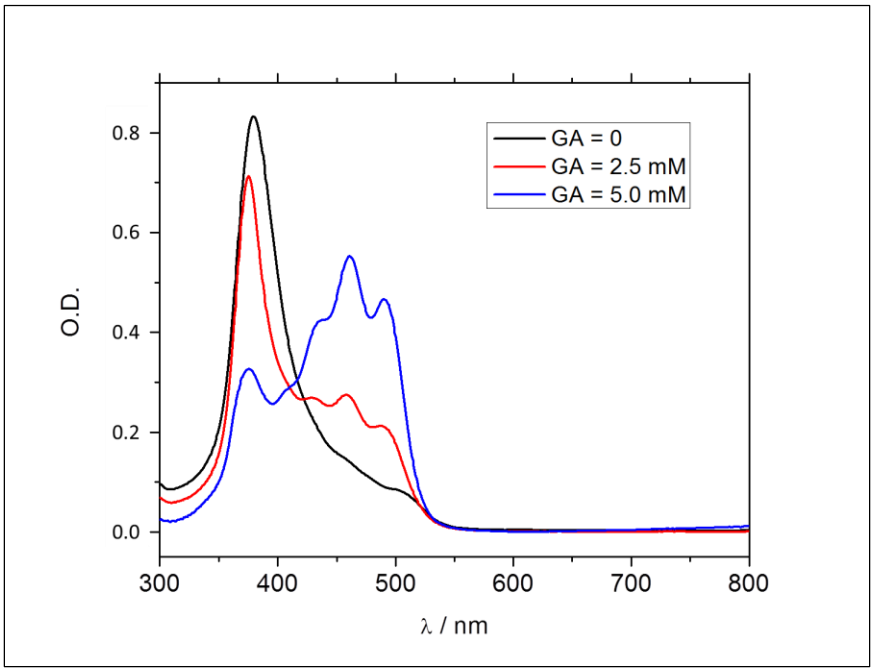

Figure 5.5: Optical absorption spectra of Lut (≈6 µM)in 25% ethanol/water mixture at different GA concentrations.

Figure 5.6 shows the molecular structure (a) and optical spectrum (c) of the Zea H-aggregate in aqueous solution and the structure of the Zea monomer (b) as it resides in the hydrophobic environment of the GA dimer along with its optical spectrum (d). The large shift from 380 nm with the loss of vibrational structure of the S_2 excited state to 450 nm and the appearance of the vibrational bands indicates the presence of the Zea monomers. From these experiments we can conclude that xanthophyll aggregation is a reversible process, and complexation with GA prevents aggregation.

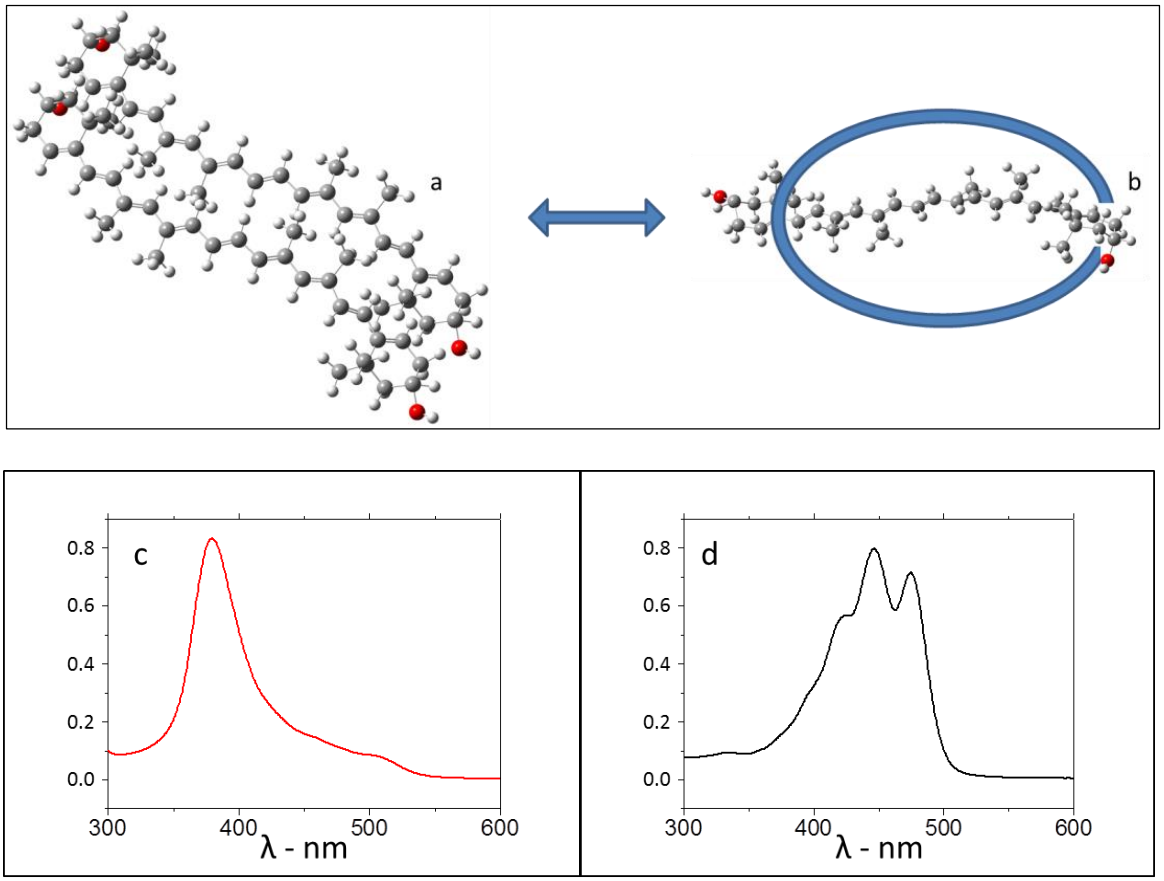

Figure 5.6: The structure of the H-aggregate (a) and monomer complexed with GA (b) of Zea. Also shown is the absorption spectrum of the H-aggregate (c) in aqueous solution and the Zea monomer (d) in the hydrophobic environment of the triterpene glycoside glycyrrhizic acid dimer. GA forms a head to tail donut hole dimer into which the Zea monomer can reside.

5.2.2 Complexation with AG Increases Photostability of Both Xanthophyll Monomers and Their H-aggregates.

Although carotenoids are known as effective photoprotectors of living cells, in aerated aqueous solution they are unstable under light irradiation, and would be unacceptable as colorants and antioxidants in foods. The reason for this is that the UV irradiation of carotenoid solutions results in a decrease of the absorption intensity with formation of reaction products which absorb light at a lower wavelength. This effect can be explained by a decrease in the

length of the conjugated chain due to the addition of oxygen to the double bonds. It is known that under irradiation carotenoids can form radical cations in various media by electron transfer to the solvent molecules or to the appropriate electron acceptor. These radical cations can be reduced by back electron transfer. However this reversible process is disrupted in the presence of water molecules which act as a proton acceptor. It results in the formation of a carotenoid neutral radical which is stabilized by the nearby proton acceptor, so a reversible electron transfer is prevented. Earlier it was demonstrated that carotenoid neutral radicals are formed from the corresponding radical cations generated electrochemically or photochemically by proton loss.[60] Although photoexcitation accelerates deprotonation of the radical cation, electrochemical measurements showed that the radical cations of a majority of carotenoids have p*K* values ranging between 4 and 7 and, therefore, can deprotonate spontaneously.[52,61] For symmetrical Zea radical cation,[62] proton loss occurs most favorably at the C4(4') carbon position with loss at C5, C9, and C13 methyl less favored to form a neutral radical. For the unsymmetrical isomer Lut, the proton loss is greatly favored only at the 4 carbon position over any other position.[63] For the Asta radical cation, deprotonation occurred at the C3(3') carbon position resulting in the lowest energy neutral radical, while proton loss at the C5, C9 of C13 methyl groups were less favored.[39] It has been shown that incorporation of carotenoids into the hydrophobic polymer environment of a GA micelle will reduce their interaction with water molecules.[11] Also, the decrease of electron transfer rate with electron acceptors was established.[9,11] During irradiation of an aqueous solution of Zea, Lut, and Asta monomers by the full light of a xenon lamp, bleaching of the solutions occurs in a few seconds. On the other hand, H-aggregates demonstrate a reduced degradation rate by about a factor of 10. This chapter investigates how complexation with GA and AG affects monomer and H-aggregate stability.

It was found that GA does not affect the photostability of Zea, Lut, or Asta. However, a significant increase (5-10 times for full light irradiation and 2 times for λ_{irr} > 380 nm) in photostability was detected for AG complexes of these xanthophylls. Moreover, the increase in photostability was detected for both the monomers and H-aggregates. This means that AG can form inclusion complexes with monomers as well as with aggregates of these xanthophylls. As an example, **Figure 5.7** demonstrates the difference in the photodegradation rate of Asta monomers in the absence (a) and in the presence (b) of 0.4 mM AG. Zea, Lut, and Asta all exhibited an increase in the photostability of H-aggregates. As an example, **Figure 5.8** shows the difference in photodegradation rate of Lut H-aggregates in the absence (a) and in the presence (b) of 0.4 mM AG.

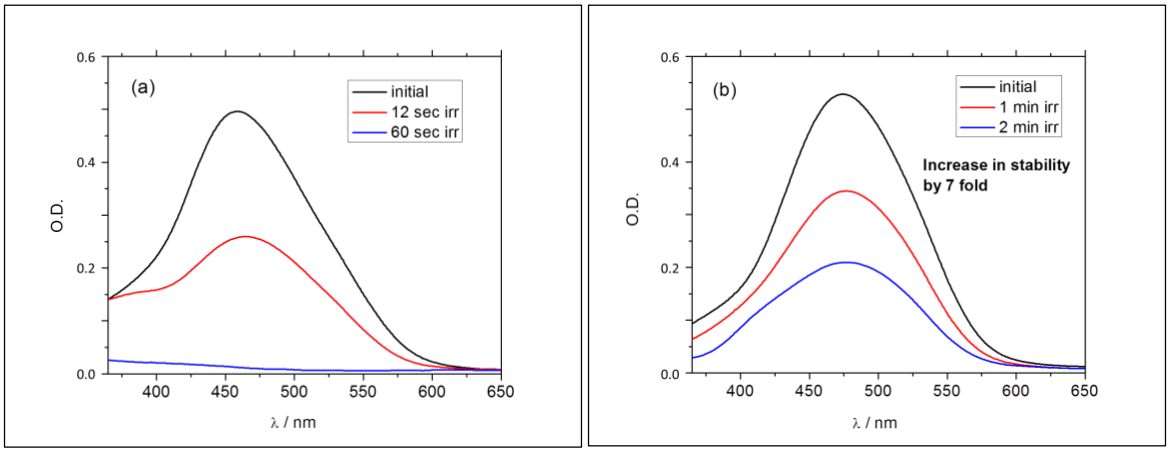

Figure 5.7: Photodegradation of Asta monomers in 25% ethanol/water solution which forms H-aggregates. Optical absorption spectra of Asta (≈4 μM) in the absence (a) and in the presence (b) of 0.4 mM arabinogalactan before and after irradiation by the full light of a xenon lamp.

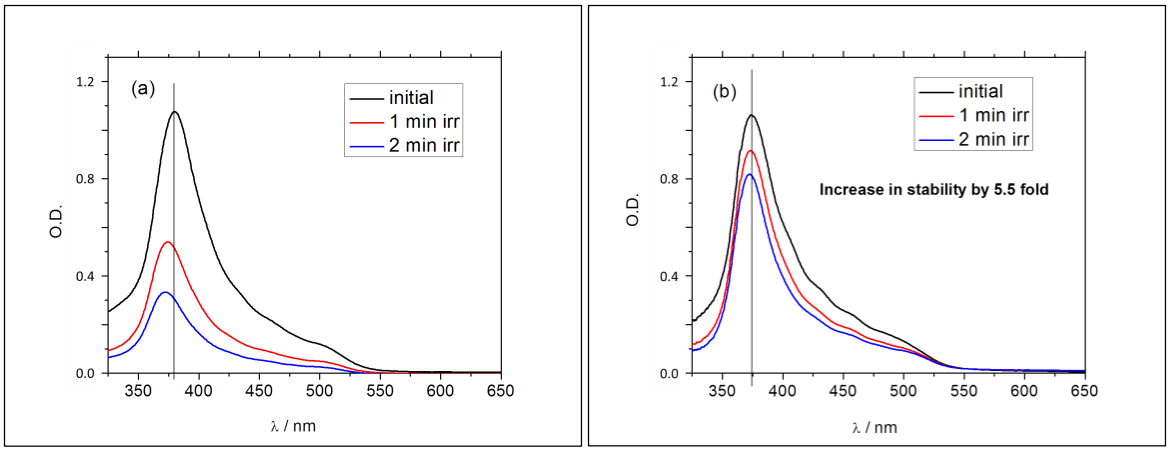

Figure 5.8: Photodegradation of Lut H-aggregates in 25% ethanol/water solution. Optical absorption spectra of Lut (≈8 μM) in the absence (a) and in the presence (b) of 0.4 mM arabinogalactan before and after irradiation by the full light of a xenon lamp.

5.2.3 EPR Spin Trapping Measurements of the Scavenging Rate Towards Peroxyl Radicals

Earlier EPR spin-trapping measurements compared the relative scavenging rates towards peroxyl radicals by different carotenoids.[49,50] This method involves measuring the yield of stable spin adduct (SA) of OOH radicals with the spin trap PBN in the presence of carotenoids. It was found that as the oxidation potential of the carotenoids increased, the radical scavenging by proton abstraction from the C4 position of the cyclohexene terminal ring increased. This is consistent with the increasing acidity of the C4 proton with increasing electron accepting character of the substituents. As an example, **Figure 5.9** shows EPR spectra of PBN-OOH radicals in the absence of Asta and in the presence of 1 mM of Asta.

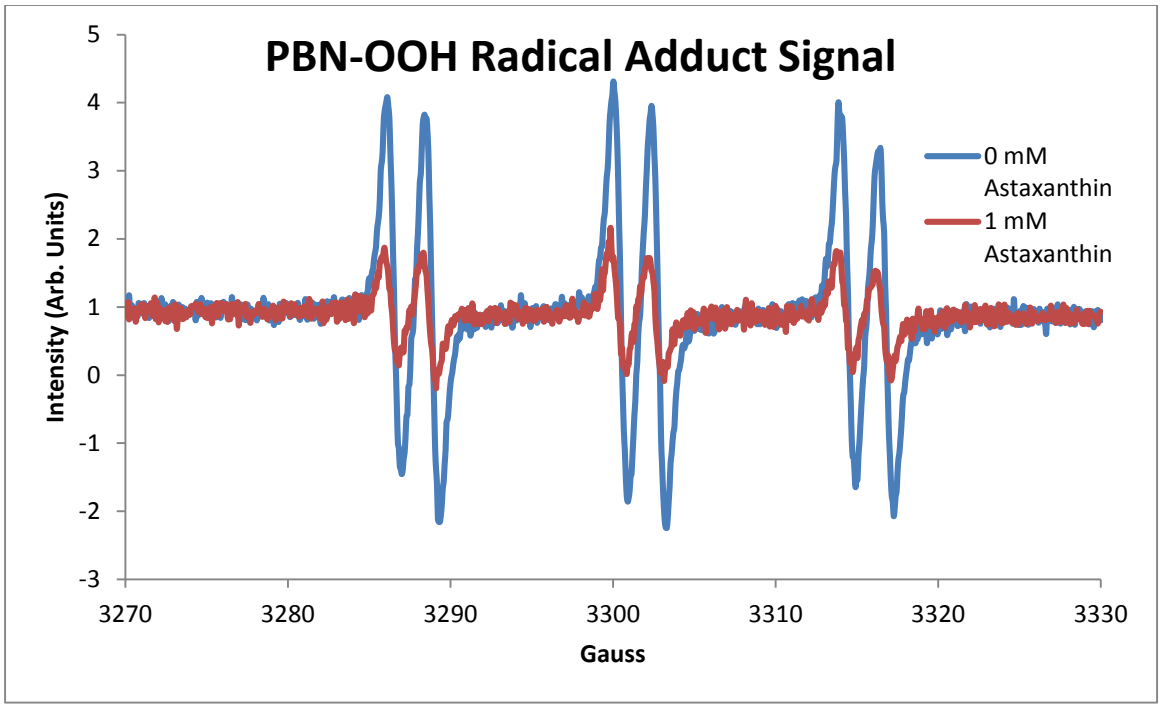

Figure 5.9: EPR signal of PBN-OOH radical spin adduct measured in the absence (blue) of Asta and the presence (red) of 1 mM Asta. The competing reactions of the carotenoid and the spin trap PBN lead to a decrease in the PBN-OOH radical spin adduct signal with increasing concentrations of carotenoids.

Because of the two competing processes, i.e., reactions of the radical with carotenoid and the spin trap, the yield of the spin adduct is proportional to the carotenoid concentration. Thus, from the experimental dependence of the spin adduct yield on carotenoid concentration, the relative rate of radical scavenging (k_{Car}/k_{ST}) by carotenoid can be assessed.

$$\frac{A_0}{A} = \frac{k_{ST}[ST] + k_{Car}[Car]}{k_{ST}[ST]}$$

Here, k_{ST} is the rate constant of radical scavenging by the spin trap (ST), A andA_0 are the values of the spin adduct signal intensity with and without carotenoid. For $k_{car} \geq k_{ST}$ only an increase in radical scavenging by the carotenoid occurs (antioxidant effect). The available kinetic database (Spin Trap Data Base: http://epr.niehs.nih.gov) provides the value of the rate constant k_{ST} measured in water ($k_{ST} \leq 10^6$ $M^{-1}s^{-1}$for the PBN spin trap). The identification of the PBN-OOH

radical spin adduct was made in previous work[49,50] using available literature data of the a(H) and a(N) splitting for the OOH, CH_3 and OCH_3 radicals. In addition to this assignment, some test experiments were carried out to prove our conclusion. In anaerobic condition the peroxyl radicals were generated in DMSO via the well-known Fenton reaction.[64]

$$Fe^{2+} + H_2O_2 \rightleftharpoons Fe^{3+} + OH^{\bullet} + OH^{-}$$

$$OH^{\bullet} + DMSO \longrightarrow CH_3^{\bullet} + CH_3(OH)SO$$

$$CH_3^{\bullet} + H_2O_2 \longrightarrow OOH^{\bullet} + CH_4$$

At low H_2O_2 concentration ($[H_2O_2]$ ~ $[FeCl_2]$ = 1 mM) only one spin adduct PBN-CH_3 was detected with ESR parameters a(H) = 3.4 G and a(N) = 14.9 G.[49] However, at higher H_2O_2 concentration ($[H_2O_2]$ = 500 mM) the reaction of CH_3 radicals with H_2O_2 becomes important and this results in the disappearance of the PBN-CH_3 adduct, and the appearance of another adduct with higher yield which was assigned to the PBN-OOH spin adduct a(H) = 2.3 G and a(N) = 13.9 G).[49] It is known that the $^{\bullet}$OOR spin adducts are relatively unstable especially in the presence of transition metal ions which can reduce $^{\bullet}$OOR radicals yielding the $^{\bullet}$OR spin adduct.[65,66] However, these facts are mainly related to alkyl peroxyl radicals. Under these experimental conditions, as H_2O_2 concentration increases the Fe^{2+} ions react primarily with the initial H_2O_2. Consequently, the stability of the $^{\bullet}$OOH spin adduct will increase. Note that there are several examples in the literature of the observation of the PBN-OOH adducts at normal conditions.[67-69] For additional confirmation of the PBN-OOH adduct formation the superoxide dismutase (SOD) test has been made.[9] The formation of all these radical species (OOH, CH_3 and OH radicals) was also confirmed by using DMPO spin trap,[49] however the measurements of radical scavenging rates by carotenoids with this spin trap have shown significant problems. First, DMPO-OOH adduct is unstable and transforms to DMPO-OH adduct via reaction with

Fe^{2+}.[70] Second, due to higher spin trapping rates of DMPO compared with some carotenoids, we have detected pro-oxidant behavior instead of an antioxidant effect.[50] This is why PBN was chosen for kinetic measurements in the previous and present studies.

Using the same approach, the reaction rates of the OOH radical with Zea and Lut monomers in DMSO solution and H-aggregates in an aqueous DMSO solution were compared. The formation of aggregates under these experimental conditions was confirmed by optical absorption measurements. It was found that Asta does not form aggregates in aqueous DMSO. In addition, the influence of GA on the scavenging ability of Lut and Zea has been investigated in an aqueous DMSO solution. **Figure 5.10** shows the time dependence of the PBN-OOH spin adduct EPR intensity in the absence and in the presence of 1 mM Lut and Zea.

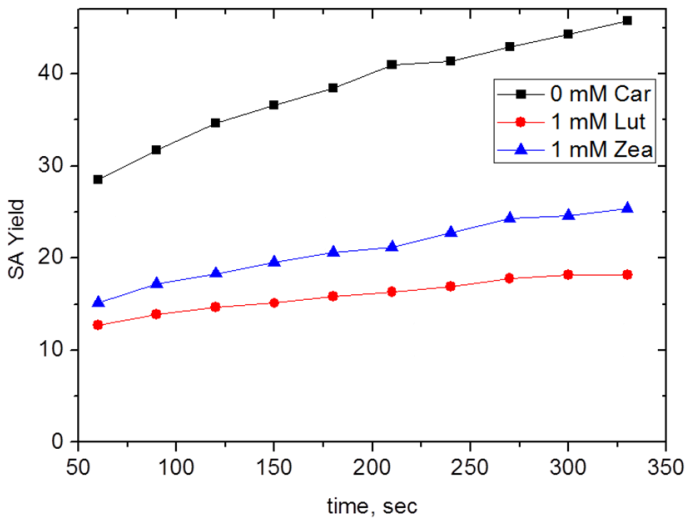

Figure 5.10: PBN-OOH SA yield in EPR spin trapping experiment at different times after the start of the reaction in DMSO solution: PBN = 5 mM, Fe^{2+}= 1 mM, H_2O_2= 500 mM, Car = 1 mM.

The initial yield of spin adduct corresponds to the free radicals produced in the Fenton reaction (k = 76 $M^{-1}s^{-1}$), but the further slow growth is due to reaction of excess of hydrogen peroxide with the reaction product, Fe^{3+} (k ~ 0.02 $M^{-1}s^{-1}$).[71,72]

$$Fe^{2+} + H_2O_2 \rightleftharpoons FeOOH^{2+} + H^+$$

$$FeOOH^{2+} \xrightarrow[\text{slow}]{} Fe^{2+} + OOH^{\bullet}$$

The significant decrease of SA yield in the presence of carotenoids is due to the reaction of these carotenoids with $^{\bullet}OOH$. As it was shown earlier, at equal concentrations, $[H_2O_2] = [FeCl_2] = 1$ mM, only the spin adduct PBN-CH_3 was detected by EPR.[49] In these experimental conditions, the SA signal was stable over 5 minutes, and no growth was observed as in the case of excess of H_2O_2. However, the SA yield decreases in the presence Zea and Lut in a concentration dependent manner.

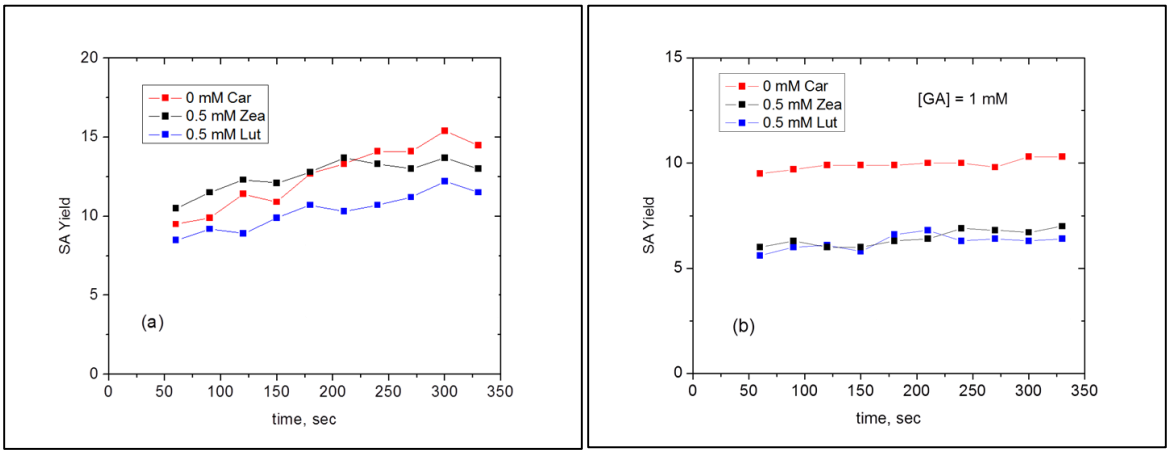

Figure 5.11: PBN-OOH SA yield in EPR spin trapping experiment at different moments after start of the reaction in 80% DMSO/water solution: PBN = 2 mM, Fe^{2+}= 0.5 mM, H_2O_2= 500 mM; (a) in the absence of GA; (b) with 1 mM GA.

Figure 5.11a shows that the formation of H-aggregates in 80% DMSO/water solution significantly reduces the scavenging ability of these xanthophylls. Moreover, the increase of SA yield (pro-oxidant effect!) was observed in the presence of Zea. Earlier[50] it was demonstrated that a pro-oxidant effect of carotenoids (an increase in the amount of free radicals formed) arises from the reduction of Fe^{3+} to Fe^{2+} by the carotenoids according to the following reactions:[50]

$$Car + Fe^{3+} \longrightarrow Car^{\bullet+} + Fe^{2+}$$

$$Fe^{2+} + H_2O_2 \rightleftharpoons Fe^{3+} + OH^{\bullet} + OH^{-}$$

This effect increases with decreasing oxidation potential of the carotenoids, with increasing H_2O_2 concentration, or with a decrease in the scavenging rate of the carotenoid. Another condition is that if $k_{car} \geq k_{ST}$; then no pro-oxidant effect occurs. However if there occurs any decay channel for free radicals, this enhances the pro-oxidant effect of carotenoids, such as reactions with lipids. For β-carotene,[50] $k_{car}/k_{ST} = 0.65$ which is a condition where the pro-oxidant effect is possible. β-carotene exhibits a low oxidation potential, measured to be the same as Zea. [52] This then explains the reason for observing a pro-oxidant effect for Zea.

We can conclude from the EPR experiments that H-aggregates demonstrate much lower spin trapping ability. The reaction of Zea with Fe^{3+} results in additional radical production at the beginning of the reaction (pro-oxidant effect), but then this reaction reduces the efficiency of Fe(III) + H_2O_2 → Fe(II) + OOH reaction, which becomes the major way for free radical formation. GA does not affect the yield of spin adduct in the absence of xanthophylls, but increases significantly their spin trapping ability (**Figure 5.11b**). We suppose that the effect of the GA dimer is due to the reduced aggregation rate of the xanthophylls, as well as the reduction of carotenoids by Fe(III) ions and by increasing the available location of the C4 proton of the carotenoid for H abstraction by $^{\bullet}OOH$. The GA dimer also shields the xanthophylls' polyene chain from reaction with Fe(III) ions. The latter process was investigated by optical absorption methods in this study.

5.2.4 Optical Absorption Study of the Reaction Kinetics of Monomers and H-aggregates with Fe_3^+ Ions and OOH Radical.

In order to explore the mechanism of antioxidant vs. pro-oxidant activity of the xanthophyll carotenoids in more detail, the decay kinetics of carotenoids Lut and Zea in the presence of Fe^{3+} ions and H_2O_2 were analyzed using optical absorption spectroscopy.

In this study we consider two main reaction ways which results in decrease of carotenoid absorption intensity, namely reaction of carotenoid with Fe^{3+} ion and with OOH radical.

$$\text{Car} + Fe^{3+} \xrightarrow{k_1^*} \text{Car}^{\bullet+} + Fe^{2+}$$

$$\text{Car} + \text{OOH}^{\bullet} \xrightarrow{k_2^*} \text{Products}$$

As it was shown in our previous study, the first reaction can play a key role in pro-oxidant activity of some carotenoids.[50] Hydroperoxyl radicals in this reaction system are formed via interaction of hydrogen peroxide with Fe^{3+} and Fe^{2+} ions, as described earlier. The measurements were made with $Fe(ClO_4)_3$ in the absence and in the presence of hydrogen peroxide in DMSO aqueous solutions: with 5% water to measure monomers (470 nm) and with 25% of water to form H-aggregates (380 nm). The decay kinetics were measured over 10 minutes, and the decay rates were calculated from the initial slopes (see **Figure 5.12** as an example). The values k_1 and k_2 are related to the reaction of H-aggregates with Fe^{3+} ion and OOH radical, and the values k_{1a} and k_{2a} are related to the reactions of carotenoid monomer with these species. Note that the calculated decay rates of absorption intensity are not equal to the corresponding reaction rates k_1* and k_2* of carotenoid with Fe^{3+} ions and OOH radicals, since the reaction products can absorb light at the same wavelength as the initial carotenoid. These decay rates might be considered as the lower limit of the reaction rates.

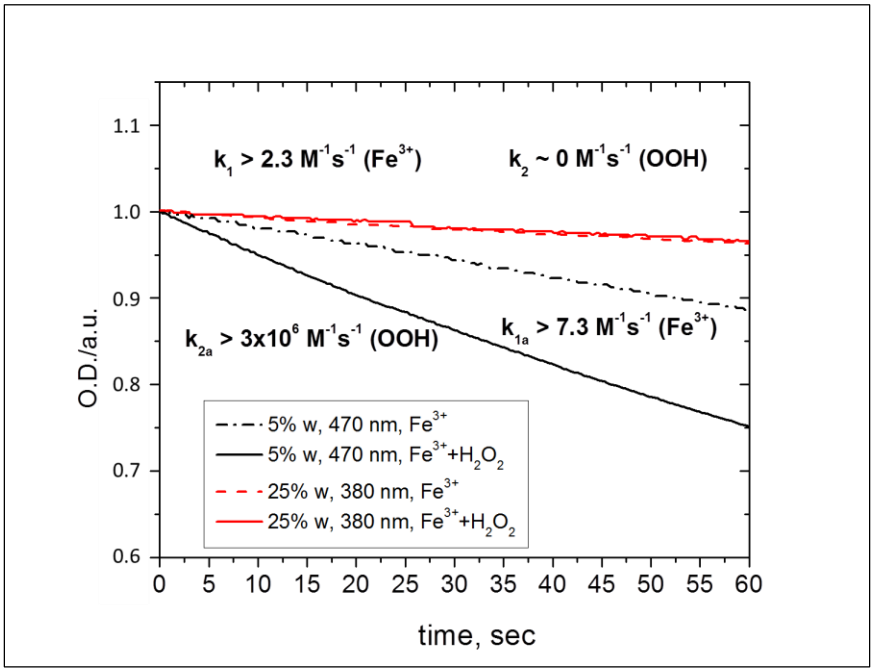

Figure 5.12: Decay kinetics of Zea detected at absorption maximum of the monomer at 470 nm and the H-aggregate at 380 nm in 5% and 25% water/DMSO solutions respectively: Fe^{3+}=0.25 mM, H_2O_2=125 mM.

One can see a threefold decrease of the Zea decay rate with Fe^{3+} ions (k_1 and k_{1a}), and complete inhibition of the reaction with OOH radical for H-aggregates (k_2) as compared with carotenoid monomers (k_{2a}). Decay rates were estimated using stationary radical concentration [OOH] ≈ 1 nM calculated from known reaction rates of the main reaction processes[71,72]: $k(Fe^{3+} + H_2O_2)$ = 0.02 $M^{-1}s^{-1}$; $k(Fe^{3+} + OOH) = 2\times10^5$ $M^{-1}s^{-1}$. We can conclude from these measurements that the pro-oxidant effect of Zea H-aggregates can arise from the reaction with Fe^{3+} ions under suppression of its ability to trap free radicals.

We have obtained the same decay rate values for the Lut monomer ($k_{2a} \geq 2.5\times10^6$ $M^{-1}s^{-1}$), but only a factor of 5 times decrease in the decay rate with $^{\bullet}OOH$ for H-aggregates. This may be a result of the unsymmetrical Lut forming a different and more open H-aggregate structure than the symmetrical Zea.

5.3 Conclusion

Formation of H-aggregates is an exclusive property of carotenoids which contain OH groups in a cyclohexene ring, as substitution of an OH with an OR group prevents the aggregation. Formation of H-aggregates significantly changes the optical and chemical properties of these carotenoids, in particular its light harvesting ability and antioxidant activity. Complexes of these xanthophylls with GA demonstrate higher antioxidant activity in aqueous solution. Reactions of the xanthophyll carotenoid inclusion complexes with OOH radicals occurs by proton loss from the most acidic proton of the carotenoid which is exposed to the environment when complexed with the donut hole GA complex. In the presence of water, Lut shows much lower antioxidant activity due to formation of H-aggregates, demonstrated by EPR spin trapping experiments using the model Fenton reaction. Zea shows pro-oxidant effect in the same conditions. Taking into account important role of these carotenoids in eye and skin health, glycyrrhizin and arabinogalactan can be considered as perspective delivery systems which provide enhanced stability and solubility of xanthophyll carotenoids.

5.4 References

(1) Polyakov, N. E.; Magyar, A.; Kispert, L. D. Photochemical and Optical Properties of Water-Soluble Xanthophyll Antioxidants: Aggregation Vs Complexation, *J Phys Chem B* **2013**, *117*, 10173-10182.

(2) Loftsson, T.; Brewster, M. E. Pharmaceutical Applications of Cyclodextrins. 1. Drug Solubilization and Stabilization, *J Pharm Sci* **1996**, *85*, 1017-1025.

(3) Szejtli, J. *Cyclodextrin Technology*; Springer, 1988; Vol. 1.

(4) Mele, A.; Mendichi, R.; Selva, A. Non-Covalent Associations of Cyclomaltooligosaccharides (Cyclodextrins) with Trans-Beta-Carotene in Water: Evidence for the Formation of Large Aggregates by Light Scattering and NMR Spectroscopy, *Carbohyd Res* **1998**, *310*, 261-267.

(5) Mele, A.; Mendichi, R.; Selva, A.; Molnar, P.; Toth, G. Non-Covalent Associations of Cyclomaltooligosaccharides (Cyclodextrins) with Carotenoids in Water. A Study on the Alpha- and Beta-Cyclodextrin/Psi,Psi-Carotene (Lycopene) Systems by Light Scattering, Ionspray Ionization and Tandem Mass Spectrometry, *Carbohyd Res* **2002**, *337*, 1129-1136.

(6) Szente, L.; Mikuni, K.; Hashimoto, H.; Szejtli, J. Stabilization and Solubilization of Lipophilic Natural Colorants with Cyclodextrins, *J Inclus Phenom Mol* **1998**, *32*, 81-89.

(7) Lancrajan, I.; Diehl, H. A.; Socaciu, C.; Engelke, M.; Zorn-Kruppa, M. Carotenoid Incorporation into Natural Membranes from Artificial Carriers: Liposomes and Beta-Cyclodextrins, *Chem Phys Lipids* **2001**, *112*, 1-10.

(8) Polyakov, N. E.; Leshina, T. V.; Konovalova, T. A.; Hand, E. O.; Kispert, L. D. Inclusion Complexes of Carotenoids with Cyclodextrins: H-1 NMR, EPR, and Optical Studies, *Free Radical Bio Med* **2004**, *36*, 872-880.

(9) Polyakov, N. E.; Leshina, T. V.; Salakhutdinov, N. F.; Kispert, L. D. Host-Guest Complexes of Carotenoids with Beta-Glycyrrhizic Acid, *J Phys Chem B* **2006**, *110*, 6991-6998.

(10) Polyakov, N. E.; Leshina, T. V.; Salakhutdinov, N. F.; Konovalova, T. A.; Kispert, L. D. Antioxidant and Redox Properties of Supramolecular Complexes of Carotenoids with Beta-Glycyrrhizic Acid, *Free Radical Bio Med* **2006**, *40*, 1804-1809.

(11) Polyakov, N. E.; Leshina, T. V.; Meteleva, E. S.; Dushkin, A. V.; Konovalova, T. A.; Kispert, L. D. Water Soluble Complexes of Carotenoids with Arabinogalactan, *J Phys Chem B* **2009**, *113*, 275-282.

(12) Polyakov, N. E.; Leshina, I. V.; Meteleva, E. S.; Dushkin, A. V.; Konovalova, T. A.; Kispert, L. D. Enhancement of the Photocatalytic Activity of TiO_2 Nanoparticles by Water-Soluble Complexes of Carotenoids, *J Phys Chem B* **2010**, *114*, 14200-14204.

(13) Haugen, L.; Bjornson, T. *Beta Carotene: Dietary Sources, Cancer and Cognition*; Nova Biomedical Books, 2009.

(14) Mazza, G. O.; Oomah, B. D. *Herbs Botanicals and Teas*; Technomic Publishing Company, Incorporated, 2000.

(15) Tolstikov, G. A.; Baltina, L. A.; Shults, E. E.; Pokrovsky, A. G. Glycyrrhizic Acid, *Bioorg Khi+* **1997**, *23*, 691-709.

(16) Odonmazig, P.; Ebringerova, A.; Machova, E.; Alfoldi, J. Structural and Molecular-Properties of the Arabinogalactan Isolated from Mongolian Larchwood (Larix-dahurica L), *Carbohyd Res* **1994**, *252*, 317-324.

(17) Medvedev, E. N.; Vavkin, V. A.; Ostroukhova, L. A. Larch Arabinogalactan - Properties and Prospects (Review) (Russian), *Chem. Nat. Comp.* **2003**, *1*, 27-37.

(18) D'Adamo, P. Larch Arabinogalactan, *J. Naturopath. Med.* **1996**, *6*, 1997.

(19) Krinsky, N. I.; Mathews-Roth, M. M.; Taylor, R. F. *Carotenoids: Chemistry and Biology*; Plenum Press, 1989.
(20) Goulinet, S.; Chapman, M. J. Plasma LDL and HDL Subspecies Are Heterogenous in Particle Content of Tocopherols Oxygenated and Hydrocarbon Carotenoids - Relevance to Oxidative Resistance and Atherogenesis, *Arterioscl Throm Vas* **1997**, *17*, 786-796.
(21) Sujak, A.; Gabrielska, J.; Grudzinski, W.; Borc, R.; Mazurek, P.; Gruszecki, W. I. Lutein and Zeaxanthin as Protectors of Lipid Membranes against Oxidative Damage: The Structural Aspects, *Arch Biochem Biophys* **1999**, *371*, 301-307.
(22) Sujak, A.; Okulski, W.; Gruszecki, W. I. Organisation of Xanthophyll Pigments Lutein and Zeaxanthin in Lipid Membranes Formed with Dipalmitoylphosphatidylcholine, *Bba-Biomembranes* **2000**, *1509*, 255-263.
(23) Li, B. X.; Vachali, P.; Bernstein, P. S. Human Ocular Carotenoid-Binding Proteins, *Photoch Photobio Sci* **2010**, *9*, 1418-1425.
(24) Khachik, F.; Spangler, C. J.; Smith, J. C.; Canfield, L. M.; Steck, A.; Pfander, H. Identification, Quantification, and Relative Concentrations of Carotenoids and Their Metabolites in Human Milk and Serum, *Anal Chem* **1997**, *69*, 1873-1881.
(25) Roberts, R. L.; Green, J.; Lewis, B. Lutein and Zeaxanthin in Eye and Skin Health, *Clin Dermatol* **2009**, *27*, 195-201.
(26) Gale, C. R.; Hall, N. F.; Phillips, D. I. W.; Martyn, C. N. Lutein and Zeaxanthin Status and Risk of Age-Related Macular Degeneration, *Invest Ophth Vis Sci* **2003**, *44*, 2461-2465.
(27) Krinsky, N. I.; Mayne, S. T.; Sies, H. *Carotenoids in Health and Disease*; Taylor & Francis, 2004.
(28) Kirschfeld, K. Carotenoid-Pigments - Their Possible Role in Protecting against Photo-Oxidation in Eyes and Photoreceptor Cells, *P Roy Soc B-Biol Sci* **1982**, *216*, 71-85.
(29) Martin, H. D.; Ruck, C.; Schmidt, M.; Sell, S.; Beutner, S.; Mayer, B.; Walsh, R. Chemistry of Carotenoid Oxidation and Free Radical Reactions, *Pure Appl Chem* **1999**, *71*, 2253-2262.
(30) Ham, W. T.; Mueller, H. A.; Sliney, D. H. Retinal Sensitivity to Damage from Short Wavelength Light, *Nature* **1976**, *260*, 153-155.
(31) Krinsky, N. I. Antioxidant Functions of Carotenoids, *Free Radical Bio Med* **1989**, *7*, 617-635.
(32) Jorgensen, K.; Skibsted, L. H. Carotenoid Scavenging of Radicals - Effect of Carotenoid Structure and Oxygen Partial-Pressure on Antioxidative Activity, *Z Lebensm Unters For* **1993**, *196*, 423-429.
(33) Edge, R.; McGarvey, D. J.; Truscott, T. G. The Carotenoids as Anti-Oxidants - a Review, *J Photoch Photobio B* **1997**, *41*, 189-200.
(34) Woodall, A. A.; Lee, S. W. M.; Weesie, R. J.; Jackson, M. J.; Britton, G. Oxidation of Carotenoids by Free Radicals: Relationship between Structure and Reactivity, *Bba-Gen Subjects* **1997**, *1336*, 33-42.
(35) El-Agamey, A.; Lowe, G. M.; McGarvey, D. J.; Mortensen, A.; Phillip, D. M.; Truscott, T. G.; Young, A. J. Carotenoid Radical Chemistry and Antioxidant/Pro-Oxidant Properties, *Arch Biochem Biophys* **2004**, *430*, 37-48.
(36) Guerin, M.; Huntley, M. E.; Olaizola, M. Haematococcus Astaxanthin: Applications for Human Health and Nutrition, *Trends Biotechnol* **2003**, *21*, 210-216.
(37) Naguib, Y. M. A. Antioxidant Activities of Astaxanthin and Related Carotenoids, *J Agr Food Chem* **2000**, *48*, 1150-1154.

(38) Palozza, P.; Krinsky, N. I. Beta-Carotene and Alpha-Tocopherol Are Synergistic Antioxidants, *Arch Biochem Biophys* **1992**, *297*, 184-187.
(39) Polyakov, N. E.; Focsan, A. L.; Bowman, M. K.; Kispert, L. D. Free Radical Formation in Novel Carotenoid Metal Ion Complexes of Astaxanthin, *J Phys Chem B* **2010**, *114*, 16968-16977.
(40) Hu, Z. Y.; Li, Y. T.; Sommerfeld, M.; Chen, F.; Hu, Q. Enhanced Protection against Oxidative Stress in an Astaxanthin-Overproduction Haematococcus Mutant (Chlorophyceae), *Eur J Phycol* **2008**, *43*, 365-376.
(41) Wu, T. H.; Liao, J. H.; Hou, W. C.; Huang, F. Y.; Maher, T. J.; Hu, C. C. Astaxanthin Protects against Oxidative Stress and Calcium-Induced Porcine Lens Protein Degradation, *J Agr Food Chem* **2006**, *54*, 2418-2423.
(42) Lennikov, A.; Kitaichi, N.; Fukase, R.; Murata, M.; Noda, K.; Ando, R.; Ohguchi, T.; Kawakita, T.; Ohno, S.; Ishida, S. Amelioration of Ultraviolet-Induced Photokeratitis in Mice Treated with Astaxanthin Eye Drops, *Mol Vis* **2012**, *18*.
(43) Mosquera, M. I. M.; Galán, M. J.; Méndez, D. H. *Pigments in Food Technology: Proceedings of 1st International Congress Pft*, 1999.
(44) Ruban, A. V.; Horton, P.; Young, A. J. Aggregation of Higher-Plant Xanthophylls - Differences in Absorption-Spectra and in the Dependency on Solvent Polarity, *J Photoch Photobio B* **1993**, *21*, 229-234.
(45) Billsten, H. H.; Sundstrom, V.; Polivka, T. Self-Assembled Aggregates of the Carotenoid Zeaxanthin: Time-Resolved Study of Excited States, *J Phys Chem A* **2005**, *109*, 1521-1529.
(46) Wang, C.; Berg, C. J.; Hsu, C. C.; Merrill, B. A.; Tauber, M. J. Characterization of Carotenoid Aggregates by Steady-State Optical Spectroscopy, *J Phys Chem B* **2012**, *116*, 10617-10630.
(47) McHale, J. L. Hierarchal Light-Harvesting Aggregates and Their Potential for Solar Energy Applications, *J Phys Chem Lett* **2012**, *3*, 587-597.
(48) Wang, C.; Tauber, M. J. High-Yield Singlet Fission in a Zeaxanthin Aggregate Observed by Picosecond Resonance Raman Spectroscopy, *J Am Chem Soc* **2010**, *132*, 13988-13991.
(49) Polyakov, N. E.; Kruppa, A. I.; Leshina, T. V.; Konovalova, T. A.; Kispert, L. D. Carotenoids as Antioxidants: Spin Trapping EPR and Optical Study, *Free Radical Bio Med* **2001**, *31*, 43-52.
(50) Polyakov, N. E.; Leshina, T. V.; Konovalova, T. A.; Kispert, L. D. Carotenoids as Scavengers of Free Radicals in a Fenton Reaction: Antioxidants or Pro-Oxidants?, *Free Radical Bio Med* **2001**, *31*, 398-404.
(51) Niedzwiedzki, D.; Rusling, J. F.; Frank, H. A. Voltammetric Redox Potentials of Carotenoids Associated with the Xanthophyll Cycle in Photosynthesis, *Chem Phys Lett* **2005**, *415*, 308-312.
(52) Liu, D. Z.; Gao, Y. L.; Kispert, L. D. Electrochemical Properties of Natural Carotenoids, *J Electroanal Chem* **2000**, *488*, 140-150.
(53) Hapiot, P. F.; Kispert, L. D.; Konovalov, V. V.; Saveant, J. M. Single Two-Electron Transfers Vs Successive One-Electron Transfers in Polyconjugated Systems Illustrated by the Electrochemical Oxidation and Reduction of Carotenoids, *J Am Chem Soc* **2001**, *123*, 6669-6677.
(54) Liu, D.; Kispert, L. Electrochemical Aspects of Carotenoids, *Recent Res Dev Electrochem* **1999**, *2*, 139-157.

(55) Liu, D.; Kispert, L. D. Recent Research Development in Electrochemistry, *Res. Devel. Electrochem.* **1999**, *2*, 139-157 and references therein.
(56) Johnson, E. J.; Hammond, B. R.; Yeum, K. J.; Qin, J.; Wang, X. D.; Castaneda, C.; Snodderly, D. M.; Russell, R. M. Relation among Serum and Tissue Concentrations of Lutein and Zeaxanthin and Macular Pigment Density, *Am J Clin Nutr* **2000**, *71*, 1555-1562.
(57) Martin, L.; Leon, A.; Olives, A. I.; del Castillo, B.; Martin, M. A. Spectrofluorimetric Determination of Stoichiometry and Association Constants of the Complexes of Harmane and Harmine with Beta-Cyclodextrin and Chemically Modified Beta-Cyclodextrins, *Talanta* **2003**, *60*, 493-503.
(58) Polyakov, N. E.; Khan, V. K.; Taraban, M. B.; Leshina, T. V. Complex of Calcium Receptor Blocker Nifedipine with Glycyrrhizic Acid, *J Phys Chem B* **2008**, *112*, 4435-4440.
(59) Kornievskaya, V. S.; Kruppa, A. I.; Polyakov, N. E.; Leshina, T. V. Effect of Glycyrrhizic Acid on Lappaconitine Phototransformation, *J Phys Chem B* **2007**, *111*, 11447-11452.
(60) Gao, Y. L.; Webb, S.; Kispert, L. D. Deprotonation of Carotenoid Radical Cation and Formation of a Didehydrodimer, *J Phys Chem B* **2003**, *107*, 13237-13240.
(61) Kispert, L. D.; Konovalova, T.; Gao, Y. Carotenoid Radical Cations and Dications: Epr, Optical, and Electrochemical Studies, *Arch Biochem Biophys* **2004**, *430*, 49-60.
(62) Focsan, A. L.; Bowman, M. K.; Konovalova, T. A.; Molnar, P.; Deli, J.; Dixon, D. A.; Kispert, L. D. Pulsed Epr and Dft Characterization of Radicals Produced by Photo-Oxidation of Zeaxanthin and Violaxanthin on Silica-Alumina, *J Phys Chem B* **2008**, *112*, 1806-1819.
(63) Lawrence, J.; Focsan, A. L.; Konovalova, T. A.; Molnar, P.; Deli, J.; Bowman, M. K.; Kispert, L. D. Pulsed Electron Nuclear Double Resonance Studies of Carotenoid Oxidation in Cu(Il)-Substituted MCM-41 Molecular Sieves, *J Phys Chem B* **2008**, *112*, 5449-5457.
(64) Lai, C. S.; Piette, L. H. Further Evidence for OH Radical Production in Fentons Reagent, *Tetrahedron Lett* **1979**, 775-778.
(65) Greenwald, R. A. *CRC Handbook of Methods for Oxygen Radical Research*; CRC Press, 1985.
(66) Dikalov, S. I.; Mason, R. P. Reassignment of Organic Peroxyl Radical Adducts, *Free Radical Bio Med* **1999**, *27*, 864-872.
(67) Buettner, G. R. Spin Trapping - Electron-Spin-Resonance Parameters of Spin Adducts, *Free Radical Bio Med* **1987**, *3*, 259-303.
(68) Harbour, J. R.; Chow, V.; Bolton, J. R. Electron-Spin Resonance Study of Spin Adducts of Oh and Ho2 Radicals with Nitrones in Ultraviolet Photolysis of Aqueous Hydrogen-Peroxide Solutions, *Can J Chem* **1974**, *52*, 3549-3553.
(69) Yoshimura, Y.; Inomata, T.; Nakazawa, H. Simultaneous Detection of Superoxide Anion, Hydroxyl Radical, and Methyl Radical by Use of High Performance Liquid Chromatography Electron Spin Resonance, *J Liq Chromatogr R T* **1999**, *22*, 419-428.
(70) Buettner, G. R. The Spin-Trapping of Superoxide and Hydroxyl Free-Radicals with Dmpo (5,5-Dimethylpyrroline-N-Oxide) - More About Iron, *Free Radical Res Com* **1993**, *19*, S79-S87.
(71) Perez-Benito, J. F. Iron(Iii)-Hydrogen Peroxide Reaction: Kinetic Evidence of a Hydroxyl-Mediated Chain Mechanism, *J Phys Chem A* **2004**, *108*, 4853-4858.
(72) Barbusinski, K. Fenton Reaction - Controversy Concerning the Chemistry, *Ecol Chem Eng S* **2009**, *16*, 347-358.

CHAPTER 6

CONCLUSIONS

6.1 Conclusions

This dissertation examined some of the properties and roles of a specific group of oxygen containing carotenoids known as xanthophylls. The xanthophylls Zea, Lut, and Asta were studied with regards to their reactivity with destructive energetic species and how the environment and structures of the xanthophylls affected their reactivity.

The deprotonation of naturally-occurring $Zea^{\bullet+}$ to form $\#Zea^{\bullet}$ and their involvement in the qE portion of NPQ was examined in Chapter 3. $Zea^{\bullet+}$ are weak acids, and readily deprotonate to a long-lived $\#Zea^{\bullet}$ that could serve as long-lived quenching sites. When $\#Zea^{\bullet}$ is eventually neutralized and Zea is reformed in the presence of D_2O, the Zea has an opportunity to undergo H/D exchange. This chapter examined evidence for H/D exchange specific to qE activity in *Arabidopsis thaliana*. It was demonstrated that $Zea^{\bullet+}$, formed chemically via oxidation of Zea by Fe(III) in the presence of D_2O, undergoes H/D exchange with a significant intensity increase of the M+1 (d_1Zea) and M+2 (d_2Zea) mass peaks in the mass spectrum compared to samples which had $Zea^{\bullet+}$ formed in the presence of H_2O or unaltered samples. Leaves were infiltrated with either D_2O or H_2O and exposed to varying levels of light intensity both above and below that needed to induce NPQ in *A. thaliana* (300 µE $m^{-2}s^{-1}$). Leaves exposed to light intensity less than needed to induce NPQ but high enough to trigger the xanthophyll cycle were measured to determine if any H/D exchange occurred during interconversion of Zea and Viol in the xanthophyll cycle. Control samples were kept in the dark to check if other physiological

processes or Zea isolation caused H/D exchange. We expected that only a fraction of Zea would undergo H/D exchange since only a fraction of the Zea participates in qE. Avenson et al demonstrated that a majority of Zea binding proteins do not undergo charge transfer quenching and thus could not undergo H/D exchange. The amount of H/D exchange is also limited because not all water molecules can be replaced by D_2O. Following infiltration of wild type *A. thaliana* leaves with D_2O or H_2O and exposure to light intensity less than or greater than that needed to induce NPQ, the carotenoids were extracted and analyzed via LC/MS. The relative mass distribution of Zea was measured to check for formation of #Zea$^{\bullet}$ during qE. It was found that only samples which were infiltrated with D_2O and exposed to qE inducing light intensity had a statistically significant increase in the M + 1 peak.

The proposed quenching mechanism requires a very specific set of conditions to be satisfied. It is imperative that the charge transfer complex has a long enough lifetime for the deprotonation to occur. Examples in the literature show proton transfer can occur in the ~30 femtosecond time range,[1-3] while Fleming's group found the charge transfer complex to last ~200 picoseconds.[4] The Zea$^{\bullet+}$ must be able to undergo deprotonation, which is evident from previous electrochemical, EPR, and DFT studies. The DFT calculations determined that the Zea$^{\bullet+}$ are weak acids and form neutral radicals on solid supports with the most likely site for deprotonation being the C4(4') position of the terminal rings. Finally the protein environment must be favorable for this deprotonation to occur. The crystal structure of the qE active protein CP29 (Protein Data Bank 3PL9) shows the C4(4') of Zea is within 4 Å of potential proton acceptors. All of these conditions are satisfied by Zea in the CP29 minor antennae component where qE occurs. It is not known if they do in the other antenna proteins, CP24 and CP26, that also support Zea$^{\bullet+}$ formation during qE because there is no structure of those complexes in the

structural databases. Although we suggested that #Zea$^{\bullet}$ may be present during qE, based on the known chemistry of Zea$^{\bullet+}$, there has been little experimental evidence of its presence during qE.

To expand upon this work, this H/D exchange method can be applied to *A. thaliana* mutants which have varying ability to carry out qE. Mutants which would be examined are the *A. thaliana npq1, npq2,* and *npq4* mutants, whose seeds are available from the Arabidopsis Biological Resource Center. The experiments would be carried out in a similar manner as in Chapter 3: leaves from the mutants will be harvested and infiltrated with H_2O or D_2O and exposed to light intensity less than or greater than that needed to trigger qE and Zea will be extracted from the leaves and be analyzed via liquid chromatography/mass spectrometry to detect H/D exchange caused by the formation of the neutral radical Zea. The *npq1* mutant is inhibited in its ability to convert violaxanthin to Zea in the xanthophyll cycle.[5] The *npq1* mutant undergoes very little qE and therefore is not expected to demonstrate H/D exchange under the experimental methods. The *npq2* mutant accumulates Zea and lacks violaxanthin and shows unimpaired qE.[6] Therefore, H/D exchange is expected to be observed under the experimental methods utilized in Chapter 3. The *npq4* mutant is defective in the qE portion of NPQ, although it exhibited no difference in synthesis of Zea in high light conditions compared to the wild-type.[7] H/D exchange is not expected to occur under the experimental methods utilized in Chapter 3 as we predict the formation of #Zea$^{\bullet}$ occurs during qE. Continuing work on the various *A. thaliana* mutants will provide further evidence for the formation of potent energy quenching neutral carotenoid radicals during qE. The H/D exchange detection could be improved with the use of ultra-high resolution mass spectrometry which would be able to distinguish a d_1Zea molecule from the C^{13} or protonated variants in the sample. This would eliminate the need for the

statistical analysis. These types of instruments are available at the National High Magnetic Field Laboratory in Tallahassee, Florida.

Chapter 4 demonstrated differences in the chemistry of geometrical isomers of Zea isolated from various sources in mass spectrometry using electrospray ionization source. Zea exhibits antioxidant activity and also plays a role in photo-protection in the retina. The long polyene structure of carotenes allow them to naturally occur in both *cis* (*Z*)- and *trans* (*E*)-isomers. Several examples of naturally occurring isomers that have been identified include 5*Z*)-, (9*Z*)-, (13*Z*)-isomers of lycopene in ketchup, [84] (9'*Z*)-, (13*Z*)-, (13'*Z*)-isomers of fucoxanthin in *Isochrysis* sp., [9 5] and (9*Z*)-, (13*Z*)-, (15*Z*)-isomers of violaxanthin in orange juice. The reasons for these naturally occurring isomers are not well understood despite their natural occurrence. As we described in Chapter 3, the protein environment is crucial in the functionality of carotenes. Much work has been done to describe the role of Zea in qE of photosynthetic systems, and the position of Zea in the crystal structure of the minor antenna component CP29 (Protein Data Bank 3PL9) suggests that the (*all-E*)-Zea configuration is necessary for the charge transfer complex to occur. The proposed quenching mechanism involving #Zea$^{\bullet}$ would not be possible with a *cis*-Zea configuration due to the position of any potential proton acceptors. Further evidence of the importance of structure on functionality is the distribution of Zea isomers in the human eyes. It has been suggested that the role of Zea in the eye is to filter out high energy blue light from reaching the underlying structures of the human retina. It can also act as an antioxidant with free radicals and reactive oxygen species to prevent peroxidation and photodamage to the retina. Isomers of Zea are regionally dominant in the eye, suggesting they play different roles. Therefore, it is crucial to examine the different chemical properties the geometrical isomers of Zea.

This study highlighted that various chemistry occurs among different geometrical isomers of Zea undergo during mass spectrometry analyses due to their unique electrochemical properties. Far more fragmentation, protonation, deprotonation, and epoxidation was observed in the mass spectra of crude Zea extracts and isolated (13*Z*)-Zea compared to the (all-*E*)-Zea in the analytical conditions described. This work demonstrates the geometrical isomers of Zea exhibit unique chemistry.

Additional work on the geometrical isomers of carotenoids which could be done would be to compare the scavenging ability of isomers towards the hydroperoxy radical utilizing EPR spin trapping techniques. It was shown that electrochemical properties play a significant role in the ability of carotenoids to react with the hydroperoxy radical[10] and that geometrical isomers undergo different reactions in ESI–MS. Therefore, it would be expected that geometrical isomers would have differing radical scavenging capabilities. This technique could be applied to multiple species if pure isomers are available. However care must be taken as *cis/trans* isomerization readily occurs when carotenoid radical cations are formed as noted in **Scheme 3.2** of Chapter 3.

Chapter 5 focuses on the xanthophyll carotenoids ability to self-assemble in aqueous solutions to form J- and H-type aggregates. This feature significantly changes the photo-physical and optical properties of these carotenoids. These aggregates are easily identified through optical measurements, with J-type aggregates being associated with a large red shift while H-type aggregates result in a large blue shift. The H-aggregate blue shift is caused by a loss of vibrational structure of the S_2 excited state of the monomer as a result of the molecular clumping. The monomers are arranged with the conjugated pi bonds stacking and becoming closely packed together, causing excitonic interaction between the closely packed xanthophyll chromophores.

The red shift of the J-type aggregation is caused by a head to tail organization of the monomers, which preserves the vibrational bands.

Practical application of carotenoids as nutritional antioxidants or components of medicinal preparations has been limited since carotenoids are highly hydrophobic, air and light-sensitive compounds. The majority of carotenoids are lipophilic molecules with near zero inherent aqueous solubility. Moving carotenoids into a pharmaceutical application requires a chemical delivery system that overcomes the problems with parenteral administration of a highly lipophilic, low molecular weight compound. Previous work has been attempted to make these compounds water dispersible, mainly focusing on the use of cyclodextrin to form inclusion complexes with the molecules. However these complexes have demonstrated low solubility and fast aggregation in the presence of water. These inclusion complexes also did not maintain the antioxidant ability of the carotenes. Identifying complexing agents that can overcome these obstacles is critical in the application of carotenes as supplements. The applicability of glycyrrhizic acid (GA) and arabinogalactan (AG) were examined in this chapter. GA is a natural compound extracted from licorice root and AG is a natural water soluble polysaccharide extracted from Siberian larch. AG has been shown in previous work to increase the photostability and photocatalytic activity of the carotenoids β-carotene and canthaxanthin.

In this study we have applied EPR and optical absorption spectroscopy to investigate how complexation can affect the aggregation ability of the xanthophyll carotenoids Zea, Lut, and Asta, their photostability, and antioxidant activity. It was shown that complexation with the polysaccharide arabinogalactan (AG) polymer matrix and the triterpene glycoside glycyrrhizin (GA) dimer reduced the aggregation rate but do not inhibit aggregation completely. Moreover, these complexants form inclusion complexes with both monomer and H-aggregates of

carotenoids. H-aggregates of carotenoids exhibit higher photostability in aqueous solutions as compared with monomers, but much lower antioxidant activity. It was found that complexation increases the photostability of both monomers and the aggregates of xanthophyll carotenoids. Also their ability to trap hydroperoxyl radicals increases in the presence of GA as the GA forms a donut like dimer in which the hydrophobic polyene chain of the xanthophylls and their H-aggregates lies protected within the donut hole permitting the hydrophilic ends to be exposed to the surroundings.

An interesting feature to examine in the future is the behavior of structural isomers in similar conditions. The formation of the aggregates is known to be a property of xanthophylls with terminal hydroxyl groups, but our work was done on purified all-*trans* isomers. Does this aggregation occur with *cis*-isomers? In continuation with the previous section, the complexation techniques could be applied to study the effect on photostability and radical scavenging of these geometrical isomers. Once again, this would require a supply of purified isomers.

To gain a better understanding of the chemistry occurring in the EPR spin trapping system, a mathematical model. Having a reliable model can produce rate constant estimates for free radical scavenging ability of compounds in our system. Preliminary work has been done on this topic, and some of the most interesting results are highlighted below. The first step is to calibrate the data acquired from the EPR measurements to determine the concentration of spin adducts formed in the system. This can be done by measuring the EPR signal of a stable radical of known concentrations to form a calibration curve. The acquired spectra can be simulated using Bruker's Xepr SpinFit software, and the signal can then be translated into concentration. A candidate for the stable radical to be used for the concentration calibration is (2,2,6,6-tetramethylpiperidin-1-yl)oxidanyl, commonly known as TEMPO. Once the calibration is

completed, the next step would be to acquire data from the spin trapping system and translate the EPR spectra into spin adduct concentration. From here, the simulation can begin. **Scheme 6.1** is a tentative list of the reactions which are occurring in the spin trapping system. Several reactions have estimated rate constants which were acquired from the NIST database (http://kinetics.nist.gov/solution/). Most of these rate constants were reported in different circumstances, such as different solvents, and may not be exact for our system. However, they do serve as good starting points in our simulation. The reactions with asterisks are those whose rate constants were found to have the greatest influence on the overall spin adduct yield in the simulations.

$$Fe^{2+} + H_2O_2 \xrightarrow{k_1\,(10^2)} Fe^{3+} + OH^{\bullet} + OH^{-}$$

$$OH^{\bullet} + DMSO \xrightarrow{k_2\,(10^9)} CH_3^{\bullet} + CH_3(OH)SO$$

$$CH_3^{\bullet} + H_2O_2 \xrightarrow{k_3\,(10^7)} OOH^{\bullet} + CH_4$$

$$CH_3^{\bullet} + CH_3^{\bullet} \xrightarrow{k_4} CH_3CH_3$$

$$PBN + OOH^{\bullet} \xrightarrow{k_5\,(10^5)} PBN(OOH)^{\bullet}$$

$$PBN + OH^{\bullet} \xrightarrow{k_6\,(10^9)} PBN(OH)^{\bullet}$$

$$PBN + CH_3^{\bullet} \xrightarrow{k_7\,(10^7)} PBN(CH_3)^{\bullet}$$

$$Car + OH^{\bullet} \xrightarrow{k_8} Car(OH)^{\bullet}$$

$$Car + CH_3^{\bullet} \xrightarrow{k_9} Car(CH_3)^{\bullet}$$

$$Car + OOH^{\bullet} \xrightarrow{k_{10}} Car(OOH)^{\bullet}$$

$$Fe^{3+} + OOH^{\bullet} \xrightarrow{k_{11}} H^{+} + Fe^{2+} + O_2$$

$$Fe^{3+} + H_2O_2 \xrightarrow{k_{12}} Fe^{2+} + OOH^{\bullet}$$

$$Fe^{3+} + Car \xrightarrow{k_{13}} Fe^{2+} + Car^{\bullet +}$$

$$Fe^{2+} + OOH^{\bullet} \xrightarrow{k_{14}} Fe^{3+} + H_2O_2$$

$$H_2O_2 + OOH^{\bullet} \xrightarrow{k_{15}} OH^{\bullet} + H_2O + O_2$$

$$CH_3^{\bullet} + O_2 \xrightarrow{k_{16}} O_2CH_3^{\bullet}$$

$$O_2CH_3^{\bullet} + O_2CH_3^{\bullet} \xrightarrow{k_{17}} \text{decay products}$$

$$Fe^{2+} + OH^{\bullet} \xrightarrow{k_{18}} FeOH^{2+}$$

$$Contaminant + OOH^{\bullet} \xrightarrow{k_{19}} \text{decay products}$$

Scheme 6.1: A list of the equations which play a role in our spin trapping system. Our spectroscopic data is the total spin adduct yield, or the sum of reactions 5, 6, and 7. The total yield is used due to difficulty in resolving the signal from the individual spin adducts. *Denotes reaction that has great influence on the overall spin adduct yield.

6.2 References

(1) Formosinho, S. J.; Arnaut, L. G. Excited-State Proton-Transfer Reactions. 2. Intramolecular Reactions, *J Photoch Photobio A* **1993**, *75*, 21-48.

(2) Kim, C. H.; Park, J.; Seo, J.; Park, S. Y.; Joo, T. Excited State Intramolecular Proton Transfer and Charge Transfer Dynamics of a 2-(2 '-Hydroxyphenyl)Benzoxazole Derivative in Solution, *J Phys Chem A* **2010**, *114*, 5618-5629.

(3) Kim, C. H.; Joo, T. Coherent Excited State Intramolecular Proton Transfer Probed by Time-Resolved Fluorescence, *Phys Chem Chem Phys* **2009**, *11*, 10266-10269.

(4) Ahn, T. K.; Avenson, T. J.; Ballottari, M.; Cheng, Y. C.; Niyogi, K. K.; Bassi, R.; Fleming, G. R. Architecture of a Charge-Transfer State Regulating Light Harvesting in a Plant Antenna Protein, *Science* **2008**, *320*, 794-797.

(5) Havaux, M.; Niyogi, K. K. The Violaxanthin Cycle Protects Plants from Photooxidative Damage by More Than One Mechanism, *P Natl Acad Sci USA* **1999**, *96*, 8762-8767.

(6) Niyogi, K. K.; Grossman, A. R.; Bjorkman, O. Arabidopsis Mutants Define a Central Role for the Xanthophyll Cycle in the Regulation of Photosynthetic Energy Conversion, *Plant Cell* **1998**, *10*, 1121-1134.

(7) Li, X. P.; Bjorkman, O.; Shih, C.; Grossman, A. R.; Rosenquist, M.; Jansson, S.; Niyogi, K. K. A Pigment-Binding Protein Essential for Regulation of Photosynthetic Light Harvesting, *Nature* **2000**, *403*, 391-395.

(8) Vallverdú-Queralt, A.; Martínez-Huélamo, M.; Arranz-Martinez, S.; Miralles, E.; Lamuela-Raventós, R. M. Differences in the Carotenoid Content of Ketchups and Gazpachos through HPLC/ESI(Li+)-MS/MS Correlated with Their Antioxidant Capacity, *J Sci Food Agr* **2012**, *92*, 2043-2049.

(9) Crupi, P.; Toci, A. T.; Mangini, S.; Wrubl, F.; Rodolfi, L.; Tredici, M. R.; Coletta, A.; Antonacci, D. Determination of Fucoxanthin Isomers in Microalgae (Isochrysis sp.) by High-Performance Liquid Chromatography Coupled with Diode-Array Detector Multistage Mass Spectrometry Coupled with Positive Electrospray Ionization, *Rapid Commun Mass Sp* **2013**, *27*, 1027-1035.

(10) Polyakov, N. E.; Kruppa, A. I.; Leshina, T. V.; Konovalova, T. A.; Kispert, L. D. Carotenoids as Antioxidants: Spin Trapping EPR and Optical Study, *Free Radical Bio Med* **2001**, *31*, 43-52.

APPENDIX A

SUPPLEMENTARY INFORMATION FOR CHAPTER 3: NEUTRAL CAROTENOID RADICALS IN PHOTOPROTECTION OF WILD-TYPE *Arabidopsis thaliana*

This appendix contains all the unsmoothed total ion chromatograms (TIC) and extracted ion chromatograms (EIC) gathered during the research described in Chapter 3 as well as all the data sets that were used in ANOVA comparisons. The *trans* peaks mentioned in the EIC figures refer to the larger and earlier peak while the *cis* peaks mentioned refer to the smaller and later peak.

The TIC's are Figures: A1, A3, A5, A7, A9, A11, A14, A17, A20, A23, A26, A29, A32, A35, and A37.

The EIC's at m/z 568.9 are Figures: A2, A4, A6, A8, A10, A12, A15, A18, A21, A24, A27, A30, A33, and A36.

The EIC's at m/z 601.9 are Figures: A13, A16, A19, A22, A25, A28, A31, A34, A38.

The data sets are Tables: A1-A13.

The ANOVA tables are Tables: A14-A29.

A.1 Chemically-Generated Zea Radicals

Figure A1: TIC from Normal

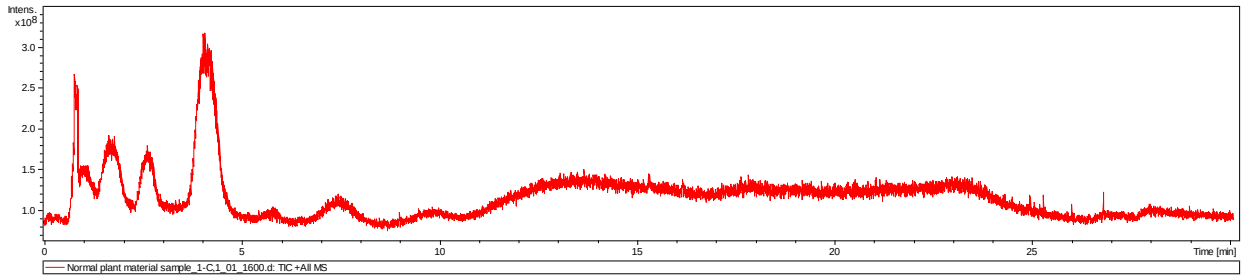

Figure A2: EIC m/z 568.9 from Normal

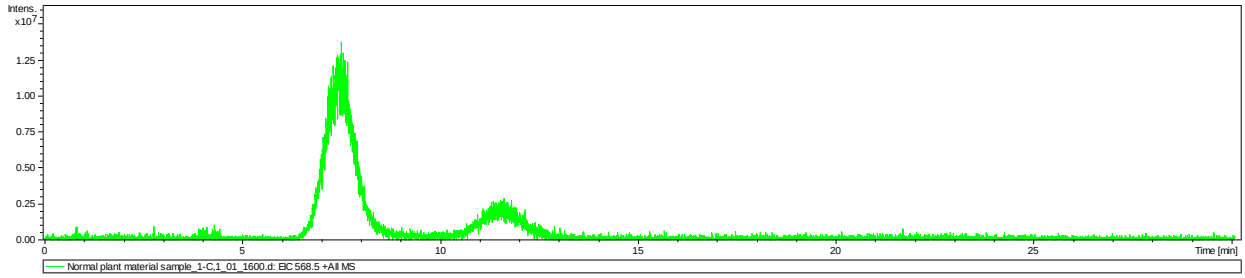

Table A1: Peak Intensities from *cis* peak of Figure A2

Normal			
m/z ratio	568	569	570
Intensity 1	640989	362724	87094
Intensity 2	736219	401538	99547
Intensity 3	758200	396416	95662
Intensity 4	717242	426165	97071
Intensity 5	700351	387126	97486
Intensity 6	659643	355469	95879
Intensity 7	595248	312168	95218
Intensity 8	520212	291685	69876

Figure A3: TIC from Short Term H_2O

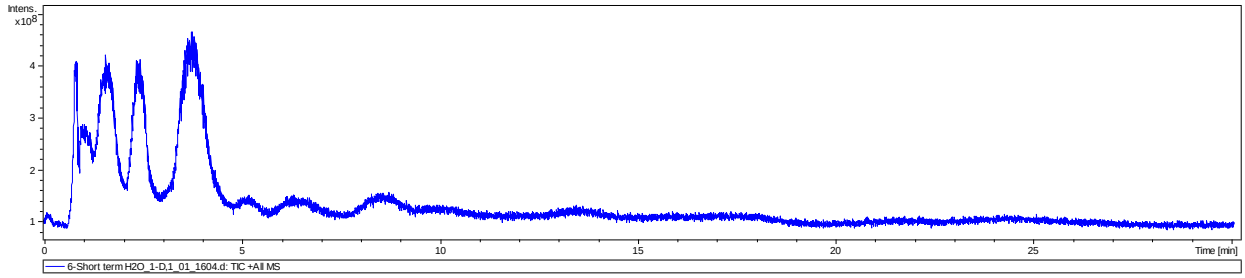

Figure A4: EIC m/z 568.9 from Short Term H_2O

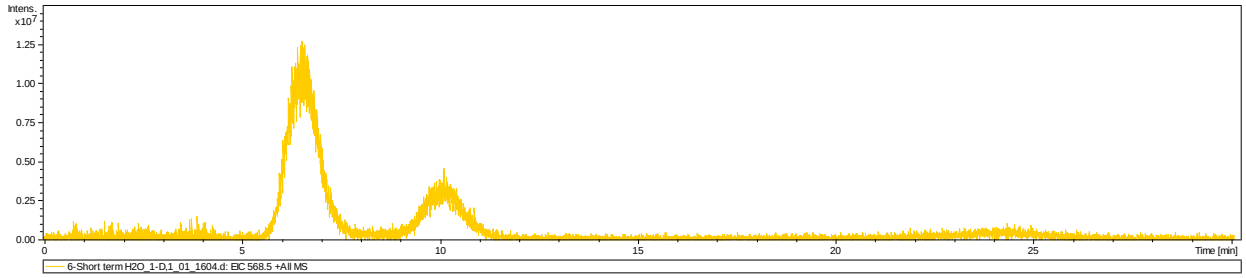

Table A2: Peak Intensities from *cis* peak of Figure A4

Short Term H_2O			
m/z ratio	568	569	570
Intensity 1	517736	324506	75389
Intensity 2	720684	354937	106315
Intensity 3	686598	388648	87504
Intensity 4	714072	411351	96604
Intensity 5	715520	369423	115318
Intensity 6	745165	384091	105511
Intensity 7	687273	377479	83044
Intensity 8	612531	335228	85189

Figure A5: TIC from Long Term H_2O

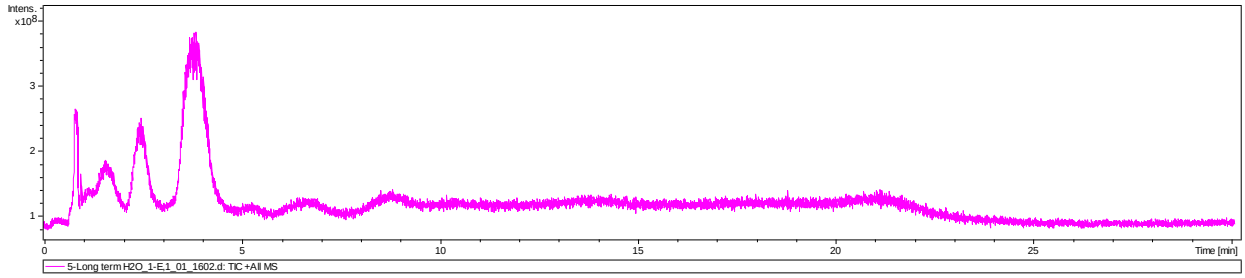

Figure A6: EIC m/z 568.9 from Long Term H_2O

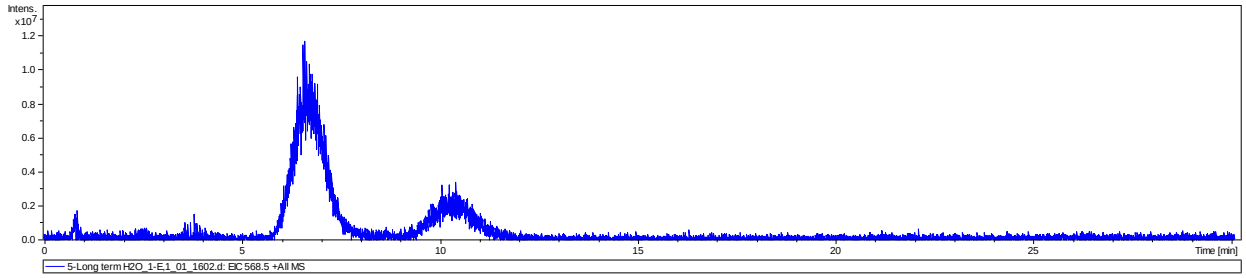

Table A3: Peak Intensities from *cis* peak of Figure A6

Long Term H_2O			
m/z ratio	568	569	570
Intensity 1	891684	469300	110798
Intensity 2	953173	561602	137907
Intensity 3	1054774	566443	129691
Intensity 4	1110002	576832	133082
Intensity 5	1076497	600643	139093
Intensity 6	968660	500512	137356
Intensity 7	969479	472607	137006
Intensity 8	801916	441198	111488

Figure A7: TIC of Short Term D_2O

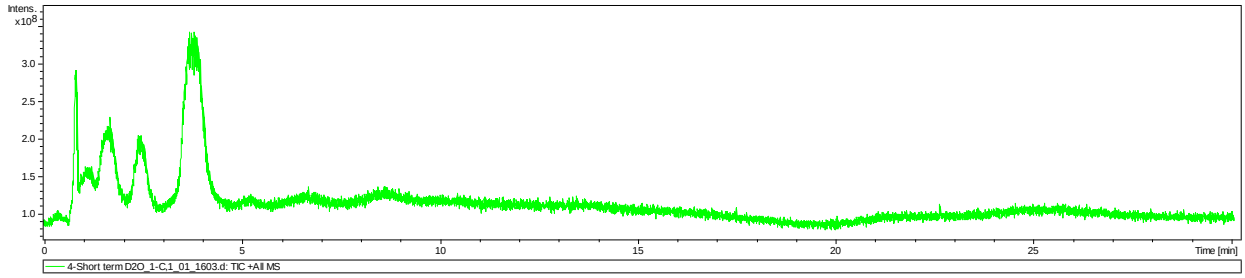

Figure A8: EIC m/z 568.9 from Short Term D_2O

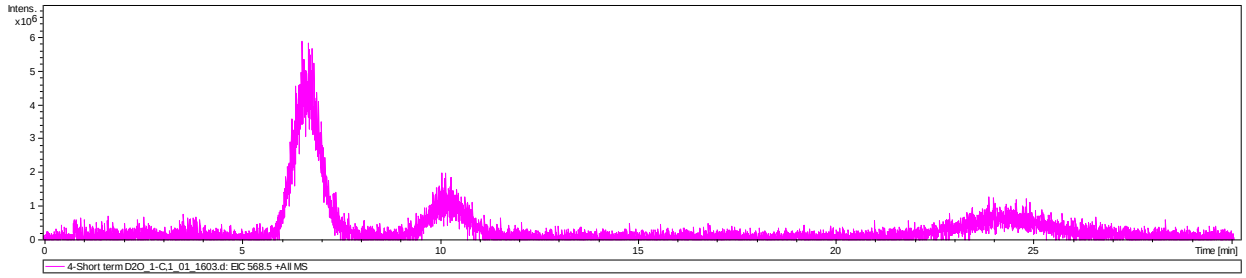

Table A4: Peak Intensities from *cis* peak of Figure A8

Short Term D_2O			
m/z ratio	568	569	570
Intensity 1	215533	152303	52767
Intensity 2	267523	172273	63460
Intensity 3	269313	174982	64077
Intensity 4	285391	186420	61758
Intensity 5	342285	213603	62828
Intensity 6	313570	210138	67230
Intensity 7	319844	210142	69252
Intensity 8	302535	181293	58246

Figure A9: TIC of Long Term D_2O

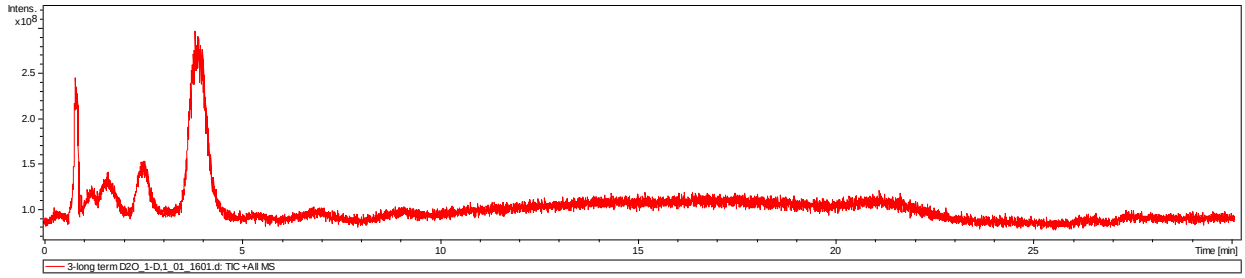

Figure A10: EIC m/z 568.9 of Long Term D_2O

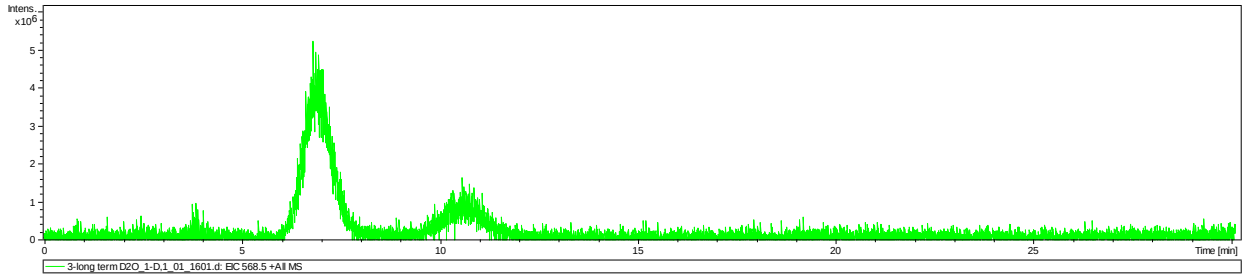

Table A5: Peak Intensities from *cis* peak of Figure A10

Long Term D_2O			
m/z ratio	568	569	570
Intensity 1	314294	194252	35453
Intensity 2	370023	210068	74256
Intensity 3	378100	241186	66020
Intensity 4	381459	235467	67921
Intensity 5	393149	226645	63494
Intensity 6	346979	205779	64832
Intensity 7	343680	191813	64484
Intensity 8	289629	169687	58907

A.2 Zea H/D Exchange in Leaves

Figure A11: TIC of BTD

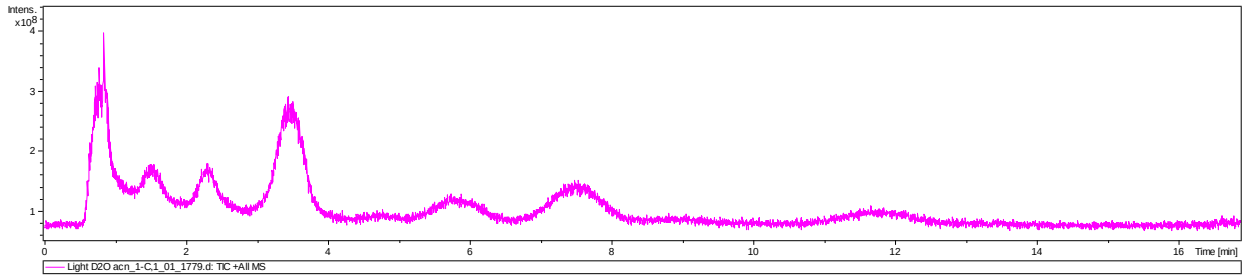

Figure A12: EIC m/z 568.9 BTD

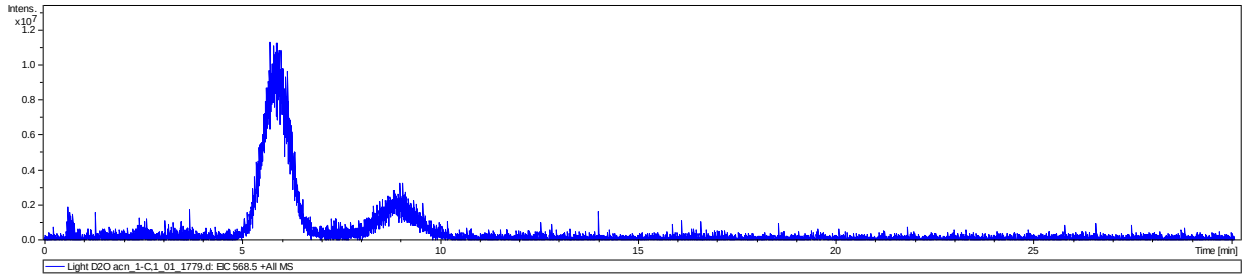

Figure A13: EIC m/z 601.9 BTD

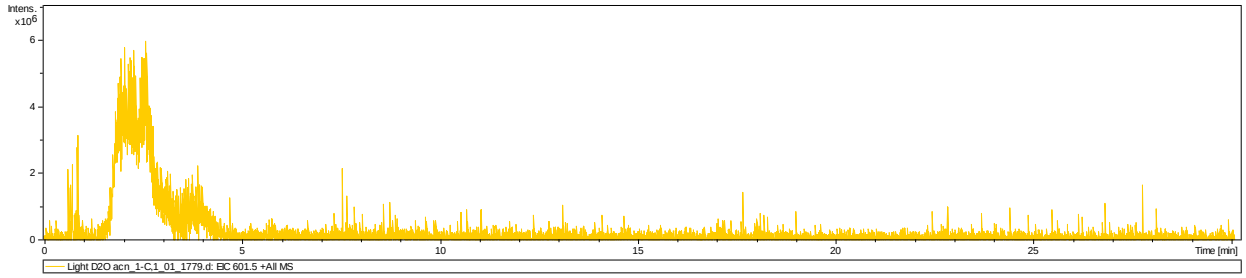

Table A6: Peak intensities from *cis* peak in Figure A12

BTD			
m/z ratio	568	569	570
Intensity 1	650829	273335	91974
Intensity 2	672163	285061	105771
Intensity 3	747193	317732	113112
Intensity 4	866889	396626	91284
Intensity 5	791162	384555	98710
Intensity 6	826385	395955	114872
Intensity 7	754752	316327	94005
Intensity 8	607869	335806	93932

Figure A14: TIC of BTW

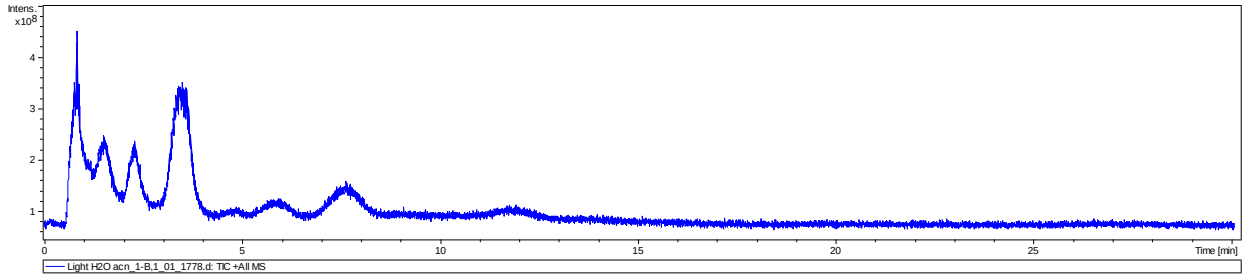

Figure A15: EIC m/z 568.9 BTW

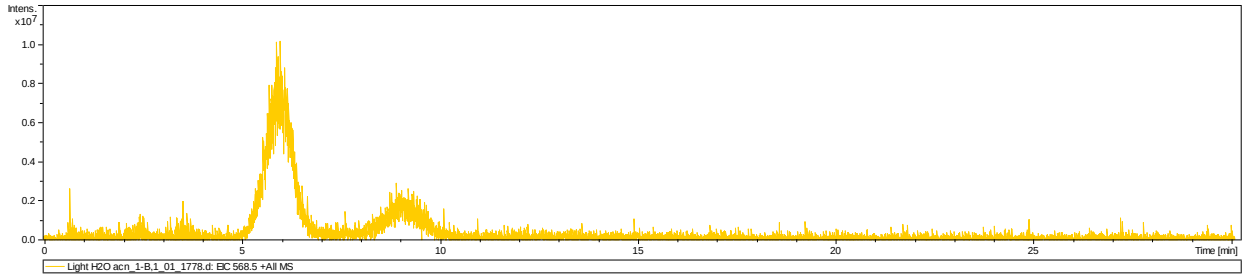

Figure A16: EIC m/z 601.9 BTW

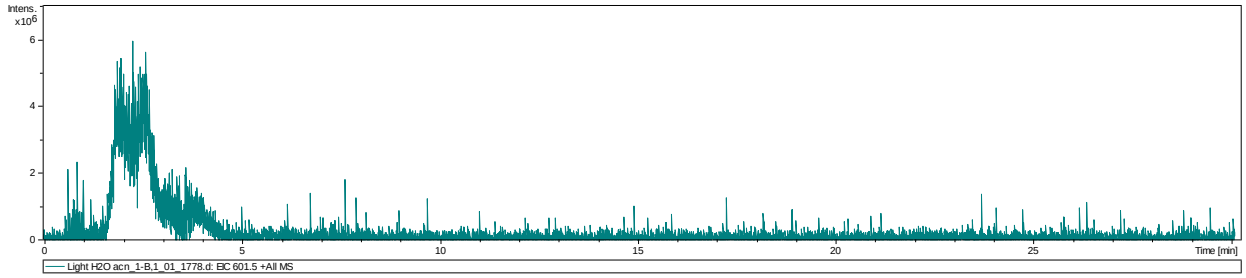

Table A7: Peak intensities from *cis* peak in Figure A15

BTW			
m/z ratio	568	569	570
Intensity 1	586667	302342	86020
Intensity 2	677951	324225	80429
Intensity 3	729339	304423	80662
Intensity 4	661067	324826	83217
Intensity 5	666619	305180	82317
Intensity 6	562181	307914	101349
Intensity 7	496845	314425	90876
Intensity 8	453779	265036	89254

Figure A17: TIC of BTD-C

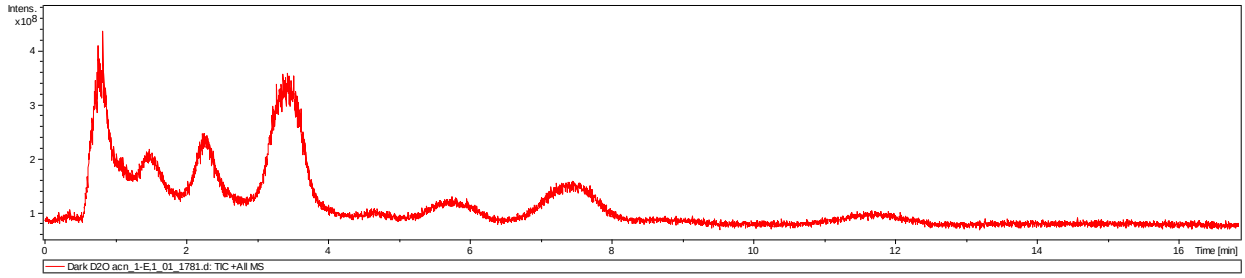

Figure A18: EIC m/z 568.9 BTD-C

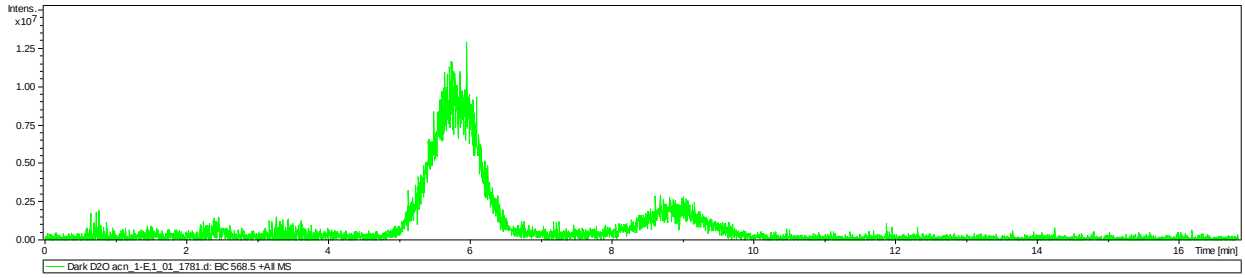

Figure A19: EIC m/z 601.9 BTD-C

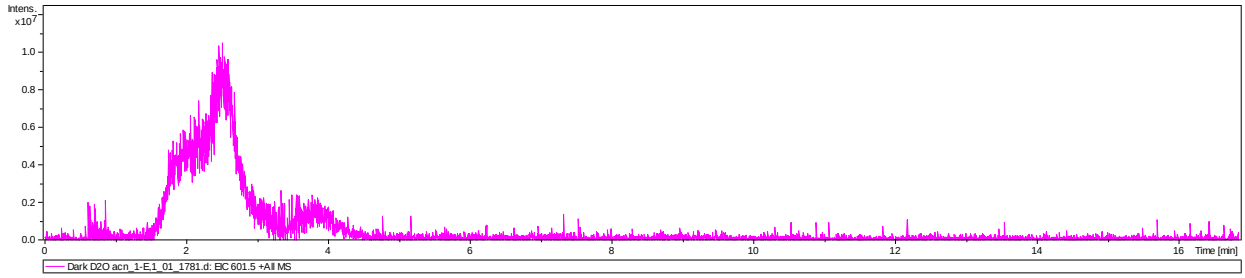

Table A8: Peak intensities from *cis* peak in Figure A18

BTD-C			
m/z ratio	568	569	570
Intensity 1	584890	263225	81661
Intensity 2	736633	342653	98059
Intensity 3	758739	356699	102576
Intensity 4	830453	355390	89740
Intensity 5	769471	379814	112574
Intensity 6	767518	387960	82837
Intensity 7	617723	311814	84960
Intensity 8	541270	288019	85531

Figure A20: TIC of BTW-C

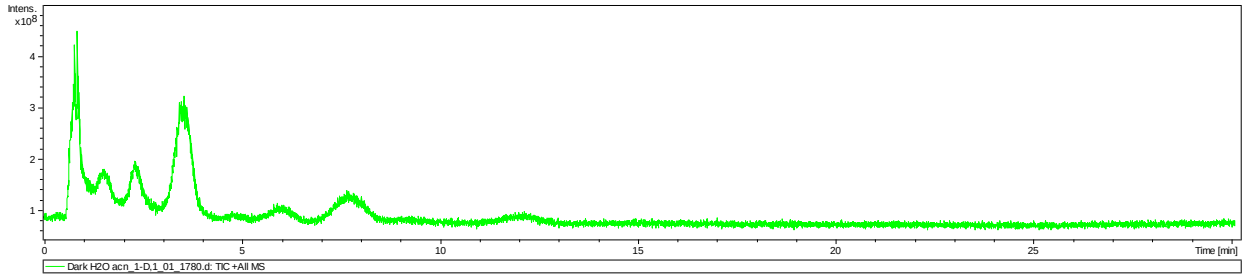

Figure A21: EIC m/z 568.9 BTW-C

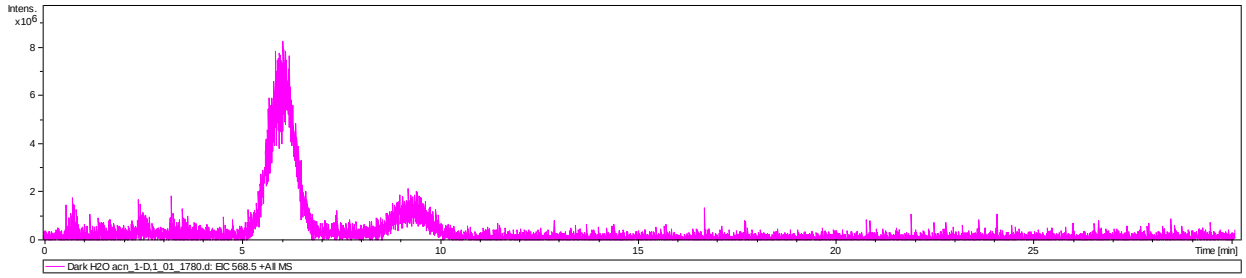

Figure A22: EIC m/z 601.9 BTW-C

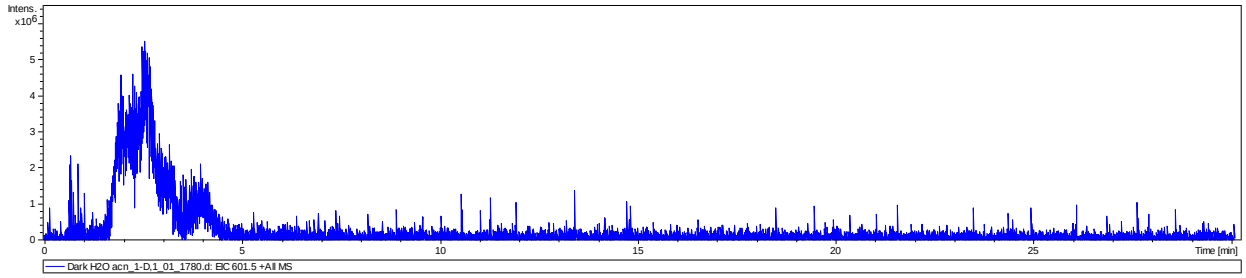

Table A9: Peak Intensities for *cis* peak in Figure A21

BTW-C			
m/z ratio	568	569	570
Intensity 1	472218	181408	61827
Intensity 2	506983	230066	65488
Intensity 3	533487	284839	62879
Intensity 4	488827	228852	78350
Intensity 5	482890	267882	78516
Intensity 6	462243	215951	60202
Intensity 7	381817	178367	56496
Intensity 8	316205	162450	48042

Figure A23: TIC of ATD

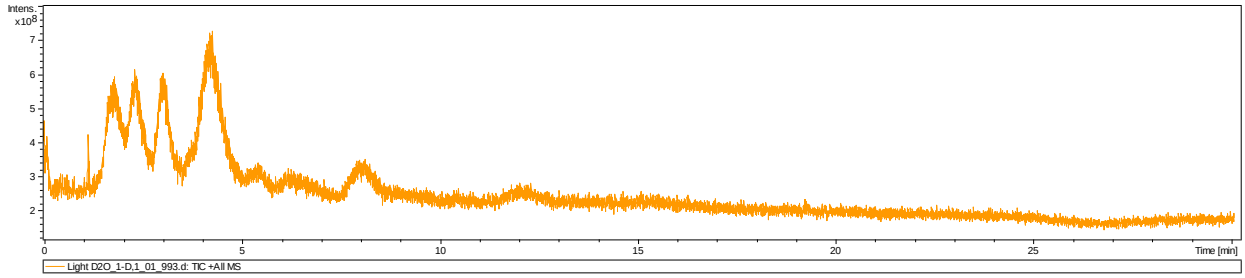

Figure A24: EIC m/z 568.9 ATD

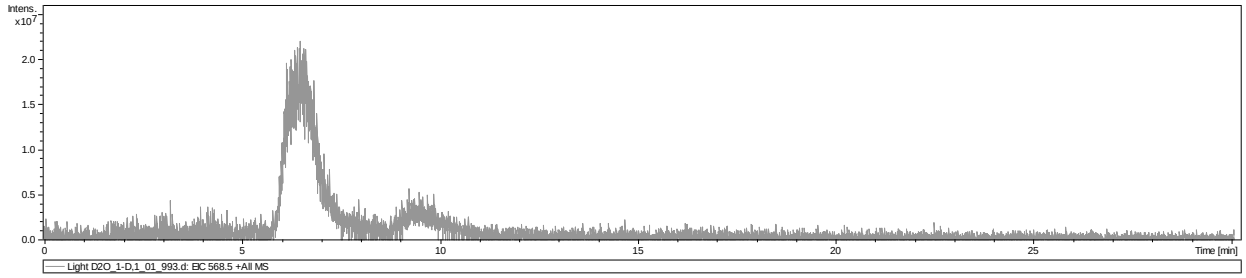

Figure A25: EIC m/z 601.9 ATD

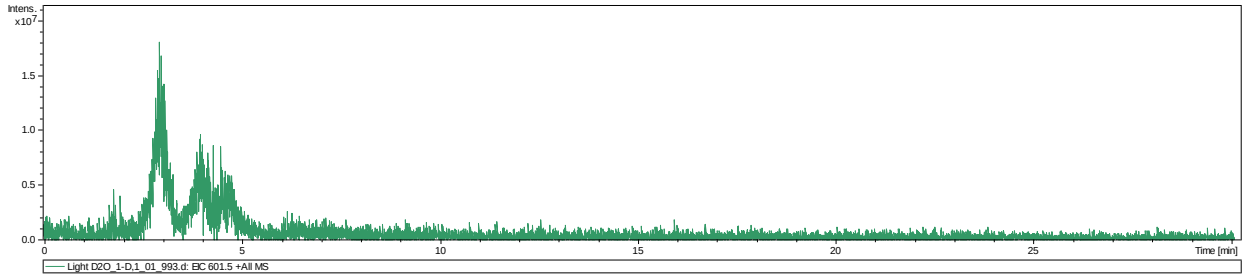

Table A10: Peak Intensities from *cis* peak in Figure A24

ATD			
m/z ratio	568	569	570
Intensity 1	919528	729228	221947
Intensity 2	1106002	755798	215951
Intensity 3	1197428	823970	226003
Intensity 4	1096679	813470	205753
Intensity 5	1204444	706466	261585
Intensity 6	1013959	748752	295286
Intensity 7	966176	732083	219543
Intensity 8	960030	644572	235215

Figure A26: TIC of ATW

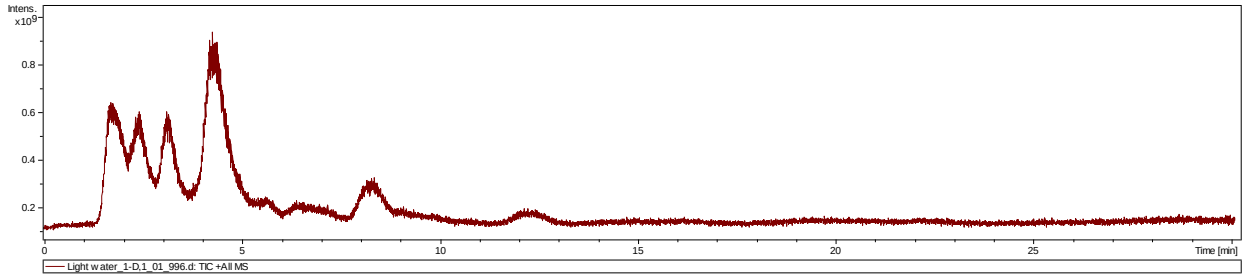

Figure A27: EIC m/z 568.9 ATW

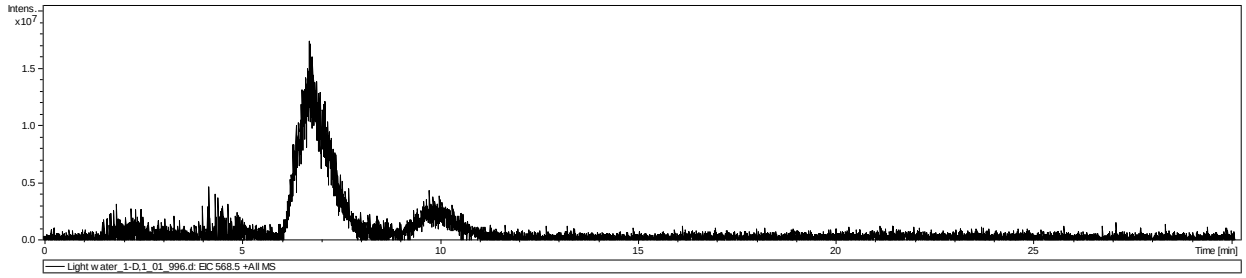

Figure A28: EIC m/z 601.9 ATW

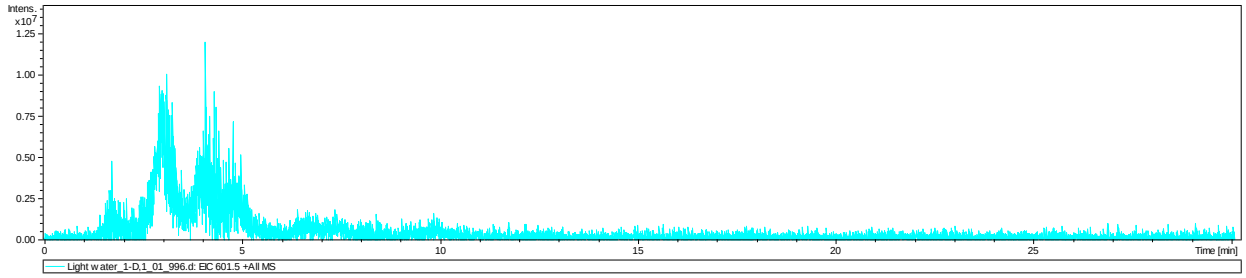

Table A11: Peak Intensities from *cis* peak of Figure A27

ATW			
m/z ratio	568	569	570
Intensity 1	625378	425953	140781
Intensity 2	786303	495532	175973
Intensity 3	885387	536160	168957
Intensity 4	915933	553186	152611
Intensity 5	916970	576487	168964
Intensity 6	865028	582236	173914
Intensity 7	811174	524882	205147
Intensity 8	817426	495505	138671

Figure A29: TIC of ATD-C

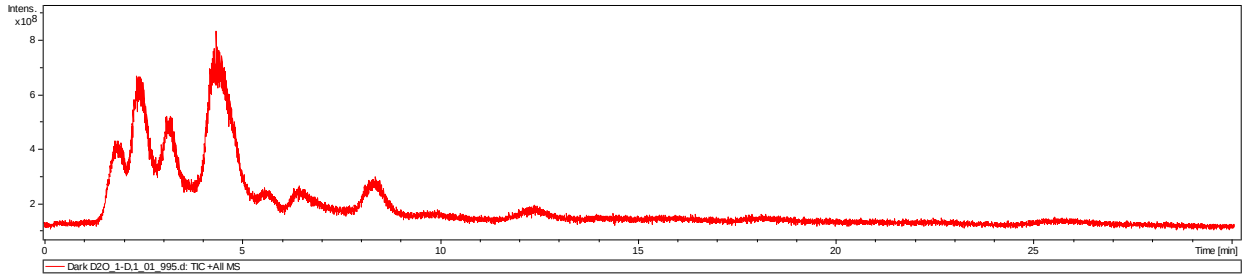

Figure A30: EIC m/z 568.9 ATD-C

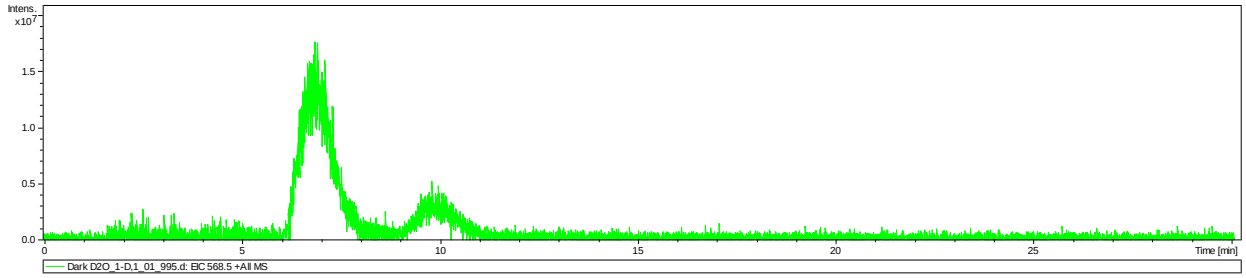

Figure A31: EIC m/z 601.9 ATD-C

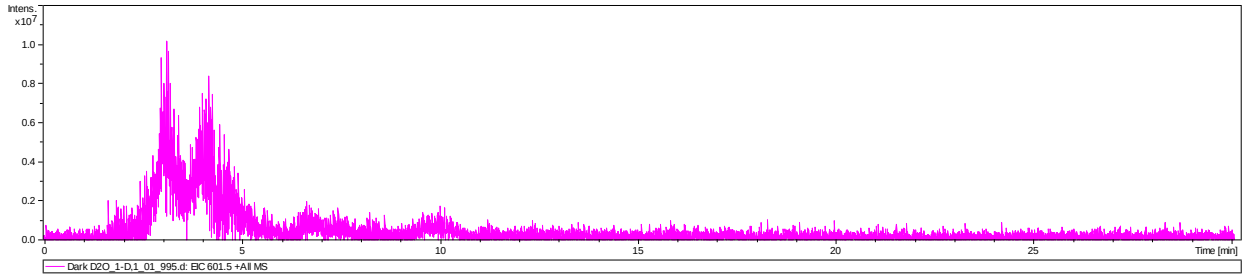

Table A12: Peak Intensities of *cis* peak in Figure A30

ATD-C			
m/z ratio	568	569	570
Intensity 1	919523	524004	195604
Intensity 2	1111534	582725	183906
Intensity 3	1203742	690477	192069
Intensity 4	1076777	698934	199874
Intensity 5	1173184	680951	210503
Intensity 6	1033511	669695	208933
Intensity 7	1060701	631689	175885
Intensity 8	888685	591807	150678

Figure A32: TIC of ATW-C

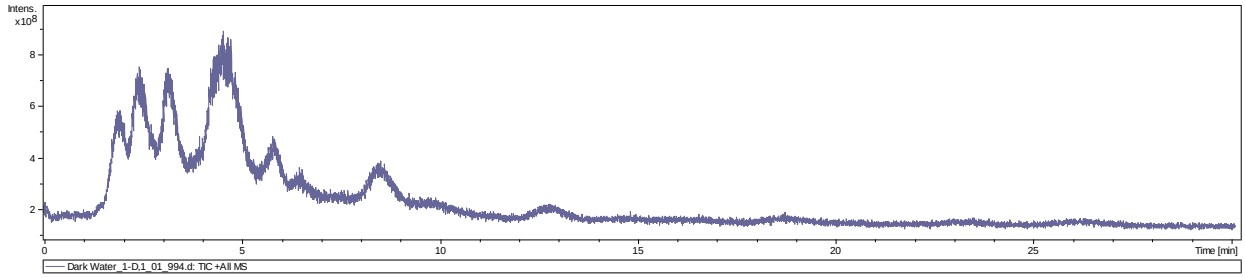

Figure A33: EIC m/z 568.9 ATW-C

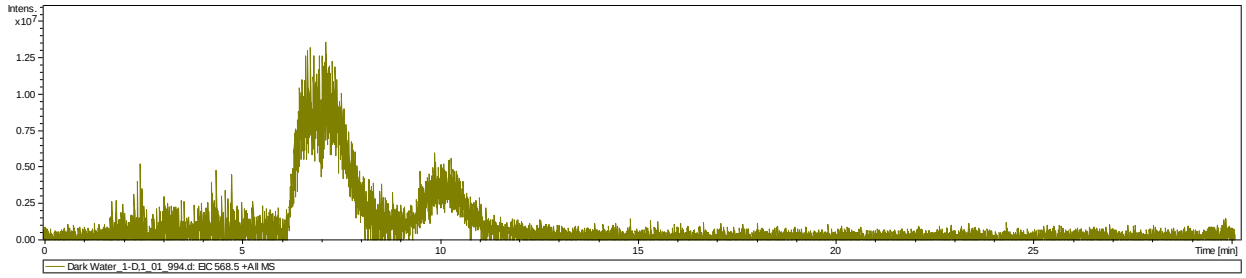

Figure A34: EIC m/z 601.9 ATW-C

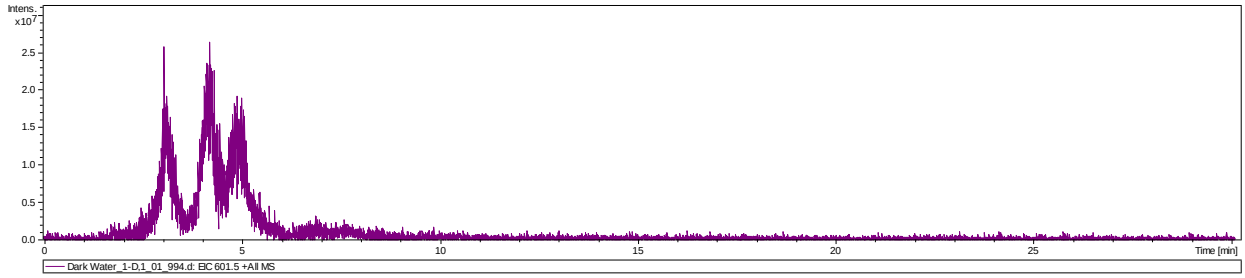

Table A13: Peak Intensities from *cis* peak in Figure A33

ATW-C			
m/z ratio	568	569	570
Intensity 1	1075169	708116	276152
Intensity 2	1395946	769533	227759
Intensity 3	1435096	848740	269273
Intensity 4	1457460	890915	306839
Intensity 5	1425688	831794	270028
Intensity 6	1326465	859095	232481
Intensity 7	1269435	828232	262357
Intensity 8	1193397	709941	199378

A.3 Confirmation of Zea/Viol Extraction

Figure A35: TIC of Zea Standard

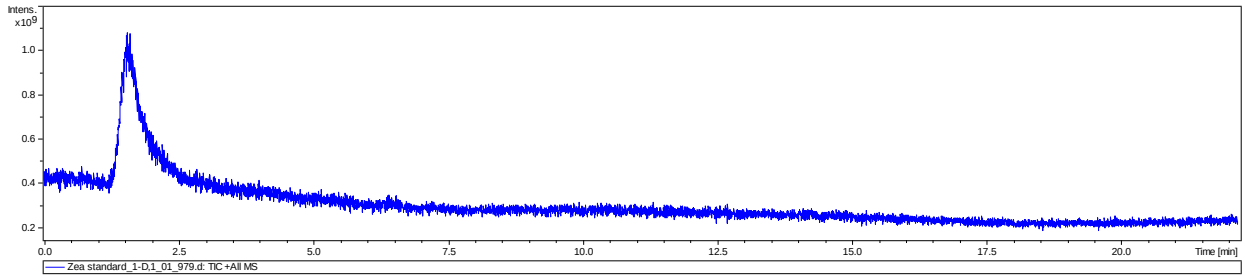

Figure A36: EIC m/z 568.9 Zea Standard

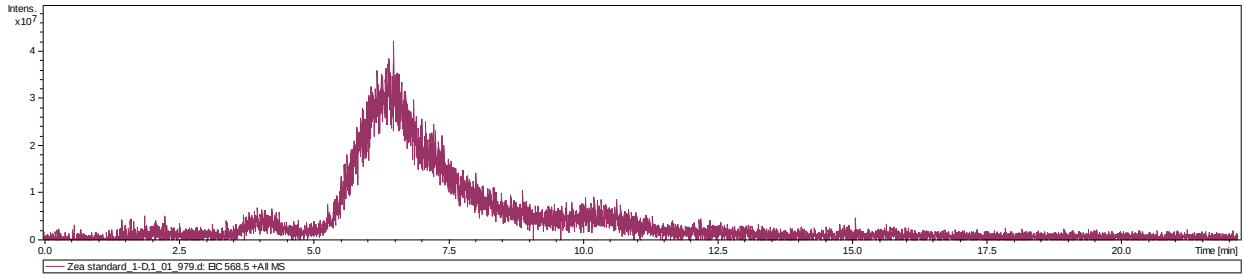

Figure A37: TIC of Viol Standard

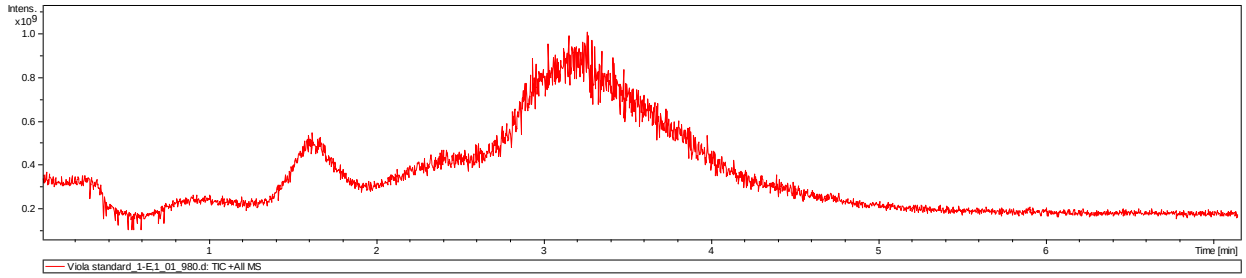

Figure A38: EIC m/z 601.9 Viol Standard

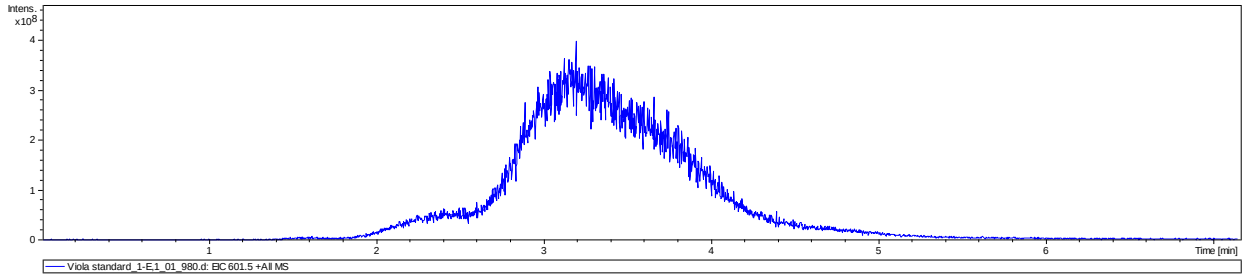

A.4 ANOVA Tables used in Manuscript

Below are the ANOVA tables used in preparation of the manuscript. The data sets were normalized to

M = 100 or M = 1 for the analyses.

Table A14: ANOVA for Normal and Short Term D_2O (M+1)

Anova: Single Factor						
SUMMARY						
Groups	*Count*	*Sum*	*Average*	*Variance*		
Normal M+1	8	440.50760	55.063450	5.5121473		
Short Term D_2O M+1	8	520.39914	65.049893	9.9382474		
ANOVA						
Source of Variation	*SS*	*df*	*MS*	*F*	*P-value*	*F crit*
Between Groups	398.91615	1	398.91615	51.638312	4.66E-06	4.6001099
Within Groups	108.15276	14	7.7251974			
Total	507.06892	15				

Table A15: ANOVA for Normal and Short Term D_2O (M+2)

Anova: Single Factor						
SUMMARY						
Groups	*Count*	*Sum*	*Average*	*Variance*		
Normal M+2	8	111.1428873	13.89286091	1.005413167		
Short Term D_2O M+2	8	174.3360763	21.79200954	4.769521262		
ANOVA						
Source of Variation	*SS*	*df*	*MS*	*F*	*P-value*	*F crit*
Between Groups	249.586195	1	249.586195	86.43775924	2.28E-07	4.60010
Within Groups	40.424541	14	2.88746721			
Total	290.010736	15				

Table A16: ANOVA for Normal and Long Term D_2O (M+1)

Anova: Single Factor						
SUMMARY						
Groups	*Count*	*Sum*	*Average*	*Variance*		
Normal M+1	8	440.50760	55.063450	5.5121473		
Long Term D_2O M+1	8	475.44811	59.431014	7.7120561		
ANOVA						
Source of Variation	*SS*	*df*	*MS*	*F*	*P-value*	*F crit*
Between Groups	76.3024595	1	76.302459	11.539819	0.004338	4.6001099
Within Groups	92.5694242	14	6.6121017			
Total	168.871883	15				

Table A17: ANOVA for Normal and Long Term D_2O (M+2)

Anova: Single Factor						
SUMMARY						
Groups	*Count*	*Sum*	*Average*	*Variance*		
Normal M+2	8	111.14288	13.892860	1.0054131		
Long Term D_2O M+2	8	140.55111	17.568889	8.3165997		
ANOVA						
Source of Variation	*SS*	*df*	*MS*	*F*	*P-value*	*F crit*
Between Groups	54.05273	1	54.05273	11.596794	0.00426	4.600109
Within Groups	65.25409	14	4.661006			
Total	119.3068	15				

Table A18: ANOVA for Long Term D_2O and Long Term H_2O (M+1)

Anova: Single Factor						
SUMMARY						
Groups	*Count*	*Sum*	*Average*	*Variance*		
Long Term D_2O M+1	8	475.44811	59.431014	7.7120561		
Long Term H_2O M+1	8	428.45265	53.556582	9.4270114		
ANOVA						
Source of Variation	*SS*	*df*	*MS*	*F*	*P-value*	*F crit*
Between Groups	138.03580	1	138.03580	16.107738	0.001281	4.6001099
Within Groups	119.97347	14	8.5695338			
Total	258.00927	15				

Table A19: ANOVA for Long Term D_2O and Long Term H_2O (M+2)

Anova: Single Factor						
SUMMARY						
Groups	*Count*	*Sum*	*Average*	*Variance*		
Long Term D_2O M+2	8	140.55111	17.568889	8.3165997		
Long Term H_2O M+2	8	106.31438	13.289298	0.9754621		
ANOVA						
Source of Variation	*SS*	*df*	*MS*	*F*	*P-value*	*F crit*
Between Groups	73.259584	1	73.259584	15.768208	0.001393	4.6001099
Within Groups	65.044433	14	4.6460309			
Total	138.30401	15				

Table A20: ANOVA for Normal D_2O and Short Term H_2O (M+1)

Anova: Single Factor						
SUMMARY						
Groups	*Count*	*Sum*	*Average*	*Variance*		
Normal M+1	8	440.50760	55.063450	5.5121473		
Short Term H_2O M+1	8	438.96609	54.870762	17.803565		
ANOVA						
Source of Variation	*SS*	*df*	*MS*	*F*	*P-value*	*F crit*
Between Groups	0.1485151	1	0.1485151	0.0127394	0.911736	4.6001099
Within Groups	163.20998	14	11.657856			
Total	163.35850	15				

Table A21: ANOVA for BTW, BTW-C, BTD, BTD-C (M+1)

Anova: Single Factor						
SUMMARY						
Groups	*Count*	*Sum*	*Average*	*Variance*		
BTW	8	4.1247832	0.5155979	0.0049188		
BTW-C	8	3.8428710	0.4803588	0.0028533		
BTD	8	3.6635869	0.4579483	0.0021904		
BTD-C	8	3.8492451	0.4811556	0.0011540		
ANOVA						
Source of Variation	*SS*	*df*	*MS*	*F*	*P-value*	*F crit*
Between Groups	0.0135859	3	0.0045286	1.6294947	0.204926	2.9466852
Within Groups	0.0778168	28	0.0027791			
Total	0.0914027	31				

Table A22: ANOVA for BTW, BTW-C, BTD, BTD-C (M+2)

Anova: Single Factor M+2						
SUMMARY						
Groups	*Count*	*Sum*	*Average*	*Variance*		
BTW	8	1.1850983	0.1481372	0.0011406		
BTW-C	8	1.1309808	0.1413726	0.0002710		
BTD	8	1.0982094	0.1372761	0.0003228		
BTD-C	8	1.0657751	0.1332218	0.0003031		
ANOVA						
Source of Variation	*SS*	*df*	*MS*	*F*	*P-value*	*F crit*
Between Groups	0.0009716	3	0.0003238	0.6357986	0.598211	2.9466852
Within Groups	0.0142641	28	0.0005094			
Total	0.0152358	31				

Table A23: ANOVA for ATW, ATW-C, ATD, ATD-C (M+1)

Anova: Single Factor						
SUMMARY						
Groups	*Count*	*Sum*	*Average*	*Variance*		
ATD	8	5.6103	0.7012875	0.0032148		
ATW	8	5.076	0.6345	0.0009198		
ATD-C	8	4.8067	0.6008375	0.0023985		
ATW-C	8	4.891	0.611375	0.0014706		
ANOVA						
Source of Variation	*SS*	*df*	*MS*	*F*	*P-value*	*F crit*
Between Groups	0.0488279	3	0.0162759	8.1339845	0.000474	2.9466852
Within Groups	0.0560276	28	0.0020009			
Total	0.1048556	31				

Table A24: ANOVA for ATD-C and ATW-C (M+1)

Anova: Single Factor						
SUMMARY						
Groups	*Count*	*Sum*	*Average*	*Variance*		
ATD-C	8	4.8067	0.600838	0.002399		
ATW-C	8	4.891	0.611375	0.001471		
ANOVA						
Source of Variation	*SS*	*df*	*MS*	*F*	*P-value*	*F crit*
Between Groups	0.000444	1	0.000444	0.229583	0.639231	4.60011
Within Groups	0.027085	14	0.001935			
Total	0.027529	15				

Table A25: ANOVA for ATW and ATD-C (M+1)

Anova: Single Factor						
SUMMARY						
Groups	*Count*	*Sum*	*Average*	*Variance*		
ATW	8	5.076	0.6345	0.00092		
ATD-C	8	4.8067	0.600838	0.002399		
ANOVA						
Source of Variation	*SS*	*df*	*MS*	*F*	*P-value*	*F crit*
Between Groups	0.004533	1	0.004533	2.731851	0.120606	4.60011
Within Groups	0.023229	14	0.001659			
Total	0.027761	15				

Table A26: ANOVA for ATW-C and ATW (M+1)

Anova: Single Factor						
SUMMARY						
Groups	*Count*	*Sum*	*Average*	*Variance*		
ATW-C	8	4.891	0.611375	0.001471		
ATW	8	5.076	0.6345	0.00092		
ANOVA						
Source of Variation	*SS*	*df*	*MS*	*F*	*P-value*	*F crit*
Between Groups	0.002139	1	0.002139	1.78963	0.202298	4.60011
Within Groups	0.016734	14	0.001195			
Total	0.018873	15				

Table A27: ANOVA for ATD and ATW (M+1)

Anova: Single Factor						
SUMMARY						
Groups	*Count*	*Sum*	*Average*	*Variance*		
ATD	8	5.6103	0.701288	0.003215		
ATW	8	5.076	0.6345	0.00092		
ANOVA						
Source of Variation	*SS*	*df*	*MS*	*F*	*P-value*	*F crit*
Between Groups	0.017842	1	0.017842	8.630487	0.010804	4.60011
Within Groups	0.028943	14	0.002067			
Total	0.046785	15				

Table A28: ANOVA for ATD-C and ATD (M+1)

Anova: Single Factor						
SUMMARY						
Groups	*Count*	*Sum*	*Average*	*Variance*		
ATD-C	8	4.8067	0.600838	0.002399		
ATD	8	5.6103	0.701288	0.003215		
ANOVA						
Source of Variation	*SS*	*df*	*MS*	*F*	*P-value*	*F crit*
Between Groups	0.040361	1	0.040361	14.38006	0.001981	4.60011
Within Groups	0.039294	14	0.002807			
Total	0.079655	15				

Table A29: ANOVA for ATW-C and ATD (M+1)

Anova: Single Factor						
SUMMARY						
Groups	*Count*	*Sum*	*Average*	*Variance*		
ATW-C	8	4.891	0.611375	0.001471		
ATD	8	5.6103	0.701288	0.003215		
ANOVA						
Source of Variation	*SS*	*df*	*MS*	*F*	*P-value*	*F crit*
Between Groups	0.032337	1	0.032337	13.80281	0.002307	4.60011
Within Groups	0.032799	14	0.002343			
Total	0.065136	15				

APPENDIX B

SUPPLEMENTAL INFORMATION FOR CHAPTER 4: CHEMISTRY OF GEOMETRICAL ISOMERS OF ZEAXANTHIN DURING MASS SPECTROMETRY WITH ELECTROSPRAY IONIZATION SOURCE

This appendix contains the unsmoothed total ion chromatograms (TIC) and unsmoothed extracted ion chromatograms (EIC) gathered during the experiment as well as tables with the mass spectrometry peak data that was used to determine the relative intensities of the ions.
The TICs are **Figures: B1**, **B2**, **B3**.

The EICs are **Figures: B4**, **B5**, **B6**.

The data sets are **Tables: B1**, **B2**.

B.1 Unprocessed Total Ion Chromatograms

Figure B1: TIC from crude plant extract

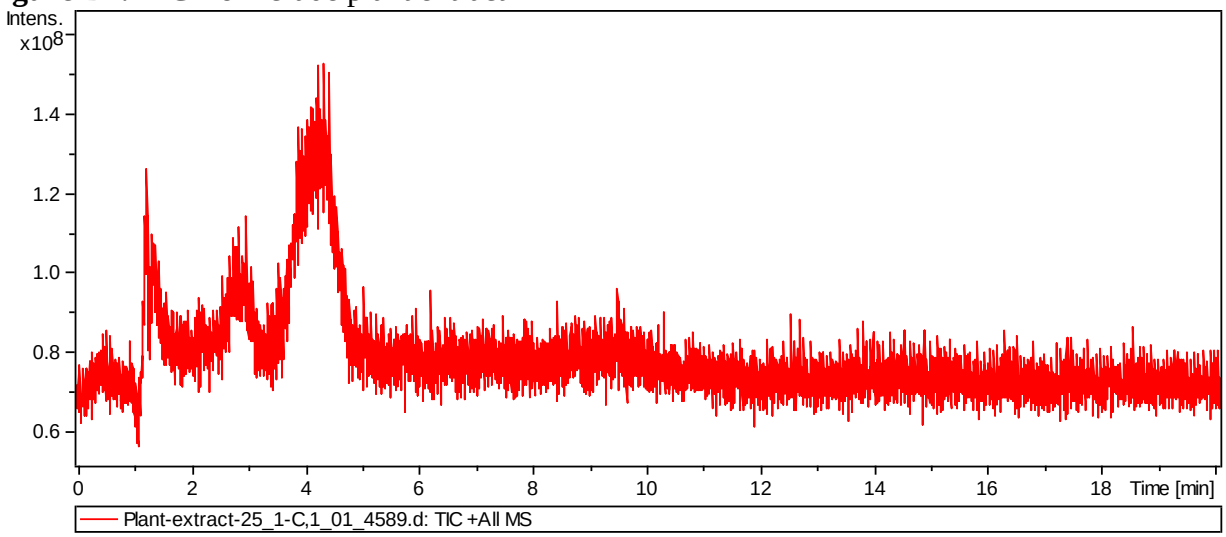

Figure B2: TIC from (13*Z*)-zeaxanthin extract

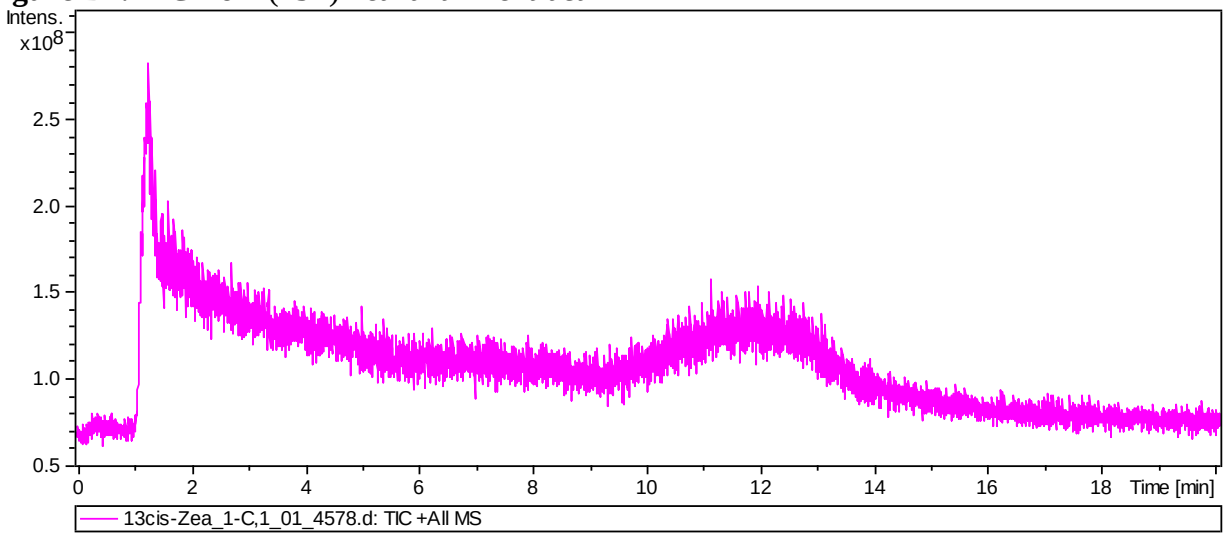

Figure B3: TIC from (all-*E*)-zeaxanthin extract

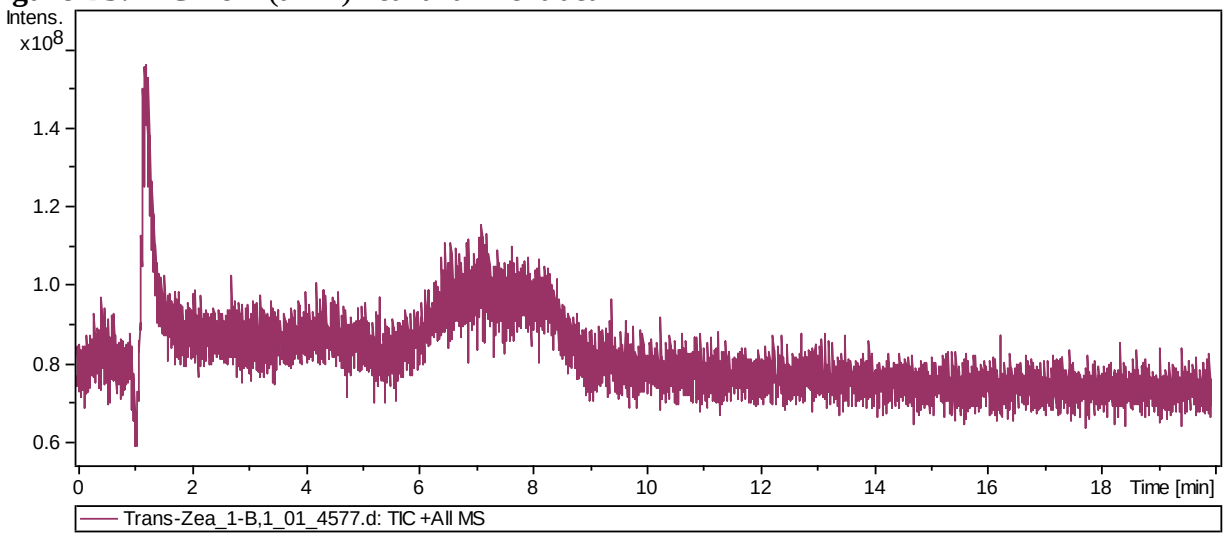

Figure B4: EIC at 568.5 *m/z* from crude plant extract

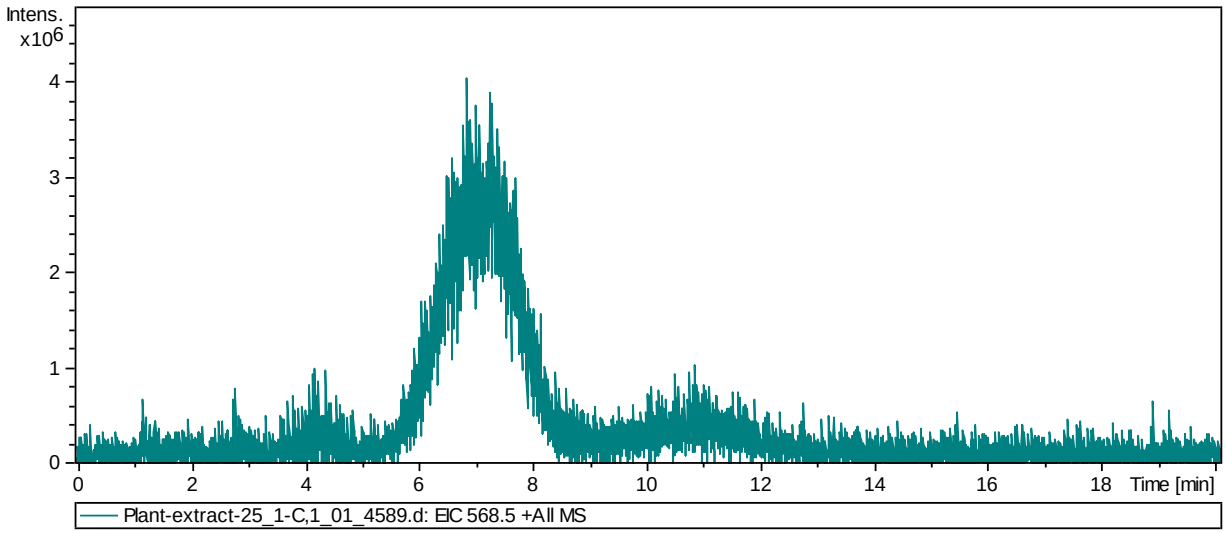

Figure B5: EIC at 568.5 *m/z* from (13*Z*)-zeaxanthin extract

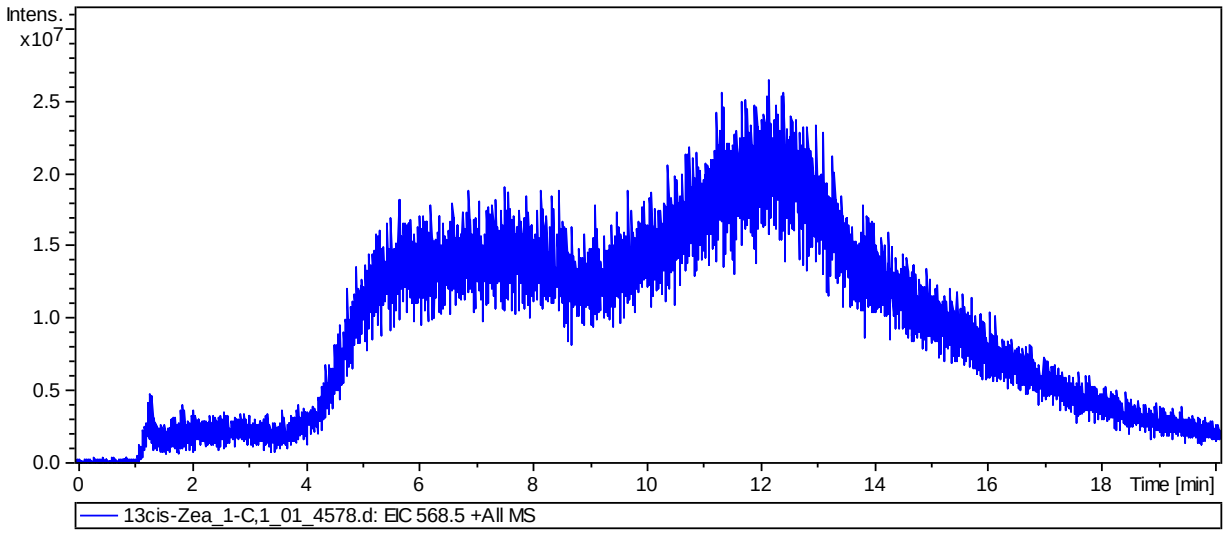

Figure B6: EIC at 568.5 *m/z* from (all-*E*)-zeaxanthin extract

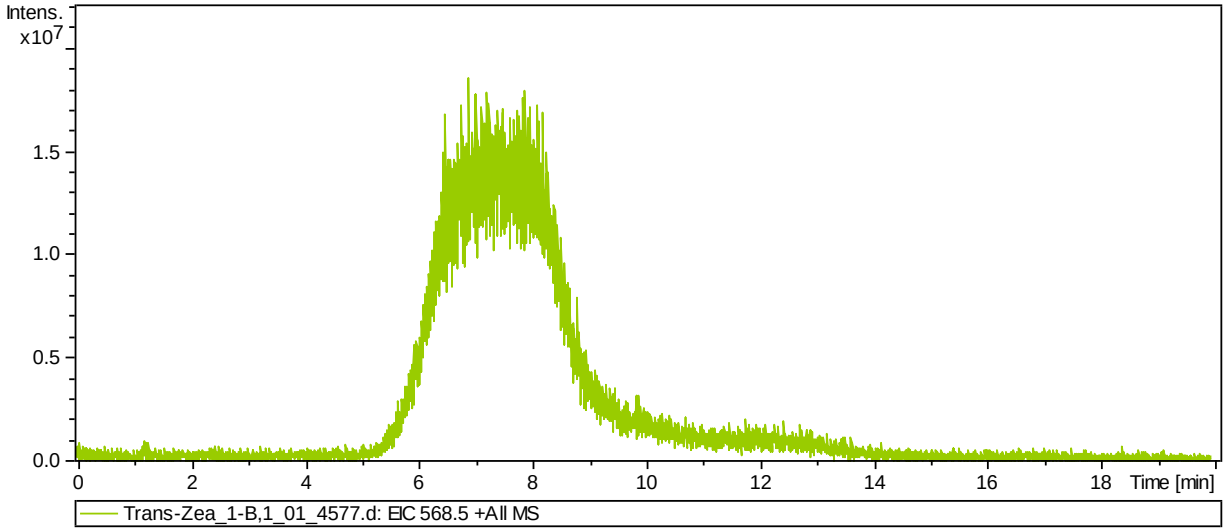

B.2 Tables with the mass peak intensities that were used to determine the relative intensity of the ions

Table B1: Mass Peak Intensities Raw Data for peaks at 6.8 - 7.7 mins

	Zea - 17	(loss water)	
trans peak 6.8-7.7	551	552	553
Plant extract	324515	132468	45033
Trans extract	noise		
cis extract	noise		

		Zea			
trans peak 6.8-7.7	567	568	569	570	571
Plant extract		921295	414414	104653	
trans extract		4656498	2152696	542283	95179
cis extract	531408	5129702	2756662	73771	144045

			Zea+17	Plus oxygen	
trans peak 6.8-7.7	583	584	585	586	587
Plant extract			noise		
trans extract	33265	47389	61717	27056	
cis extract	522267	498392	1910602	777065	181208

				Zea + 32	Plus 2 Oxygen		
trans peak 6.8-7.7	597	598	599	600	601	602	603
Plant extract				noise			
trans extract		17678	57691	32699	31516		
cis extract	35569	30287	250577	123301	89732	40826	18895

Table B2: Mass Peak Intensities Raw Data for peaks at 9.9 - 11.8 mins

	Zea - 17	(loss water)	
cis peak 9.9 - 11.8	551	552	553
Plant extract	243353	94514	35088
trans extract	noise		
cis extract	534428	283519	77402

		Zea			
cis peak 9.9 - 11.8	567	568	569	570	571
Plant extract	58119	120760	63146	25241	21355
trans extract		461570	220531	65235	
cis extract	904538	6285355	4590114	1470055	295774

			Zea+17	Plus oxygen	
cis peak 9.9 - 11.8	583	584	585	586	587
Plant extract			75664	32115	20895
trans extract			noise		
cis extract	412025	248030	390035	159332	43273

		Zea + 32	Plus 2O		
cis peak 9.9 - 11.8	599	600	601	602	603
Plant extract		noise			
trans extract		noise			
cis extract	1510276	675933	357442	122644	